THE UNIVERSITY *of* EDINBURGH

The Role of Heat and Mass Transfer on the Effluent Generated by Fire Flames

Jonathan Reep

A thesis submitted for the degree of Doctor of Philosophy

The University of Edinburgh

2025

This page has been intentionally left blank.

The Role of Heat and Mass Transfer on the Effluent Generated by Fire Flames

Written by
Jonathan Reep

This thesis has been supervised by

Prof. Rory M. Hadden
Prof. Jose L. Torero

The examining committee consisted of

Dr. Christine Switzer
Prof. Luke Bisby

This page has been intentionally left blank.

Abstract

The precise chemical composition of fire effluent has eluded scientists for decades. When solid materials burn, gaseous chemical species are initially generated. The production of gaseous volatile species occurs via pyrolysis, initiated by heat transfer. Pyrolysis products are subsequently oxidised by a flame to produce combustion products. These combustion products, alongside a proportion of partially oxidised pyrolysis products, are the species entrained in air forming the aforementioned effluent. It is therefore important to consider both preceding processes in order to fully understand the composition of fire effluent.

The resultant analytical problem is twofold: to be able to identify the combustion products being produced, a study must be confident in identifying the initial volatile species being generated. This generation stems from a combination of the initial material composition, the rate at which mass is being lost, the geometry of the flame and the imposed combustion environment. Increasing the oxidative environment using existing methodologies results in the mass loss rate (MLR) of a sample increasing as the fire intensifies. This elevated MLR causes the pyrolysis rate to increase, enabling a greater proportion of oxidation reactions to occur. This increased volume of exothermic oxidative processes causes the overall heat release rate (HRR) to rise. Such effects result in the surface of the sample reaching greater temperatures, resulting in thermal gradients being established within the material under investigation. These thermal gradients alter the pyrolysis pathways available, preventing comparisons between experiments conducted under differing oxidative environments being linked to a single changeable variable.

This thesis attempts to decouple the link between the MLR of a sample and the oxidative environment, thus enabling an insight into the role of heat and mass transfer on the composition of fire effluent. Initial room-scale experiments were conducted to attempt to obtain representative fire effluent for analysis. The combustion environment obtained during these room-scale experiments enabled the interaction between a descending smoke layer and the flames to be assessed, however the flow of oxidiser could not be independently adjusted without altering other variables such as the MLR, thus, an alternative approach was required.

Reducing the scale of the problem was found to enable a greater level of control over experimental variables. The modified means of controlling the Fire Propagation Apparatus (FPA) allowed the MLR of a sample to remain fixed under differing oxidative environments. A proportional, integral derivative (PID) controller was used to adjust the voltage controlling the FPA lamps based upon a live reading from the inbuilt load cell. This resulted in a means of enabling a steady state MLR whilst recording the mass and observing the sample throughout an experiment. The combination of such data enabled near real-time yields to be calculated and linked to observed flame geometries.

Furthermore, the heat flux being sent to control the MLR was recorded, enabling the quantification of various oxidative processes when used in conjunction with the effluent analysis. The use of a combination of analytical techniques enabled a greater proportion of

the species generated in the effluent to be identified, providing insights into both pyrolysis and combustion processes. Such a setup enabled the effects of oxygen on pyrolysis and flaming combustion over a range of materials to be investigated in a novel manner.

Decoupling the MLR from the oxidiser has enabled the effect of flame geometry to be linked to the effluent composition for condensed-phase fuels. By demonstrating that these flames behave as diffusion flames, the fire science field can begin to move away from treating fire flames as point sources for chemical species to enter the effluent. It is hoped that the methodology developed in this thesis will continue to enable effluent composition to be linked to changing oxidative environments in a manner that successfully decouples the symbiotic relationship between the MLR and the oxidiser.

Lay Summary

As a fire burns, smoke containing a mixture of different chemicals is generated. To understand how fires behave, we must work out what is in this smoke and how it changes with the type of fire that has been formed. Once we understand what is in the smoke and the factors that affect how it is produced, buildings can be designed to limit the interactions between people and harmful gases during fires.

There are two processes that lead to the production of the gases that form smoke. The first begins when the heat provided to a sample is large enough to enable the transition from the solid or liquid material to form a gas. This process is called pyrolysis, meaning breakdown through heating. After pyrolysis, the produced gases interact with the flame in oxidation reactions (combustion). The shape of the flame will control the extent of this oxidation and therefore the ratio of carbon monoxide, carbon dioxide and other unoxidised species entering the smoke.

When a material is heated up, pyrolysis gases are produced. If the heat source is large enough or provided for a long time, these pyrolysis gases build to a level where they may be ignited. Once ignited, a flame will form which will act as the source of heat to warm the material. As long as a fuel and oxygen are available, this positive heat feedback cycle stops the flame from going out. When oxygen is plentiful, the flame burns brighter and releases more heat. This heat causes additional pyrolysis gases to be produced by the material and the fire increases in size. When oxygen is reduced, the reverse happens and the fire gets smaller.

Current test methods used to measure smoke under different oxygen levels do not account for these changes in surface temperature or flame structure. As a result, experiments under high oxygen conditions lead to brighter, hotter flames that heat the surface more than weaker flames at lower oxygen levels. The hotter flames cause extra pyrolysis gases to be produced by the material that is burning, fuelling the fire and altering the composition of the smoke. The link between the oxygen conditions and this additional gas production may be recorded by measuring the mass being lost by a sample, the mass loss rate (MLR). As the MLR and the oxygen levels are both changing, changes in the smoke cannot be linked to a single changeable variable using existing methods.

In this thesis a new method to assess the heat and mass transfer processes that impact smoke composition is proposed. By keeping the MLR of a sample at a set value, changes in the MLR caused by different oxygen availabilities altering the flame intensity can be prevented. The new method used heat lamps to control the heat flux sent to a sample. The lamps were automatically adjusted based upon the mass of the sample. By controlling the MLR, the effect of varying the oxygen composition could be used to investigate flame structure alongside pyrolysis and charring processes.

The method shows that the flames generated by solid fuels behave as diffusion flames. The shape of these flames is shown to vary with the oxygen availability, where the flames fan out under low oxygen environments. When the flame opens up in this way, unoxidised

species are more likely to enter the smoke. The methodology allows the effects of flame shape to be linked to smoke composition while also providing the heat fluxes required to maintain these processes.

Such results allow the field to move away from treating flames as points from which smoke is produced. Evacuation models can use the data generated by the presented methodology to more accurately model existing fire point sources as diffusion flames. The changes in the oxygen conditions may now be linked to differing flame shapes and therefore differing species entering the smoke. The results enabled by the methodology increase our understanding of smoke composition and the heat and mass transfer processes that determine how smoke is produced.

Acknowledgements

During the last few years I've been supported massively by the welcoming atmosphere in the John Muir building, from the supportive staff to the all the students that pass through, John Muir really is a special place. I just want to thank all the John Muirians that I will have bored to death with my endless tales about running, perhaps now you will have some respite. I've tried to keep this section brief, the fact it is still over a page long shows how amazing you all are.

Thank you Mark, I'm not sure how you brought the FPA back to life, at one point it was a very expensive water feature. Without your technical knowledge I could never have finished my bench-scale work. You've taught me the importance of doing things right and doing them once. You're a great technician and the fire group are very lucky to have you.

Sticking with the team, a massive thank you has to go to all the academic staff but in particular both Angus and Rory for making the PhD experience a genuine pleasure. Angus has saved me from burning a few things that were literally too big, cough cribs cough, whilst Rory simultaneously encouraged it. The atmosphere you guys foster is truly special. On the theme of the academics, Jose and Mike (an academic at heart) deserve a special mention. From the biweekly project meetings to in-person meetings in London you both encouraged my ideas and helped to steer me away from potential pitfalls.

A massive thank you has to go to Sergio and Cameron for sacrificing a week of their lives and coming to Belfast with me. I couldn't have wished for nicer people to spend a week in a disused power station with. From trekking through the snow for tapas to posing with the big fish, it was a week I don't think any of us will ever forget.

Thanks to James and Laura for all the support and putting up with me organising Fired Up 2024 with you, I hope all the stress was worth it to help implement a poster session, perhaps this is our legacy? It is a great conference and I'm happy to have helped play a small part in organising it as a team.

I simply had to thank Hussein and Sam for spending a week with me in Japan. Being covered by micro pigs in Tokyo is one of the most surreal things to have happened during my PhD and perhaps my life, thank you for both for making that adventure feel like home.

David, I'm not sure if I should be thanking you or ruing the day I met you, you have been the biggest distraction during my PhD. It all started when we burned a chair together on Valentine's day, since then we have created whisky and successfully won the coveted silver pinecone from NIST. It has been an absolute pleasure to work alongside you, I'm sure I won't be able to escape you in the future.

A massive thank you to my mum and dad, my sisters Ally and Suzy, and close friends including Mr. Smith, Dr. Hutchings, and Mr. Leckie for dealing with my tales of burning things whilst technically being unemployed. Feigning an interest in fire while you all worked full time jobs, I really appreciated it. You guys are the real heroes, maybe I'll eventually get a real job...

Finally, thank you so much Victoria for dealing with 340 miles between us for 3 years. I reckon constantly taking those LNER and LUMO trains between England and Scotland really boosted the economy post pandemic. Let's hope next time we hear "This is an LNER AZUMA service..." we are on the train together. Seriously though, thank you for supporting my crazy adventures academic or otherwise, I couldn't do it without you.

Publications

Thesis Specific Publications

The below list contains a summary of the relevant peer-reviewed publications related to the content of this thesis.

- **J. Reep**, J.L. Torero, R.M. Hadden, **An approach for the improved measurement of pyrolysis products**, Fire Saf J 142 (2024) 104037. https://doi.org/10.1016/j.firesaf.2023.104037.
- **J. Reep**, J.L. Torero, M. Spearpoint, R.M. Hadden, **Identifying the different processes occurring during the steady state charring of solids**, J Phys Conf Ser 2885 (2024). https://doi.org/10.1088/1742-6596/2885/1/012023.
- **J. Reep**, J.L. Torero, R.M. Hadden, **Assessing the effect of oxidizer on flame geometry and effluent composition from burning solids**, Fire Saf J (2025) 104347. https://doi.org/10.1016/j.firesaf.2025.104347.
- **J. Reep**, S.V. Cordoba, C.E. MacLeod, Y. Kanellopoulos, K. Chotzoglou, T. Fateh, M. Spearpoint, J.L. Torero and R.M. Hadden, **An evaluation of large-scale testing to assess effluent composition during the combustion of building materials**, Fire Saf J UNDER REVIEW.

Conference Proceedings

The following list details the conferences that papers directly related to this thesis have been presented at:

- The 14^{th} International Association of Fire Safety Science (IAFSS) - Tsukuba, Japan 2023
- The 4^{th} European Symposium on Fire Safety Science (ESFSS) - Barcelona, Spain 2024

Additional Publications

The following publications summarise peer-reviewed work that has been completed beyond the specific thesis topic.

- D. Morrisset, **J. Reep**, I. Ojwang, R.M. Hadden, A. Law, **Repeat Fire Tests of Upholstered Furniture: Variability and Experimental Observations**, Fire Technol (2024). https://doi.org/10.1007/s10694-023-01523-3.

- D. Morrisset, **J. Reep**, I. Ojwang, R.M. Hadden, A. Law, **Repeat Fire Tests of Upholstered Furniture: Influence of Experimental Conditions**, J Phys Conf Ser 2885 (2024). https://doi.org/10.1088/1742-6596/2885/1/012043.
- **J. Reep**, D. Morrisset, S. Martin, R.M. Hadden, **Assessing the Extent of Charring and its Impact on the Whisky Ageing Process**, Food Physics, 2 (2025) 100055. https://doi.org/10.1016/j.foodp.2025.100055.

Declaration

This thesis and the work described within has been conducted solely by Jonathan Reep under the supervision of Professor Rory Hadden and Professor Jose Torero at the University of Edinburgh. Where others have contributed, or other sources are quoted, references have been given in full.

.....

Jonathan Reep

2025

This page has been intentionally left blank.

Table of Contents

Terminology

Abbreviations

The following abbreviations are used throughout this thesis. Definitions for selected terms can be found in the subsequent section.

APM - Aerosol Particle Mass Analyser.

CACC - Controlled Atmosphere Cone Calorimeter.

CC - Cone Calorimeter.

CID - Collision-induced Dissociation.

DCM - Dichloromethane.

FPA - Fire Propagation Apparatus.

FT-IR - Fourier Transformed - Infrared Spectroscopy.

GC-MS - Gas Chromatography - Mass Spectrometry.

HPLC - High-performance Liquid Chromatography.

HRR - Heat Release Rate.

IMS - Ion-mobility Mass Spectrometry.

ISO - International Organisation for Standardisation.

L_v - The latent heat of vaporisation.

MALDI - Matrix-assisted Laser Desorption Ionisation.

$\dot{m}''_b$ - The burning rate.

MeOH - Methanol.

MMA - Methyl Methacrylate (Methyl 2-methylpropenoate).

m/z - Mass to charge ratio.

NMR - Nuclear Magnetic Resonance.

PID - Proportional Integral Derivative.

PID - Photoionisation Detector.

PIR foam - Polyisocyanurate foam.

PMMA - PolyMethylmethacrylate (Poly methyl 2-methylpropenoate).

POM - Polyoxymethylene (Polyformaldehyde).

ppb - Parts per billion.

ppm - Parts per million.

PS - Polystyrene.

PUF - Polyurethane Foam.

PVC - Polyvinyl Chloride.

$\dot{Q}''_E$ - The heat flux, per unit area, arising from external heat sources during a fire.

$\dot{Q}''_F$ - The heat flux, per unit area, arising from a flame during a fire.

$\dot{Q}''_L$ - The heat losses, per unit area, to the environment from a fire.

SBI - Single Burning Item.

SEM - Scanning Electron Microscopy.

SPME - Solid-phase Microextraction.

SSM - Solid-state Modulator.

SSTF - Steady State Tube Furnace.

TACO - Transportable Analyser for Calorimetry Outside.

TGA - Thermogravimetric Analysis.

UV - Ultraviolet.

VOC - Volatile Organic Compound.

Definitions

The terms featured here appear throughout this thesis and are defined below to give context to the discussion.

Aerosol - A dispersion of solid particles or liquid droplets in air.

Anisotropic - Any material property that varies with direction. A taken measurement will yield different values depending on the direction from which it was taken.

Burning Rate - The mass of fuel being converted to combustion products through oxidation reactions per unit of time.

Condensed-phase Fuel - A solid or liquid phase material that may be used to generate a gaseous fuel stream for combustion.

Chemical Environment - A description of the atoms that immediately surround the atom being analysed during NMR. Different chemical environments cause different shifts in the resultant spectra.

Diffusion Flame - A type of flame where a central fuel flow is surrounded by a flow of oxidiser. The shape of the flame is dictated by the rate of oxidiser diffusing towards the flame envelope.

Deuterated - A compound, usually a solvent, that has had one (or more) of the hydrogen atoms replaced with deuterium atoms.

Ex-situ Sampling - Any analytical technique where species are removed from their sampling environment, to be analysed at a later date.

Fire Effluent - All gases and aerosols, including suspended particles, created by combustion or pyrolysis and emitted into the environment.

Flame Anchoring - The stabilisation of a flame above a specific location.

Flame Envelope - The location where combustion reactions are actively occurring. The size and the shape of a flame is determined by this boundary.

Headspace - The volume of air immediately above a surface of interest.

Impinger - A piece of glassware containing a collection solution and two glass tubes. Gasses are bubbled between the tubes encouraging analytes to diffuse into the collection solution.

Inverse Diffusion Flame - A type of flame in which the fuel is introduced as an outer jet surrounding an inner air jet, the reverse of a standard diffusion flame.

In-situ Sampling - Any analytical technique that occurs whilst an experiment is ongoing, providing real-time data.

Mass Loss Rate - The mass of fuel transitioning from the condensed phase into the gaseous state per unit of time. The mass loss rate is analogous to the pyrolysis rate.

Oligomer - A chemical species containing a couple of repeating units, a short polymer.

One-dimensional Heat Transfer - Heat transfer that occurs in a single spatial dimension.

Optical Density - A measure of a material's ability to absorb/ scatter a beam of light.

Orthogonal Separation - A chromatographic process in which multiple separation techniques are applied to a sample. Typically samples will be run through two columns, each having differing selectivities for analyte molecules.

Premixed Flame - A flame formed when a fuel and oxidiser are mixed before combustion, usually in a predetermined ratio.

Pyrolysis - The production of small volatile molecules from larger molecules, where the thermal decomposition is initiated by heat.

Speciation - The identification of a specific molecules utilising analytical data.

Stationary Phase - Typically the solid phase for which molecules have a differing affinity for, resulting in the separation of a mixture as the mobile phase is flowed past.

Temperature Field - The difference between the temperature of the environment and the mean integral volume temperature of the sample.

Toxicity - Capable of causing an adverse effect upon a living organism such as irritation, narcosis or death.

Wavenumber - The inverse of wavelength, typically used to compare spectroscopic techniques and the amount of energy being transferred to analytes.

Chapter 1

Introduction

"Why must a building burn before a lesson is learned?"

– Maxïmo Park
Why Must a Building Burn? (Nature Always Wins, 2021)

This page has been intentionally left blank.

1.1 Heat and Mass Transfer in Fire Flames

The arbitrary example of polypropylene burning has been used to contextualise the discussion throughout this introductory chapter. To understand the impact of heat and mass transfer on fire flames, we need to acknowledge how a material burns, whilst accounting for the mass and energy flows within a fire system. The burning of a condensed-phase fuel like polypropylene, a thermoplastic consisting of propylene monomer units, enables these flows to be visualised. The fuel starts in a condensed phase, whether that be a solid or a liquid, before transitioning into the gas phase to enable combustion reactions to occur. Figure 1.1 details the key features of a molten polypropylene pool fire [1].

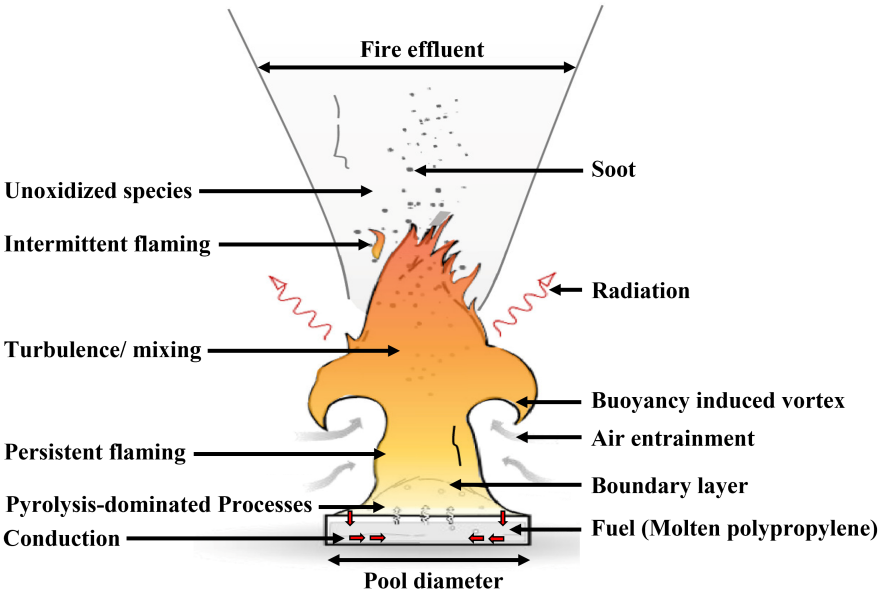

Figure 1.1: An annotated sketch of a pool fire, modified from Y. Chen *et al.*, Pool fire dynamics: Principles, models and recent advances [1].

Fundamentally, combustion is an exothermic chemical process. Once the polypropylene fuel has formed volatile species through pyrolysis-dominated and evaporative processes, these species are oxidised, liberating energy in the form of heat and light whilst generating combustion products. The rate at which this process occurs is known as the burning rate ($\dot{m}''_b$), which refers to the rate at which this gas-phase fuel molecules are consumed via oxidation. This $\dot{m}''_b$ term is dependent on the net heat flux at the surface of the pool, including contributions from external heating ($\dot{Q}''_E$), the flame ($\dot{Q}''_F$), heat losses from the surface of the pool ($\dot{Q}''_L$) and the heat of vaporisation (pyrolysis) of the fuel (L_v) [2, 3]. This relationship is summarised in Equation 1.1.

$$\dot{m}''_b = \frac{\dot{Q}''_E + \dot{Q}''_F - \dot{Q}''_L}{L_v} \tag{1.1}$$

Each term within Equation 1.1 is influenced by a range of variables, incorporating a combination of both material-specific and environmental factors. As $\dot{Q}''_E$ is the external heat flux supplied to the pool fire, this factor largely depends on the external environment. If the pool fire is in an enclosed space, heat transfer via radiation from the walls, ceiling and any established smoke layer back to the fire, will be much greater than the comparative open-air case. Experimentally, $\dot{Q}''_E$ is often the independent variable, as it is the easiest to set and therefore control via external heat sources. The use of a constant $\dot{Q}''_E$ results in $\dot{Q}''_F$ and $\dot{Q}''_L$ becoming time dependent and changing based upon the burning behaviour, the material properties and the flame dynamics. As a result, the net heat flux absorbed by the sample changes as the material burns.

$\dot{Q}''_F$ refers to the energy provided by the flame back to the surface of the fuel. The temperature of the flame and the soot fraction will alter the value of $\dot{Q}''_F$, thus, $\dot{Q}''_F$ varies with the extent and completeness of the combustion. The concept of differing completeness of combustion can be illustrated by adjusting the volume of air flowing into a Bunsen burner. The manner by which the flow of oxidiser is introduced to the fuel has a significant impact on the completeness of the combustion. When the fuel and air are premixed, an essentially soot-free, blue, premixed flame is formed. Alternatively, situations when the fuel and oxygen are not premixed, a more luminous sooty diffusion flame is produced. Under both conditions the same volume of fuel is being burned, yet the flame geometry, heat release rate and species being generated differ significantly. For the pool fire scenario, the base of the flame close to the surface of the pool is blue, indicative of compete combustion. However, moving away from the pool, the decreased combustion efficiency results in a more luminous flame. Eventually at the top of the plume the flame transitions into an intermittent flame, where pockets of fuel only burn when buoyancy induced vortexes and turbulence causes the fuel:oxidiser ratio to fall back into the flammable range. This demonstrates the importance of understanding the mixing of streams of fuel and oxidiser in determining the flame properties.

The heat loss term, $\dot{Q}''_L$, is dependent on the orientation and thickness of the sample, the properties of the fuel, radiation from the surface and factors that influence $\dot{Q}''_F$ (the presence of flame retardants etc.). The orientation of a fuel helps to dictate the dominant method of heat transfer thus, impacts the flame geometry. Once the polypropylene has completely melted in the pool fire scenario, $\dot{Q}''_L$ varies with the diameter of the resultant pool that is formed. A larger surface area results in greater heat losses from the surface of the pool, however these losses may be compensated for by increased $\dot{Q}''_E$ and $\dot{Q}''_F$ terms depending on the specific scenario [4]. For solid fuels, the orientation of a sample impacts how the flame anchors and spreads. A solid material in a vertical orientation will have much greater convective losses compared to the same situation in a horizontal orientation [5].

Flame retardants can be integrated into materials to promote $\dot{Q}''_L$, decreasing $\dot{Q}''_F$ and $\dot{m}''_b$, with the overall aim to promote flame quenching. Halogenated flame retardants form highly reactive radicals that quench the hydroxyl and hydrogen radicals generated during combustion. After several catalytic cycles, halogens are released into the headspace, diluting combustible volatile species [6]. Other retardants like aluminium hydroxide break down endothermically to produce aluminium oxide and water vapour. This endothermic process

removes energy from the fire system, promoting $\dot{Q}''_L$, whilst diluting pyrolysis gases below the lower flammability limit through the emission of water vapour [7]. Flame retardants and other additives complicate the balance shown in Equation 1.1 and enable a further subsection of theoretical species to form.

The multiple variables that impact each of the terms that contribute towards $\dot{m}''_b$ are intrinsically linked. To investigate the role of heat and mass transfer on fire flames, these variables need to be decoupled, thus, enabling methodologies to independently assess the impact of each variable on fire dynamics.

1.2 Mass Loss Rates

Before a pool fire is established, a sequence of chemical and physical processes occur as the fuel is heated. During this initial heating, the fuel undergoes several physical processes including melting, pyrolysis and evaporation, resulting in volatile species being released into the local headspace [8]. The produced volatiles are the components that burn in the presence of an oxidiser and an appropriate thermal environment, producing a flame. The rate of these gaseous volatile species being generated by the fuel can be monitored by recording the reduction of mass from the condensed-phase fuel. This variable is known as the mass loss rate (MLR) of the material.

The MLR is largely determined by pyrolysis-dominated processes as it encompasses all the fuel mass transitioning from the condensed phase into the gaseous state. The MLR is not equal to $\dot{m}''_b$ as the burning rate only incorporates the combustion (oxidation) of the pyrolysis products. In the pool fire scenario described in Figure 1.1, some gaseous fuel molecules may not be oxidised by the intermittent flaming, resulting in species entering the effluent not accounted for by $\dot{m}''_b$. The MLR must therefore be used to describe the flow rate of gaseous fuel molecules arising from a condensed-phase fuel.

The extent of the fuel oxidation is intrinsically linked to the MLR and the oxygen availability in the surrounding environment. During the polypropylene pool fire, the polymer is initially cleaved to produce short-chain, volatile species. When these species are oxidised, heat is transferred to the surroundings. This heat flux encourages additional polypropylene molecules to undergo pyrolysis processes, increasing the MLR and creating, at least initially, a positive feedback cycle [9].This concept, known as the surface energy balance, creates a cycle that will cause the pool fire to grow rapidly. An increase in oxidiser availability is likely to increase the heat being generated by the flame and therefore drives an increase in the pyrolysis rate. It therefore follows that altering the oxidative conditions may cause the MLR of a sample to vary. Altering the MLR impacts the rate of fuel oxidation and therefore the heat generated by the flame. Thus, it follows that the interconnected nature of these variables cannot be ignored when interpreting fire processes.

To fully understand ignition, combustion, flame spread and quenching events, a basic comprehension of the chemical composition of the gaseous fuel is needed [10, 11]. The identification of the species being generated and in particular, how these products vary in relation to the MLR of the investigated material, is necessary in order to increase our understanding of fire dynamics. The interconnected nature between the MLR and the oxidiser composition currently prevents a single variable being investigated, thus MLRs should be controlled and stabilised when adjusting oxidiser compositions to assess the impact on the species in the generated fire effluent.

1.3 Hazards Associated with Fire Effluent

Gaseous species within fire effluent, can be broadly classified into three clusters: asphyxiants, irritants and other, with the final category containing typically inert species [12]. Asphyxiants are species that reduce the body's ability to uptake oxygen while irritants encompass species that cause sensory or pulmonary irritation, incapacitating individuals, decreasing their chances of a successful escape. Irritants like hydrogen chloride (HCl), generated during the combustion of PVC, have been shown to prompt irritation to the eyes and lungs. Once inhaled, HCl readily dissociates, producing H^+ ions that damage mucus membranes leading to lung irritation and inflammation. Depending on the concentration of the gas and the length of exposure, this damage can be irreversible, with prolonged exposure eventually leading to death.

Irritants function by harming the skin, including irritating the eyes and internal linings of the airways. Such effects reduce a person's mobility, disrupting their means of escape and rendering the evacuee susceptible to any asphyxiants present in the effluent. It is however more common for asphyxiants to be the direct cause of fire fatalities, due to the reduced oxygen carrying capacity of blood. Carbon monoxide (CO) is the most notorious asphyxiant in fire effluent as it preferentially binds to haemoglobin, displacing an oxygen ligand, hindering the body's ability to uptake oxygen. Figure 1.2 shows a simplified mechanism for this interaction.

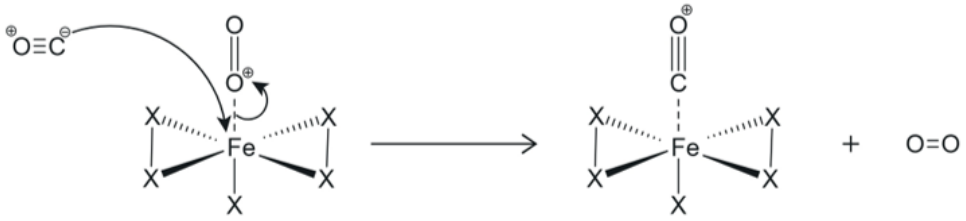

Figure 1.2: A simplified mechanism showing the displacement of an oxygen ligand from the iron ion at the centre of the haemoglobin protein when in the presence of CO. Note that X refers to nitrogen binding sites within the protein.

The CO ligand has a stronger affinity for the iron ion than oxygen, and as such displaces the oxygen ligand from the haemoglobin protein. Hydrogen cyanide (HCN), another asphyxiant, behaves in a similar manner, as the cyanide ion binds to the iron ion in the mitochondrial enzyme cytochrome oxidase. Once bound, the HCN prevents aerobic metabolic processes occurring as the mitochondria cannot obtain oxygen from the blood. Anaerobic metabolism ensues, generating lactic acid leading to metabolic acidosis [13].

The effects of CO and HCN as chemical asphyxiants have been extensively documented throughout literature, with blood carboxyhaemoglobin levels post-mortem being used to identify cause of death [14].Despite this documentation, the additive impacts caused by the combination of specific asphyxiants and irritants is largely undiscussed. A reliable means of identifying and quantifying these species in fire effluent must first be determined to enable meaningful discussion surrounding the hazards associated with fire effluent.

CO and HCN formation are known to vary in part based upon the availability of oxidiser, with both species being preferentially generated under low oxygen environments. Given the hazards associated with these species, their yields in fire effluent have been assessed as a function of the oxidative environment. Figure 1.3 summarises some literature yields for these asphyxiants obtained during the combustion of insulation foams utilising a single piece of apparatus: the steady state tube furnace [15–17].

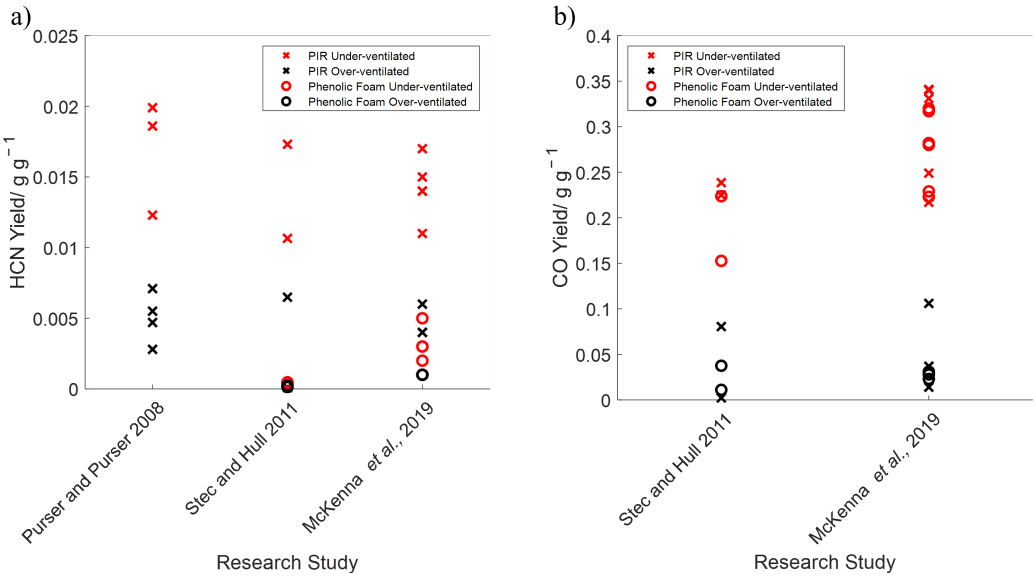

Figure 1.3: A compilation of a) HCN and b) CO yields obtained from polyisocyanurate (PIR) and phenolic foam using the steady state tube furnace in existing literature [15–17].

The HCN yields obtained from polyisocyanurate (PIR) foam spanned between 0.0001 and 0.020 g g^{-1}, depending on the oxidative conditions being investigated, with under-ventilated conditions resulting in increased cyanide yields. In contrast, the CO yields recorded in the phenolic foam effluent were an order of magnitude larger, ranging from 0.01 to 0.32 g g^{-1}, where under-ventilated conditions promoted the formation of CO. The literature demonstrated the impact of the oxidative conditions on the species being produced, with the dominance of CO across both foams suggesting that differing combustion processes contribute to asphyxiant generation. The extent of the oxidation achievable during these combustion processes hinges partially on the geometry of the flame, a factor itself dependent on the oxidative environment.

1.3.1 Pyrolysis Products

For most materials it is difficult to identify the entirety of the chemical species being generated during pyrolysis, although there are a few notable exceptions including polymethylmethacrylate (PMMA). To simplify things, the generation of volatile species in the effluent is often defined arbitrarily by using the MLR to represent $\dot{m}''_b$. A greater understanding of the species being generated and their respective concentrations during the pyrolysis of polypropylene would provide a starting place to model the oxidation reactions occurring during the pool fire presented in Figure 1.1. Once the undefined pyrolysis prod-

ucts have been produced, partial and complete oxidation reactions occur, causing the range of unknown species present in the effluent to increase. Precisely defining the composition of pyrolysis products will enhance our understanding of the gas-phase chemistry arising from condensed-phase materials and will facilitate a greater understanding of the processes relevant to diffusion flames.

During pyrolysis, polymeric materials undergo both chain scission and chain stripping processes. These processes reduce the molecular weight of the polymer, generating a range of volatile species including dimers and monomers. The elevated temperatures associated with fires enable cross-linking, cyclisation, rearrangement and degradation reactions to simultaneously occur, further complicating the problem [18]. The volatile species arising from different materials may theoretically interact, potentially producing additional species. Figure 1.4 shows the mechanism by which polyvinyl chloride (PVC) may generate chlorinated by-products when in the vicinity of polypropylene [19]. Such scenarios are increasingly plausible when products consisting of a mixture of materials become involved in fires.

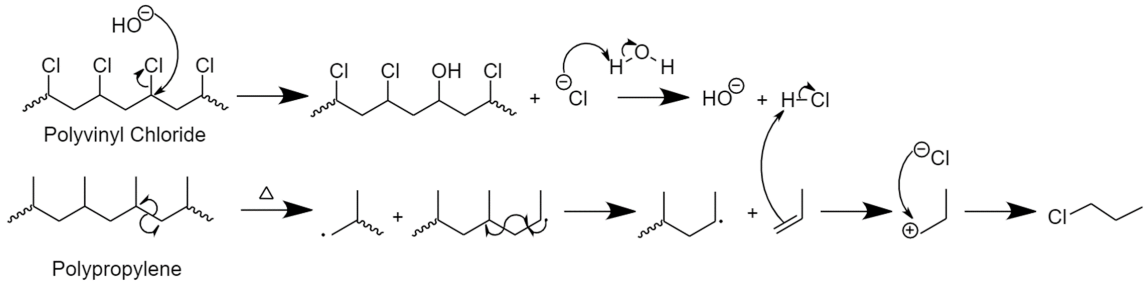

Figure 1.4: A theoretical means by which chlorinated hydrocarbons may be generated when polyvinyl chloride and polypropylene are burnt together. A substitution mechanism is shown for the PVC while the polypropylene is depicted as undertaking a chain scission process [19].

It therefore follows that the chemical structure of the material being investigated will impact which pyrolysis mechanisms can occur. For example, strong aromatic structures have higher bond energies due to the strength afforded by the conjugated π-bonded systems. In such scenarios, the weaker, non-aromatic σ-bonds are initially cleaved, as the π-bonds have a greater resistance to the imposed heat flux, influencing the likelihood of certain volatile species being formed.

Predicting which bonds will cleave during pyrolysis is not straightforward. For a simple polymer comprising of a single type of monomer in an unbranched chain, like PMMA, basic pyrolysis mechanisms, result in monomer yields ranging from 90 % to 98 % [20, 21]. More complex natural polymers, like the cellulose in timber, may cleave in numerous places, generating a range of differing pyrolysis products [22]. Such results reflect the complexity and interconnectivity of the numerous variables that impact pyrolysis processes.

1.3.2 Combustion Products

Flaming combustion requires the fuel to be in the gaseous state. Fire scenarios typically involve an oxidising flame, reducing the prevalence of pyrolysis products as they are preferentially oxidised to form carbon dioxide (CO_2) and water vapour (H_2O). To determine the impact of these interconnected variables on the concentration of generated species, the flame and its resultant geometry must also be considered.

Once volatile species and an oxidiser are present in a flammable ratio, an ignition source can be introduced to initiate flaming combustion. This involves a flame becoming established above the surface of the fuel, anchoring above regions of pyrolysis. Equation 1.2 shows the complete combustion of propene, a pyrolysis product formed from polypropylene.

$$2\ C_3H_{6\ (g)} + 9\ O_{2\ (g)} \rightarrow 6\ CO_{2\ (g)} + 6\ H_2O_{\ (g)} \tag{1.2}$$

The increased temperatures within the flame envelope enable oxidative processes to occur, which in turn release energy, increasing the extent of oxidation. Once formed through pyrolysis gaseous species, largely short chain hydrocarbons like propene, are oxidised, where CO_2 and H_2O form the majority of the effluent. The ratio of CO_2 to partially oxidised products like carbon monoxide (CO) is expected to vary with oxygen availability.

Combustion can still occur in the absence of a flame via smouldering. The rate of smouldering combustion is much slower than that of flaming combustion as it is dictated by oxygen attacking a solid-phase fuel [23]. CO and CO_2 are still generated, but at a greatly decreased rate in comparison to a flaming process. This flameless form of combustion has a lower heat release rate (HRR) than its flaming counterpart, resulting in a lower temperature process. These lower temperatures decrease the combustion efficiency, leading to the generation of partially oxidised products like the asphyxiant CO. Despite the decreased MLRs, the yield of these products can still be large however, it is the high proportion of unoxidised pyrolysis products entering the effluent alongside CO and CO_2 that signifies that smouldering combustion may be occurring.

1.4 Flame Types

During fires, combustible gases are generated when a condensed-phase fuel undergoes pyrolysis due to heat transfer from the flames and the surrounding environment. These combustible gases are transported by buoyancy effects alongside the entrainment of air, supplying the oxygen necessary for combustion. As the fire increases in size, the characteristic flow velocity also increases, eventually transitioning to turbulence. It is the combination of these factors, the heat feedback, the buoyancy and the turbulence, that controls the transport of both the fuel and the oxidiser towards the flame. These coupled phenomena ultimately establish the location of the flame and the characteristics of the combustion chemistry.

To fully understand the composition of fire effluent it is essential to be able to identify and quantify both the pyrolysis products and the combustion products being generated. The produced species will vary, in part, with the type of flaming combustion that occurs. Diffusion flames are usually formed during the combustion of condensed-phase fuels where the mixing between the fuel and oxidiser occurs at the flame envelope. The other common flame type, premixed flames, are usually induced for gas-phased fuels where the oxidiser is uniformly mixed with a gaseous fuel stream prior to combustion. Both types of flame influence the composition of the generated effluent.

1.4.1 Diffusion Flames

Diffusion flames are controlled by the rate of an oxidiser propagating towards a fuel. The flow of oxidiser into the reaction zone is rate-determining compared to the relative rate of the oxidising reactions occurring within the flame envelope [24]. The shape of the resultant laminar diffusion flame is therefore influenced primarily by the co-diffusion of oxygen and fuel. This subsequently determines the size and geometry of the flame envelope, including whether any pyrolysis or partially oxygenated species are generated and emitted [11].

The shape of these diffusion flames is defined by the region in which the fuel and oxidiser are consumed by combustion reactions, a process outlined by the Burke-Schumann development [25]. Burke and Schumann proposed that a fuel and an oxidiser cannot coexist beyond the flame envelope, thus, any combustion reactions are assumed to have occurred instantaneously. This approximation enabled the diffusion between the gaseous fuel and air within a co-flow burner to be identified as the dominant contributor to diffusion flame geometry, greater than any contribution from velocity differences between the streams [26]. Following on from this work, diffusion flame shapes for gas-phase fuels have been predicted with a remarkable degree of accuracy, aligning well with experimental results [27]. The size and geometry of the resultant laminar diffusion flame is therefore influenced primarily by the co-diffusion of fuel and oxygen towards the flame.

However, as the majority of fuels involved during fire scenarios begin in the condensed phase, the injection rate of gaseous fuel is controlled by the pyrolysis rate (approximated by the MLR). This MLR varies as a function of the combustion environment incorporating

the effects of any external heating. As a result, the gaseous fuel injection rate becomes highly coupled to the external environment, where simplified configurations, such as those found in counter-flow burners, no longer enable interrogation of all the relevant variables.

The species produced during the pyrolysis and combustion of condensed-phase materials are therefore not currently well defined. When the changing flame structures, temperatures, flow fields and oxidiser availabilities above a pool fire are factored in, predicting the products that will form and hence the energy released during their subsequent combustion becomes extremely complex. Once additional factors like the geometry of the diffusion flame and the partial oxidation of pyrolysis products are considered, the resultant mixture of species comprising fire effluent is currently too complex to reliably predict.

The uncertainty surrounding the combustion products being generated by fires can be considered to primarily arise from diffusion flames. During fire scenarios, like the polypropylene pool fire, there is no control over the fuel injection rate or the mixing of the fuel and the oxidiser, thus, diffusion flames are generated. Diffusion flames are intrinsically linked to the combustion environment, with the flame geometry being dictated by a combination of the oxygen in the local atmosphere, the MLR of the sample, the temperature field and the composition of the material being investigated. Accurately predicting the pyrolysis products for materials beyond simple polymeric fuels is not currently possible. As a result, predicting the effects of oxygen on a diffusion flame sustained by a condensed-phase fuel, in terms of combustion efficacy and the resultant species being generated, requires more research.

1.4.2 Premixed Flames

Moving away from diffusion flames, a fuel and oxidiser may be mixed prior to combustion leading to the formation of a premixed flame. Premixed flames occur when a gaseous fuel is mixed with a set volume of oxidiser and the resultant blend is flowed at a set rate prior to combustion. Control over the fuel:oxidiser ratio allows the composition of the combustion products to be reliability predicted, enabling the HRR of combustion processes to be controlled. As a society, we have moved away from the uncertainty of diffusion flames, preferring the control and predictability that premixed flames enable. Premixed flames are used to control combustion processes, facilitating modern comforts like cooking with gas hobs and travel via modern internal combustion engines [24]. Modern internal combustion engines limit diffusion flames via the introduction of liquid fuels as small droplets. These droplets are gasified in the engine prechamber where the nozzle introduces turbulence to encourage mixing with an oxidiser. The control over the injection rate, nozzle and droplet size enables quasi premixed conditions [28]. By preventing diffusion flames from forming, the heat released by these processes has become predictable and controllable, hence their prevalence in society.

As the fuel and the oxidiser are already mixed, diffusion does not control the flame geometry for premixed flames. Instead, the ratio between the fuel and the oxidiser becomes critical. The equivalence ratio, shown in Equation 1.3 enables the relationship between these two factors to be quantified, where n represents the number of moles [29].

$$Equivalence\ Ratio\ (\Phi) = \frac{(n_{fuel}/n_{air})_{actual}}{(n_{fuel}/n_{air})_{stoichiometric}} \tag{1.3}$$

If Equation 1.3 generates a value greater than one, the environment is said to be fuel rich. In this scenario, there are insufficient moles of oxygen to enable complete combustion to occur, thus partially oxygenated products are produced. Conversely, when the equivalence ratio is lower than one, a fuel lean environment is generated. The abundance of oxygen facilitates complete combustion, increasing the yields of CO_2 and H_2O. A low equivalence ratio therefore leads to a cleaner combustion process. To enable a lower equivalence ratio, an abundance of oxygen is required, reinforcing the link between effluent composition and oxygen availability.

Such ratios may be useful for the bench-scale analysis of premixed flames, however for the more common diffusion-controlled flame, the movement of oxygen towards the flame envelope becomes rate determining, rather than the equivalence ratio. As a result, methodologies should focus on assessing diffusion flames at representative scales. Under these scenarios it is the flow of oxidiser in relation to the burning rate has a greater impact on the overall geometry of the flame and hence the composition of the effluent rather than the equivalence ratio.

As the oxygen diffusing towards the flame controls the combustion processes, the oxidiser flow may be varied in order to screen a range of flame geometries. However, changing the airflow induces changes in the burning rate, altering the combustion processes being investigated. To successfully vary the oxygen reaching the flame, the MLR needs to be set, and independently controlled, enabling the impact of the airflow on flame geometry to be independently assessed. Such conditions can only be obtained if manipulation of the oxidiser flow occurs alongside a set MLR.

1.5 Aims and Objectives

This thesis aims to develop a method to assess the chemical species that are generated during fire scenarios involving diffusion flames. This problem has manifested itself in the fire community in the form of toxicity, screening fire effluent for specific asphyxiants or irritants. However, understanding the chemical composition of fire effluent has much wider applications, enabling insights into the solid and gas-phase processes of burning.

For gaseous fuels, fire effluent is typically studied using experimental arrangements where the flows of both a fuel and an oxidiser can be independently controlled, e.g., in a co-flow burner [25]. However, when studying combustible solids, the pyrolysis rate controls the gaseous fuel flow rate. The pyrolysis rate is determined by the surface energy balance which includes external heat fluxes and any heat feedback provided by the flame. The combination of these effects results in a strong coupling between the fuel flow rate and the oxidiser. To study how the amount of available oxygen alters the burning of solid fuels, it is therefore necessary to be able to independently control the pyrolysis rate, in the form of the MLR. This thesis attempts to find a mechanism to decouple these phenomena through the following chapter objectives:

Chapter 2 – Literature Review:

- To summarise existing strategies to sample fire effluent.
- To identify the best methodology to generate, sample and analyse effluent.
- To evaluate the key features of an appropriate sampling methodology.

Chapter 3 – Large-scale Evaluation of Effluent Composition:

- To assess effluent composition during realistic fire scenarios.
- To generate effluent in a repeatable manner at a large-scale.
- To assess the representativeness of large-scale methodologies.

Chapter 4 – Improving the Measurement of Pyrolysis Products:

- To develop a representative effluent generating methodology focused on a fixed MLR.
- To assess the pyrolysis products generated by simple synthetic polymers.
- To identify chemical species via a combination of appropriate analytical techniques.

Chapter 5 – Investigating Charring Materials:

- To assess more complex charring materials utilising the developed methodology.
- To determine the transition from pyrolysis into charring via energy inputs.
- To use the species detected in the effluent to determine which combustion processes are occurring.

Chapter 6 – Assessing the Impact of Flame Geometry on Effluent Composition:

- To extend the developed methodology to flaming combustion with a fixed MLR.
- To investigate the effect of oxidative conditions on flame shape.
- To determine the impact of diffusion flame geometry on overall effluent composition.

Chapter 7 – Conclusions:

- To consolidate an overall means for assessing the products generated by fires.
- To outline the applications of this research in the wider fire science community.
- To recommend approaches for future research in this field.

It is hoped that an improved understanding of the role of heat and mass transfer on the effluent generated by fire flames can be obtained through the development of a new methodology. Such an approach must be able to identity and quantify the chemical species being generated alongside controlling and recording the MLR of a sample, enabling the decoupling of the gaseous fuel flow rate from the oxidiser flow. Currently there is no single analytical approach to attain such information.

By developing an improved methodology that focuses on decoupling the gaseous fuel flow rate from the oxidiser flow, more prominent links between surface conditions, including flame geometry, and the composition of the effluent can be made. Implementing appropriate sampling strategies is likely to improve both the speciation and the quantification of the effluent enhancing our understanding of pyrolysis and combustion processes as additional species are identified. The development of such techniques will reduce the complexity surrounding the interconnected nature of the factors that impact effluent composition, improving the reliability and reducing the uncertainty in current effluent predicting models. Such improvements will increase our understanding of the factors that influence effluent composition, aiding decisions to avoid scenarios that would facilitate the generation of products of concern.

This page has been intentionally left blank.

Chapter 2

Literature Review

"A burning beacon, burning through the fog."

– Courteeners
Sunflower (Concrete Love, 2014)

This page has been intentionally left blank.

2.1 A Universal Methodology?

The conservation of matter law, proposed by Lavoisier, states that matter, within a closed system, may not be created or destroyed [30]. As such, the smoke (fire effluent) generated during a fire reflects the chemical composition of the burning material. Applying this principle to the sampling of fire effluent indicates that the type and concentration of chemical species present in the effluent will vary depending on both the mass of air entering the system and the mass of the sample burning. A greater oxygen (O_2) availability will favour oxidation reactions, leading to higher flame temperatures and inevitably a greater burning rate. The coupling between these variables and the attempt to individually control them has resulted in the creation of multiple methodologies to assess the composition of fire effluent.

The challenges involved in identifying and quantifying the gaseous species being generated during both pyrolysis and any subsequent oxidative processes, across a range of materials, scales and scenarios has resulted in analytical methodologies being tailored towards individual experiments. A variety of different heat sources, heating rates, sampling techniques, sampling locations, testing scales and means of obtaining the mass of a sample during an experiment have enabled multiple methodologies to be developed. This chapter aims to highlight the challenges associated with the generation, sampling and analysis of fire effluent, explaining why a universal means of sampling fire effluent is yet to be finalised.

2.2 Effluent Generation

To identify and verify the impacts of variables such as oxygen availability on fire effluent, it is important that a robust and repeatable methodology exists. Obtaining a repeatable means of quantifying fire effluent is a complex challenge requiring the control over several factors including the generation, the sampling and the chemical analysis of the effluent. The end goal for experimental work should always involve the application and implementation of experimental findings. Ideally, data should be collected via controlled full-scale combustion studies, establishing direct links between experiment and reality. Unfortunately, due to physical and economic constraints, full-scale tests are not usually plausible. Instead, a compromise is reached with bench-scale testing offering insights into full-scale fire dynamics.

Large-scale testing methodologies are less common than bench-scale methodologies, existing primarily as a means of verifying the results obtained at smaller-scales. Larger-scale experiments often involve room-sized fires, leading to debates over representative sampling locations. At the bench-scale, the combustion mass balance remains unresolved as the species generated by 'simple' fuels result in complex mixtures of several components [31]. As the complete chemical analysis of fire effluent is still largely in its infancy, small-scale testing is a necessity for the development of a standardised methodology for the assessment of fire effluent.

By controlling the variables that impact a material's mass loss rate (MLR), apparatuses in turn control the species passing into the effluent. While the previous chapter discussed the composition of fire effluent, this section focuses on the means by which the effluent can be generated, trapped and analysed. The first of these sections covers existing techniques used to generate effluent for analysis.

2.2.1 Thermogravimetric Analysis

Thermogravimetric analysis (TGA) is a common methodology used to distinguish between combustion phases. The process involves a small mass of a sample ($\sim$0.015 g) being placed in a pan on a load cell within a furnace, whereby the temperature is gradually raised at a set rate [32]. Figure 2.1 details the experimental setup for the TGA in the vertical orientation [33].

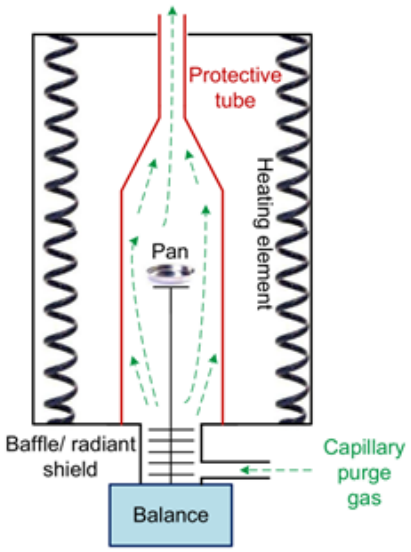

Figure 2.1: The vertical TGA setup in which a pan containing a sample is heated inside an oven. Reproduced from N. Saadatkhah *et al.*, Experimental methods in chemical engineering: Thermogravimetric analysis - TGA [33].

Mass will be lost by the sample at particular temperatures, specific to the material under investigation, enabling differing processes to be identified. Typically, an initial drying phase occurs as water is evaporated from the sample before a subsequent pyrolysis phase. However, the technique can also identify other solvent losses alongside more complex processes such as the loss of carbon dioxide (CO_2) from carboxylic acids (decarboxylation) [34]. The temperature at which these mass losses occur provides material property data, which is usually used to guide experimental parameters for subsequent studies.

Organic fuels that often differ in structure, like peat, may be screened via TGA to assess the differing composition of volatile components. Figure 2.2 shows a TGA plot for peat, where distinct vertical regions show mass is being lost from the sample [35].

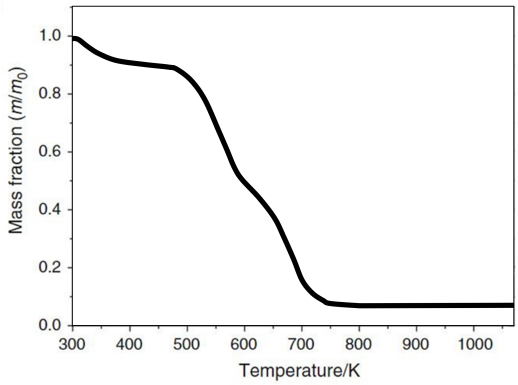

Figure 2.2: A TGA plot for the thermal decomposition of peat. The vertical sections represent mass losses, suggesting the loss of volatile compounds. Modified from J. Yang *et al.*, Combustion kinetics and emission characteristics of peat through the use of TG-FTIR [35].

TGA experiments are usually conducted under nitrogen, preventing oxidation reactions and therefore favouring pyrolysis-dominated processes. In Figure 2.2, at 373 K water was driven off the peat, a common TGA observation. Beyond this point pyrolysis-dominant processes are responsible for the observed mass loss. The plots indicate that pyrolysis of this specific peat sample began at around 500 K with additional information on chemical composition being provided via coupling to external analytical techniques. Any differences observed between TGA experiments using the same peat samples may have arisen due to the non-uniform behaviour of the peat, arising from the small sample sizes utilised during TGA analysis.

TGA has its place as an effluent generating tool; however, it is more of an initial technique used to guide experimental design rather than a tool to act as a fire-based model. The small sample sizes alongside the one-dimensional heating and slow ramp rates prevent the technique from being a representative means of assessing the thermal gradients present across larger, more realistic, samples. These thermal gradients across real-world samples facilitate alternative pyrolysis pathways, potentially generating effluent with a differing chemical composition to that generated by TGA. The combination of the small sample size and the slow thermal ramp rate prevent a continuous effluent stream being generated. As such, TGA may not enable an insight into some of the more complex interactions encountered during genuine fire scenarios.

It is therefore plausible to use TGA as a guide to determine an appropriate experimental setup based upon the aim of a study. Through tailoring an experimental study towards a specific temperature, work can focus on pyrolysis or combustion phenomena. For example, the determination of the pyrolysis temperature for polymethylmethacrylate (PMMA) via TGA enabled the robustness of a novel temperature sensing technique to be assessed [36]. TGA enables a reproducible dataset to be obtained, attributed to the high level of control over the external conditions that a sample is exposed to, yet the small sample size must be kept in mind if utilising TGA for speciation.

2.2.2 The Smoke Density Chamber

In an attempt to retain fire effluent for analysis the smoke density chamber was developed, containing a set volume of smoke inside a chamber for a standardised analysis [37]. Figure 2.3 shows the standard setup for a smoke density chamber (International organisation for standardisation, ISO, 5659-2:2017) [38]. During each test, a standardised square of material (75 mm $\times$ 75 mm $\times$ 25 mm) is placed on a load cell and undertakes one of four different scenarios detailed in Table 2.1.

Table 2.1: A comparison of the four standard experimental conditions assessed using the smoke density chamber based on information presented in ISO 5659-2:2017.

Heat Flux / kW m^{-2}	Ignition Source	Fire Scenario Modelled
25	N/A	Pyrolysis
25	Pilot	Initial flaming
50	N/A	Non-flaming combustion
50	Pilot	Flaming combustion

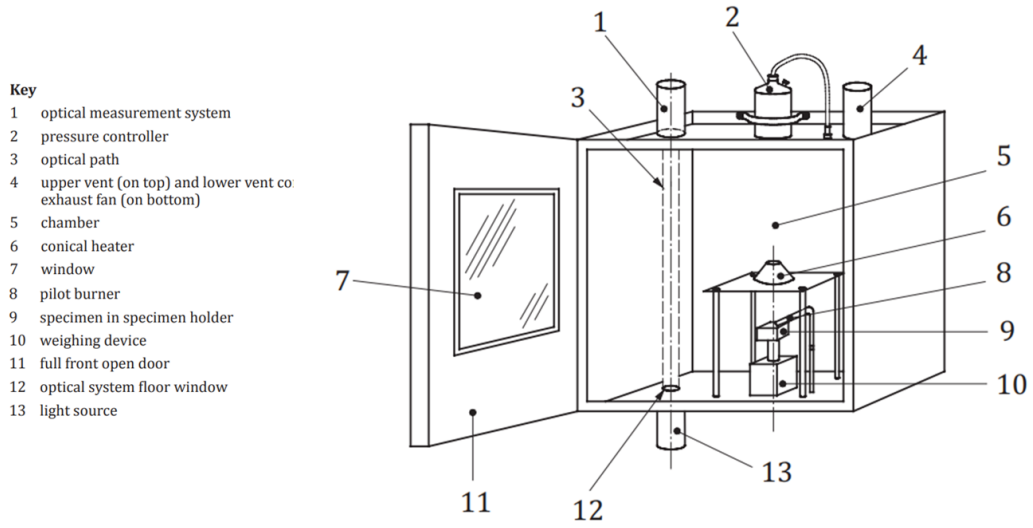

Figure 2.3: The standard method (with a material inside the chamber) for sampling combustion products using the smoke density chamber (ISO 5659-2). Reproduced from ISO 5659-2:2017 — Plastics - Smoke generation - Part 2: Determination of optical density by a single-chamber test [38].

As a sample is subjected to one of the scenarios outlined in Table 2.1, the generated effluent is retained in the surrounding 0.51 m^3 enclosure, restricting the mixing of species and preventing the entrainment of fresh air. Such scenarios are also material dependant, thus the imposed conditions may need to be altered based on the sample being assessed. The recycling of the air within the chamber results in unique burning behaviours, reducing the repeatability of the technique. Throughout this process the optical density of the effluent is recorded via a photocell and lamp system. As the effluent begins to fill the chamber, oxygen is consumed, decreasing the oxygen concentration within the chamber thus, increasing the generation of incomplete combustion products. As such, the species being generated vary throughout the sampling period.

This variation in the concentration of the species being generated resulted in a paradox when determining an appropriate sampling strategy. As the chamber gradually fills with an increased proportion of incomplete combustion products, regular sampling appears preferable. However, the process of taking a sample removes gas from the chamber, disturbing the retained smoke, inducing artificial mixing. Such disturbances cause artificial flows that enable unburnt hydrocarbons to pass back down towards the flame to generate additional combustion products. As a result, sampling frequency is usually decreased to one reading every few minutes in an attempt to reduce these artificial interactions. Such compromises decrease the resolution achievable with the apparatus.

The smoke density chamber also enables a non-invasive optical density measurement, allowing data to be gathered without effluent disruption. Such results allow an overview of how the effluent composition develops rather than being a technique for specific speciation. This approach has been used to monitor the optical density of the effluent produced

during the combustion of reinforced fibres [39]. Figure 2.4 details these results, providing insights into how the smoke develops over time. The Kevlar-based synthetic polymer, polybenzoxazine, generated much denser smoke than any of the other investigated materials. Therefore, synthetic polymers were identified as materials of interest when assessing effluent generating methodologies.

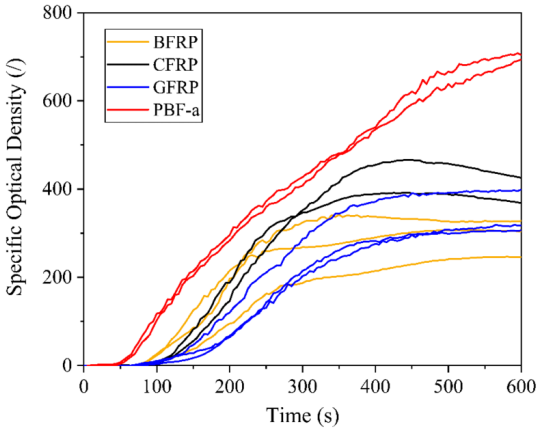

Figure 2.4: The optical densities recorded in a smoke density chamber during the combustion of carbon (CFRP), glass (GFRP), basalt (BFRP) and polybenzoxazine (PBF-a) reinforced fibres. Reproduced from N. Wolter *et al.*, Carbon, Glass and Basalt Fibre Reinforced Polybenzoxazine: The Effects of Fibre Reinforcement on Mechanical, Fire, Smoke and Toxicity Properties [39].

A further complication associated with the smoke density chamber arose from the location of the sampling point. The representative gas sample, removed for analysis, is usually taken from the top of the chamber. During the combustion process, the produced volatiles rise to the top of the enclosure displacing cold, denser air. This warm upper gas layer will have artificially higher levels of volatile species compared to lower portions of the compartment. Sampling from the top of the chamber will therefore result in inflated concentrations of combustion products, relative to the total volume of the chamber. Existing works that used smoke density chambers may use an uncertainty factor of two to correct for this variance, but it is not entirely clear as to why this value is appropriate [39].

Following a standardised procedure (ISO 5659-2:2017), the concentration of detected gases is reported only at the peak optical density reading of the smoke, as this is deemed to be the most important in terms of life threat. During recent testing of both polyvinylchloride (PVC) cladding and PVC veneer, hydrochloric acid (HCl) was only detected after the optical density had peaked in the smoke density chamber [40]. Other species like hydrogen cyanide (HCN) failed to be recorded at all during separate polyurethane foam tests, contrary to analysis with the same samples using the cone calorimeter [41]. Under the current standards, HCl and potentially other species of concern would fail to have been detected in the effluent using the smoke density chamber, suggesting that the current smoke density chamber methodology masks the production of certain volatile species.

The smoke density chamber offers a relatively simple means of generating combustion products, trapping the entirety of the effluent as it is generated. However, its scope is rather limited as the closed chamber restricts the oxygen availability, particularly noteworthy towards the end of an experiment, in theory favouring the generation of

partially oxygenated species. This decreased oxygen availability often causes inflated carbon monoxide (CO) levels, whilst simultaneously underestimating the concentrations of other generated products [42]. The flaws stem from the closed chamber concept, preventing emitted species from being identified the moment they are produced. This oversight enables species to participate in further reactions within the retained system, producing unrepresentative products. Subsequent sections will examine the various flow-through techniques that aim to mitigate these problems.

2.2.3 The Controlled Atmosphere Cone Calorimeter

Given the multiple variables that impact the mass loss rate of a sample, it is imperative to control both the thermal exposure and the oxygen availability when assessing the hazards associated with fire effluent. As a result, novel apparatuses began to be developed to incorporate a controlled airflow passing over the sample.

One example, the Controlled Atmosphere Cone Calorimeter (CACC), involves a sample (100 mm × 100 mm × 25 mm) being placed into a steel sample holder, situated on a load cell. The sample holder ensures that the edges of the material are covered, exposing only the surface of the material to the radiant heat flux imposed by the conical heater. The delivered heat flux can be adjusted up to a maximum of 100 kW m^{-2} and can be used in combination with a sparked ignition source to ignite the material of interest [43]. After the emitted gases have passed through a cold trap, removing water vapour, the levels of various species (CO, CO_2 and O_2) are monitored in real-time using a combination of spectroscopic and paramagnetic techniques. Heat release rates are subsequently calculated from the concentrations of these gases using the oxygen consumption calorimetry technique pioneered by Janssens [44].

The CACC is an adaption of the cone calorimeter that enables control over atmospheric conditions. The most recent adaptation, ISO 5660-5:2020, contains the sample within an enclosed box where the local atmosphere can be controlled through the addition of oxygen and nitrogen [45]. Figure 2.5 shows the modified setup for the CACC, ISO 5660-5:2020 [46].

The ability to control the atmosphere within the cone calorimeter enabled fire effluent to be studied under differing combustion environments. However, the absence of an oxygen sensor at the air inlet alongside the omission of nitrogen and air premixing potentially decreases the uniformity the investigated atmospheres established within the CACC. A number of existing CACC setups have also reported issues with the seals in the atmospheric chambers, with some studies being unable to create a completely inert (0 % O_2) environment [40]. Furthermore, sample preheating as a result of radiation from the chamber walls prior to an experiment beginning remains a common concern with the technique. Water cooling of the chamber walls has begun to be implemented to reduce sample preheating prior to an experiment commencing.

The relative infancy of the technique, becoming standardised in 2020, has resulted in a few studies being published to date. Existing studies vary the location of the sampling point in the chimney and even debate whether the chimney is necessary. The conclusion

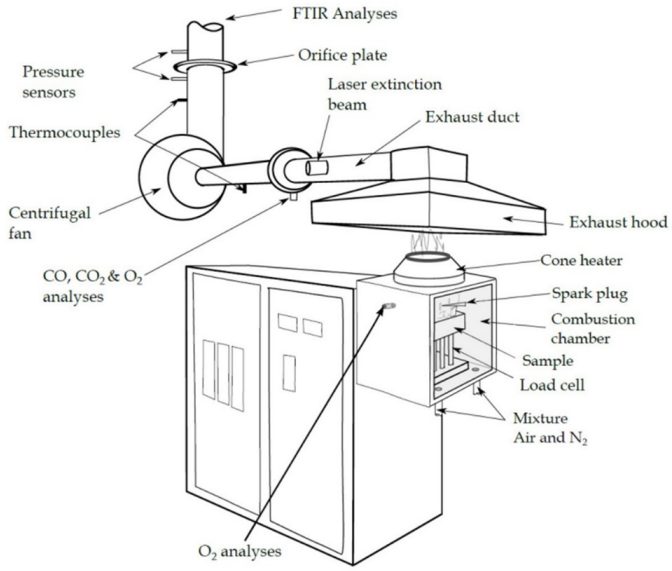

Figure 2.5: The controlled atmosphere cone calorimeter setup (ISO 5660-5:2020). The sample is retained in a closed chamber where the atmosphere can be artificially controlled. Reproduced from ISO 5660-5 Reaction-to-fire tests - Heat release, smoke production and mass loss rate [47].

that the absence of a chimney rendered the CACC unsuitable for the investigation of gas-phase phenomena under vitiated conditions has been reached, with further discussions on the impact of chimney types (metal or quartz) also expected to impact obtained results [48]. Despite obtaining repeatable data, some studies have had to modify the CACC to record oxygen concentrations 50 mm from the sample, an attempt to define and control the combustion environment. It is clear that the CACC requires further iteration before it is truly standardised.

The experimental repeatability that the CACC enables, facilitated the rise of the apparatus to prominence within the fire science field, particularly under oxygenated conditions. However, the control over the combustion environment, in terms of the applied conical heater being in the effluent path, alongside the mixing of the gases to establish the oxidative conditions, could be improved in future iterations of the apparatus.

2.2.4 The Fire Propagation Apparatus

A bench-scale technique that facilitates control over both the thermal exposure and the oxygen availability for a sample is the Fire Propagation Apparatus (FPA). The FPA uses a combination of four infrared lamps alongside a quartz tube chimney to separate the heat source from the sample, limiting the prevalence of any post-combustion oxidation reactions [49]. The FPA requires a sample (of approximately 100 mm $\times$ 100 mm $\times$ 25 mm) to be placed onto a stage mounted on a load cell. For the FPA, the sample stage is centred between the four tungsten filament lamps, delivering a combined heat flux of up

to 65 kW m^{-2} [50]. The height of the pedestal connected to the load cell can be adjusted, enabling the surface of the sample to sit precisely where the supplied heat flux is well defined. Figure 2.6 shows the conventional setup for the FPA [51].

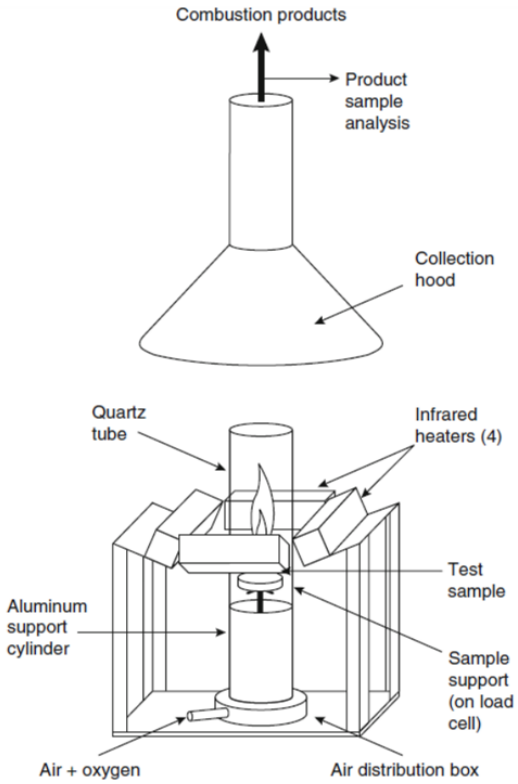

Figure 2.6: The experimental setup for the FPA (ISO 12136:2011). Four tungsten filament lamps supply a heat flux onto a sample situated in the centre of the apparatus. A quartz chimney prevents the lamps being in direct contact with the produced pyrolysis/combustion gases. Reproduced from A. Tewarson *et al.*, Carbon, Glass and Basalt Fibre Reinforced Polybenzoxazine: The Effects of Fibre Reinforcement on Mechanical, Fire, Smoke and Toxicity Properties [51].

The FPA uses a flow-through technique to monitor combustion products. The setup enables a controlled mixture of nitrogen and oxygen to be passed around a sample, creating the desired combustion atmosphere. This airflow carries any produced species into the effluent line for analysis. A standard setup primarily detects CO, CO_2 and O_2, enabling heat release rates to be calculated via oxygen consumption calorimetry, however additional sampling lines can be readily introduced [44].

Combustion products generated via the FPA rise up the quartz chimney, unobstructed by heated elements like the conical heater present in the cone calorimeter. The positioning of the FPA lamps therefore prevents them acting as a heat source for the ignition of generated products. This increase in sample representativeness does however result in a slightly shorter wavelength heat flux, < 2 µm, being delivered to the sample [52]. The

discrepancies in ignition times for materials with a specific wavelength absorbance have been evidenced to have arisen due to this phenomenon [53]. Thus, care must be taken when comparing data gathered from the FPA to that of other bench-scale techniques.

The FPA is designed to enable control over the combustion environment, achieved via an inlet situated beneath the sample stage. Oxygen and nitrogen are premixed at the desired ratio prior to entering the chamber, enabling the overall rate of airflow to be controlled. A forced pyrolysis experiment can be achieved under an inert environment, 100 % nitrogen, whilst maintaining the same overall flow rate. The light produced by the lamps illuminates the effluent being generated by a sample throughout an experiment, enabling the onset of pyrolysis, the colour and the intensity of the effluent and the surface response of the sample to be viewed and filmed with ease. As the FPA allows the oxidative environment and the heat flux to be controlled, it has promise as a suitable means of assessing fire effluent.

There are drawbacks to the FPA, most notably with the lack of control over the mass of a sample. Despite having a load cell, the mass loss rate of a sample is left uncontrolled, altering based upon the oxidative conditions, generating an effluent stream of changing chemical composition. Given the transient behaviour, measurements of effluent in the duct are unlikely to reflect the conditions that the sample is exposed to. Further issues arise when low flow rates are used. Whilst the FPA can control the heat flux and flow variables independently, there are some limitations. These primarily arise due to the poorly defined flow fields around the sample, including the effects of the bluff body, buoyancy and turbulence. Low flow rates induce pressure profiles inside the quartz tube and also highlight potential leaks between the seal connecting the quartz tube and the aluminium support cylinder.

When combustion is necessary, an ethene diffusion flame can be positioned above the sample to encourage ignition of the pyrolysis gases. This ethene pilot flame, if used, will generate combustion products that must be accounted for in the subsequent gas analysis. Alternative ignition sources, such as a spark igniter, are less disruptive to the overall effluent composition, thus, could be worth including as alternative ignition options if the FPA were to be modified.

2.2.5 The Steady State Tube Furnace

The steady state tube furnace (SSTF) can be used to generate fire effluent via sample manipulation. During the experimental process, a sample is slowly passed into an open furnace, gradually being subjected to an escalating heat flux throughout the experiment. The control over the airflow being supplied to the furnace allows different equivalence ratios (as mentioned in Chapter 1) to be mimicked, enabling under- and over-ventilated environments to be assessed. It is this ease of manipulation combined with a rapid screening process that has increased the prevalence of the technique for material assessment.

A standard experimental setup for the SSTF (ISO/TS 19700:2016) is summarised in Figure 2.7 [54]. A 1700 mm quartz tube connects a 30 L effluent chamber to a primary air supply via a combustion furnace. The sample, typically weighing $\sim$20 g, is placed into an 800

mm silicon specimen boat which is passed into the furnace at a constant rate of ∼40 mm min^{-1} ± 10 %. This rate is determined based upon the uniformity and the density of the sample, with alternative rates being utilised for uniform rods of material [55].

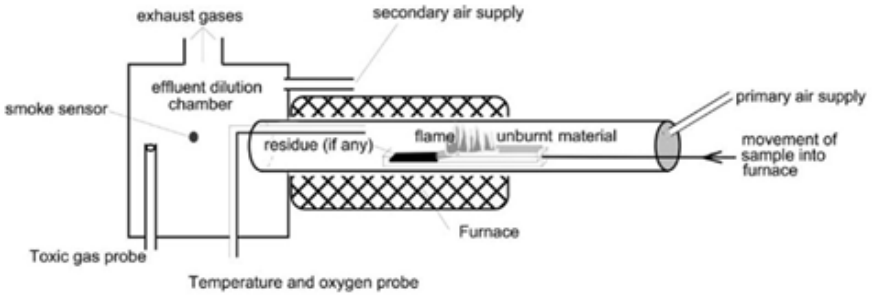

Figure 2.7: The steady state tube furnace (ISO/TS 19700:2016). A sample is horizontally passed into the furnace under a continuous (primary) airflow. Effluent is analysed after entering the mixing chamber where a secondary airflow dilutes the produced species prior to analysis. Reproduced from A.A. Stec *et al.*, A Comparison of Toxic Product Yields Obtained From Five Laboratories Using the Steady State Tube Furnace (ISO TS 19700) [55].

A secondary air supply is flowed directly into the effluent chamber, ensuring that the produced gases are mixed. This gas mixing attempts to prevent any air temperature stratification profiles present vertically within the tube. The total airflow, across both air supplies, is maintained at 50 L min^{-1}, where the primary air supply will usually be below 25 L min^{-1} in an attempt to minimise the cooling effect on the air temperature inside the furnace [56].

As the sample is passed further into the furnace, an increasing heat flux is delivered, eventually triggering spontaneous ignition. After stabilising for a few minutes, the flame front becomes established in a set position, marking the commencement of an initial run. Rather than the more commonly used mass loss rate (MLR), CO_2 and O_2 measurements help identify the steady state combustion period. From this point it is assumed that the mass loss will be constant during the central part of the run, with the mass loss determined based upon a combination of the residual sample mass and the readings obtained from the secondary oxidiser. Typically, the produced effluent is only assessed during this period.

Control over the movement of the sample into the furnace, combined with the manipulation of both the furnace temperature and the primary airflow rate enables the apparatus to simulate differing combustion conditions and a variety of different equivalence ratios. These values are selected using the rudimentary definition that under- and over-ventilation combustion requires 2.6 L min^{-1} and 26 L min^{-1} of air per gram of sample respectively [57]. Once generated, the gaseous species flow through the remainder of the heated furnace and into the effluent dilution chamber. Differing equivalence ratios are achieved via manipulation of the primary airflow rate. Well-ventilated conditions typically involve a primary airflow rate of 10 L min^{-1}, while under-ventilated conditions drop the primary airflow rate to around 5 L min^{-1} [56].

Under elevated temperatures, the SSTF is subject to the development of furnace hotspots. The non-uniformity of the furnace can be indirectly detected, in part, by increases in the oxidised products being produced as the species pass through the flame, i.e., slight spikes in CO_2. However, during the assessment of pyrolysis, the presence of these hotspots may cause pyrolysis rates to fluctuate, unnoted in the absence of a flame. These risks reinforce the importance of having a real-time mass loss reading to link the mass loss rate of the sample to the generated species via yield calculations.

The SSTF does not enable a real-time mass loss reading, and as such, monitored emissions cannot be directly linked to the burning rate in real time. Instead, preliminary trials must be conducted, feeding samples into the furnace at differing rates to determine the actual testing conditions. These trials test samples under differing furnace temperatures, air flows and specimen boat moving rates, all requiring visual observation of the sample to determine key timestamps e.g., the onset of pyrolysis, ignition, flame quenching and extinction. ISO 19700:2016 states that this can be achieved via monitoring the CO_2 emissions, typically waiting for a plateau, or via the use of a convex mirror to attempt to view the sample inside the furnace.

A lack of optical access into the furnace itself obstructs the sample from view, preventing pyrolysis and/or burning processes being directly observed. A spike in CO_2 may be a means of determining when ignition occurs; however, other effluent generating techniques can correlate this spike in CO_2 with the visual observation of the flame, allowing for any delay times between sampling methods to be accounted for.

Solely taking the mass of a sample at the start and end of an experiment prevents changes in the burning rate being associated with changes in effluent composition over the course of a trial. The mass of the sample cannot be measured at the point of ignition (or the start of the steady period). As such, mass will be lost prior to the steady state period commencing, mass which cannot be quantified or accounted for during subsequent yield calculations.

Prior to analysis, effluent enters the dilution chamber where it is mixed before sampling. Given the differing secondary airflows required to make the overall airflow 50 L min^{-1}, which may range from 1 – 25 L min^{-1}, work has occurred to ensure that the effluent is well-mixed. Percentage yields of HCl taken from the bottom of the effluent mixing chamber matched the yields of those taken at the top of the chamber across two different temperatures when the primary airflow was as low as 2 L min^{-1} [58]. The need for appropriate mixing is understood, however it appears to restrict the range of airflows that can be screened by the steady state tube furnace through the implementation of an upper limit (50 L min^{-1}).

The SSTF recognises the importance of a controlled burning rate and has successfully been used to identify HCN produced during the combustion of polyisocyanurate (PIR) foam, with yields exceeding 15 mg g^{-1} under under-ventilated conditions [16]. These yields have been evidenced to align with other studies, reinforcing the importance of maintaining control during combustion to enable sampling of a constant effluent stream [15]. Given the focus on the steady state burning rate, the lack of a mass measurement seems somewhat of an oversight, perhaps warranting inclusion in a future iteration of the apparatus.

2.2.6 The Single Burning Item Method

Moving beyond the bench-scale methodologies, real-scale assessment techniques are increasingly being applied to construction materials. Techniques focused on how fires develop have been designed to improve our understanding of how fire growth occurs at a larger-scale. The single burning item (SBI) method, BS EN 13823:2020, aims to simulate an item burning in the corner of a $3 \times 3 \times 2.4$ m^3 room [59]. During a test, two panels of a material, 0.5×1.5 m and 1×1.5 m, are positioned alongside a triangular propane burner to form a corner. Figure 2.8 details the full experimental setup [60].

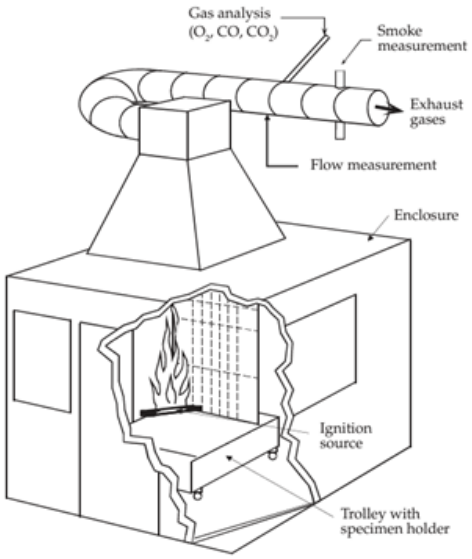

Figure 2.8: The experimental setup for the single burning item test. Reproduced from R. Mierlo *et al.*, The Single Burning Item (SBI) Test Method - A Decade of Development and Plans for the Near Future [60].

A 30 kW burner, imitating a waste paper bin fire, is switched on throughout the experiment, providing the heat and ignition source for the material under investigation. Generated effluent is gathered for analysis over the entire twenty-minute run while a heat release rate (HRR) is calculated based upon the CO, CO_2 and O_2 gas analysis. The corner configuration restricts the airflow towards the burner, prompting an increase in the flame length. The SBI test therefore performs as a large-scale flame spread test rather than acting as a methodology designed to generate effluent in a controllable manner.

Despite the larger scale, the SBI test has made a few assumptions that decrease the realism of the methodology. During the test, gas analysis occurs from the exhaust duct. The precise location of this gas sampling, including the means by which the effluent is filtered and dried remains undefined. Sampling earlier on in the extraction duct may prevent unrepresentative secondary oxidation reactions, however the effluent may be subject to inadequate mixing. Poor mixing may prevent species being detected depending on the sampling location and the extraction rate. Sampling at this scale is yet to be unanimously optimised.

Furthermore, the mass flow rate, required for yield calculations, remains set at 1.5 m^3 regardless of the experimental setup [60]. Such flow rates are suitable to assess larger fires; however, the noise introduced for smaller fires (around 10 kW) or materials that do not readily combust result in O_2 readings getting lost in the background noise, impacting HRR calculations. Such discrepancies, or "exotic products", introduce a degree of uncertainty to the SBI and should be noted when interpreting emissions data [61].

2.2.7 ISO Room Testing

Scaling beyond the corner of a room, full-scale room testing has been developed with a standardised room configuration being established in ISO 9705-1:2016 [62]. For the test, a 3.6 × 2.4 × 2.4 m room is lined with inert boards, with a 0.8 × 2.0 m opening created on one of the shorter walls. Figure 2.9 details this experimental setup [62].

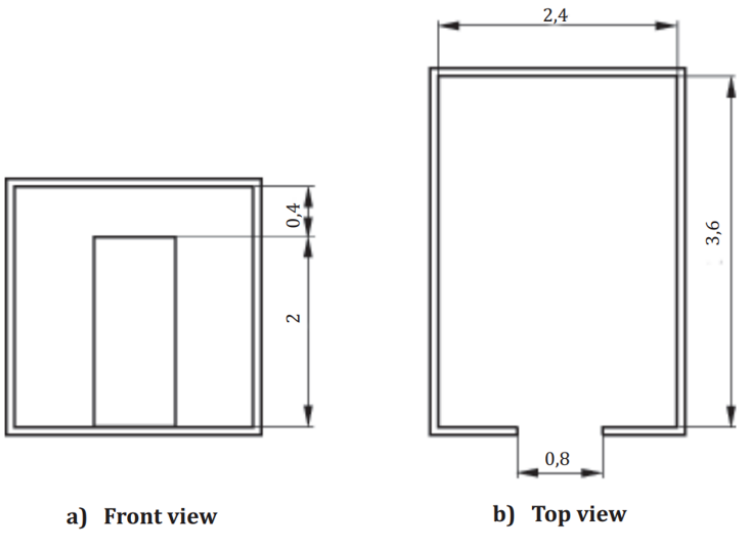

Figure 2.9: The dimensions, in metres, of the ISO 9705 room for fire testing. Reproduced from ISO 9705-1 Reaction to fire tests - Room corner test for wall and ceiling lining products [62].

The material being tested is mounted onto each of the uninterrupted walls in Figure 2.9, and optionally the ceiling. A 0.17 × 0.17 m burner is used to ignite the rear wall of the room and the fire is allowed to develop. Effluent exits the ISO room via the front opening, passing into a hood duct for analysis. HRRs are calculated based on the CO, CO_2 and O_2 concentrations detected in the effluent over the course of the run [44]. Mass loss readings are possible but require the whole ISO room to be raised up onto a load cell.

The standard ISO room dimensions have been adopted throughout literature to enable a universal model room for experimentation. Designs where fuel packages are placed inside the room on load cells and ignited directly, rather than using a burner, to assess wall linings have enabled large-scale effluent to be sampled in a repeatable manner [63]. The combination of a crib ignition source and an ISO room have enabled PIR wall linings to be investigated with the results compared to tests conducted in a half scale ISO room

[15]. Despite being slightly lower, the CO yields aligned with the half-scale ISO 9705 room-corridor rig, 0.0768 to 0.1050 g g^{-1}, with the difference likely to have arisen from the differing ventilation between the tests [15].

If correctly instrumented, ISO room testing can provide a multitude of data helping to characterise the combustion environment being investigated. As with the SBI, determining how and what to sample remains an issue. The room may be placed under an extraction duct and sampling can occur from this exhaust line, akin to the SBI. However, the same issues persist regarding secondary oxidation and adequate mixing. Gas sampling can occur inside the ISO room, providing insights into the effluent composition. The removal of effluent will impact the smoke layer dynamics in the room and potentially introduce artificial mixing. Effluent may also be sampled from the opening to the ISO room, but once again, the sampling probe must be carefully placed to avoid introducing secondary oxidation as the effluent mixes with external air.

Information on temperature, flows, mass and chemical species can be combined alongside images from inside the compartment to define the precise experimental conditions. Despite being able to monitor these conditions, control over several variables including the MLR or the flow into the compartment remains coupled to multiple factors. Thus, it is tough to predict let alone implement specific experimental conditions in advance of a trial.

2.2.8 Critical Summary of Generative Methods

A comparative summary of the advantages and disadvantages of each discussed methodology is summarised in Table 2.2, enabling the techniques to be compared in full. Each technique has merits and flaws when generating fire effluent for speciation.

As Table 2.2 details, the reviewed methods of generating effluent each offer a unique advantage, cementing their places as effluent generating methodologies. The correct means of effluent generation will vary depending on the individual experimental setup and the aims of the investigation. For the purposes of assessing the impact of combustion conditions on the composition of fire effluent, the selected methodology requires the ability to control both the flow of the oxidizer and the fuel. As such, the FPA was selected due to the control afforded over the composition of air being flowed across a sample. It is likely that the modification of the FPA will enable circumnavigation of some of the limitations, in particular the inability to obtain a constant MLR. Moving forward, a modified means of controlling the FPA was deemed an appropriate technique to produce fire effluent for speciation.

Table 2.2: A comparison of the key advantages and disadvantages offered by a range of fire effluent generating methodologies.

Apparatus	Advantages	Disadvantages
Thermogravimetric Analysis	• Quick screening tool • Controllable external environment	• Sample obstructed from view • Unrepresentative sample size
Smoke Density Chamber	• All effluent retained for analysis • Non-invasive photocell records optical density	• Sampling induces artificial mixing • Atmospheric conditions change uncontrollably throughout an experiment • CO yields overestimated • Some species only detected after the optical density had peaked
Cone Calorimeter	• Highly repeatable technique • Conical heater can be calibrated to deliver a specific heat flux • Sample visible throughout • Mass loss rate calculated in real time	• Steady state combustion not possible under existing standards • Conical heater in path of effluent • CACC nitrogen/ oxygen gases not premixed
Fire Propagation Apparatus	• Sample visible throughout • Lamps can react instantaneously, enabling the heat flux to be adjusted in real time • Mass loss rate calculated in real time	• Quartz tube enables soot deposits • Wavelength supplied by lamps is different to traditional heat sources • Steady state combustion not possible under existing standards
Steady State Tube Furnace	• Several equivalence ratios can be screened as a sample is always forced to combust, even under low oxidative conditions • An adjustable conveyor allows the controlled decomposition of a sample at a 'steady state'	• No mass loss reading to confirm burning behaviour • Sample obscured from view • Significant effluent dilution occurs before sampling • Preliminary runs with additional samples must occur to identify experimental parameters
Single Burning Item	• Repeatable test methodology • Large-scale combustion of a single material under investigation	• No mass loss reading to confirm burning behaviour • Burner size not appropriate for all test scenarios • Test duration makes it more of a flame spread test that an effluent generating technique
ISO Room Testing	• Mass loss rate recorded • Fire allowed to develop as it would in a room • Lots of different variables can be measured enabling combustion environment to be precisely defined (post-experiment)	• Mass data has low accuracy due to high load • Precise control over several external variables (volumetric flow, MLR, smoke temperature etc.) not possible

2.3 Sampling Strategies

Once generated, effluent must be sampled prior to chemical analysis. To facilitate the calculation of product yields, sample masses must also be obtained when sampling fire effluent. The relatively low concentrations of volatiles generated by a sample are rapidly entrained in air, producing large volumes of gas. Sampling can occur either in-situ, with analysis happening whilst an experiment is running, or ex-situ, where analytes are removed from the sampling environment. For these gases to be analysed remotely, a representative sample must be obtained and remain unchanged until analysis has been conducted. This problem is particularly prominent when sampling small gaseous species being generated by fires.

When a sampling strategy has been settled upon, the frequency of the sampling needs to be selected. Sampling intervals must occur regularly enough to monitor changes in effluent composition, whilst still enabling analytical functionality. This section discusses some of the strategies deployed, separating them based on the physical phase of the obtained sample.

2.3.1 Gaseous Sampling

The most common sampling method involves directly assessing fire effluent in its gaseous state. Generated volatiles are largely in the gas phase thus, it is logical to sample them with minimal interference. Two sampling strategies are generally deployed: inline analysis and gas trapping, usually involving gas bags. The vast majority of studies tend to use inline gas analysis, enabling near real-time data to be collected.

During inline gas analysis effluent often passes along ducts before reaching extraction vents. Orifice plates within the ducts enable the calculation of flow rates, providing an opportunity to sample gases under known flows. Inline gas sampling involves drawing a sample of the effluent from these ducts and passing the gas sample through to analytical apparatus. If combined with a compatible analytical technique, inline sampling enables real-time data collection and visualisation. The use of filters and unheated sampling lines may result in certain species of interest being omitted from the eventual effluent stream that is analysed, however the main gases of interest for the calculation of heat release rates, CO_2, CO and O_2, will be present. As such, inline infrared (IR) and paramagnetic analysis is often used to describe the composition of effluent.

Sampling from the exhaust duct means that many species of interest will cool down, condensing on inner surfaces. Furthermore, soot filters, used to protect instrumentation, remove particulates and provide additional surfaces for condensation to occur. These issues prompted alternative means to sample gases from fire effluent to be investigated.

A proposed alternative sampling approach involves the use of gas bags to retain gaseous effluent for analysis at a later date. Once a bag has been filled, it is sealed and retained for analysis. This storage period is not indefinite. Bags are prone to leaks, at different

rates, especially during filling and prior to analytical sampling. Furthermore, effluent will slowly diffuse from the bags regardless of the lining, reducing the representativeness of the sample. Table 2.3 summarises some of the materials used to create these bags [64].

Table 2.3: The composition of gaseous sample bag linings [64].

Bag Type	Inner Lining
Aluminised	Inner polyethene layer with five outer aluminium layers
Halar	Trifluoroethene
Saran	Poly(1-fluoroethylene)
Tedlar	Fluorinated ethylene propylene
Teflon	Fluorinated ethylene propylene

The chemical composition of the bag lining will result in different interactions with different analytes. For example, the lining of Tedlar bags has been shown to react with many sulphur-based compounds present in cigarette smoke, skewing analytical results [65]. Despite the context, these results highlight the stability issues surrounding gas bag sampling, reinforcing the importance of rapid analysis upon sample collection.

In theory, aluminised bags should retain analytes for a longer period than their polymer counterparts. The packed metal structure should limit diffusion of the volatiles from within the bag. However, as Figure 2.10 shows, polymer bags tended to retain a greater proportion of analyte over an eight hour period post sampling [64].

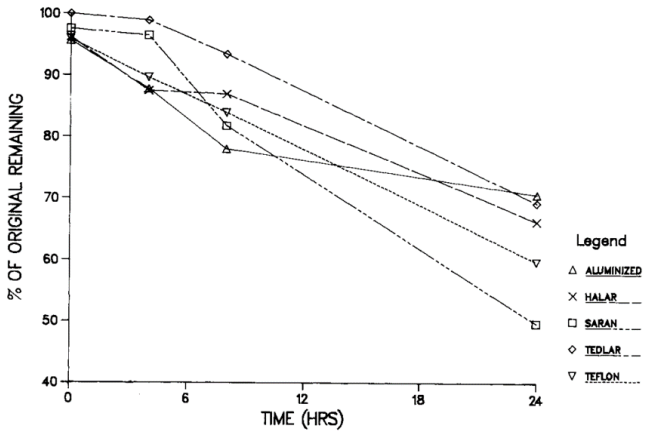

Figure 2.10: A comparison between the sampling bags described in Table 2.3 and their ability to retain 100 ppm of acetone. Reproduced from J.C. Posner *et al.*, Sampling with Gas Bags I: Losses of Analyte with Time [64].

The actual retention times obtained for analytes will vary based upon the chemical species being trapped and the concentration gradient across the bag. Figure 2.10 can only act as a rough guide to enable the retaining power of the bags to be compared. The leaks from the seals on the bags must also be considered when retaining gaseous samples.

The use of alternative trapping techniques, for example glass gas sampling bulbs or

canister sampling, has improved analyte retention. However, the same issues remain, the composition of the sampled gas is likely to change, particularly if stored for prolonged time frames prior to analysis.

2.3.2 Liquid (Condensate) Sampling

Different species within the effluent will change phase at differing temperatures thus, the selected cooling temperature for liquid sampling will depend on the species that a study is attempting to isolate. Liquids are intrinsically easier to handle than gases, they occupy much smaller volumes and tend to be more resistant to decay due to a combination of the solvation and the lower temperatures involved. The production and subsequent analysis of liquid samples obtained from fire effluent is therefore a plausible concept, warranting discussion.

Generated fire effluent can be passed through an ice bath to condense gaseous species [66]. The 273 K offered by ice alone may be insufficient to condense products of interest thus, cryogenic mixtures are used. Figure 2.11 shows an acetone/ dry ice bath, reaching 195 K, being used as part of an experimental procedure.

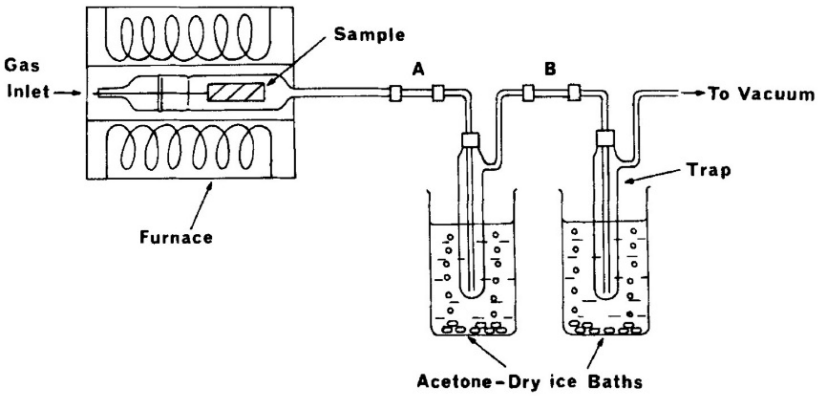

Figure 2.11: An example of an experimental setup that uses two acetone/ dry ice baths to condense species from the effluent. Reproduced from J.H. Hodgkin *et al.*, Combustion Products from Burning Polyethylene [66].

Alternative ice baths that can reach lower temperatures, like liquid nitrogen baths, risk condensing oxygen, forming liquid oxygen in an explosive environment. It is usually unsafe to conduct such extractions in settings with open flames, thus ice bath sampling strategies tend not to condense species with boiling points below 200 K. Therefore, ice bath sampling strategies will always fail to trap a proportion of the most volatile species until these risks can be mitigated.

Alternatively, effluent gases can be passed through impingers, also known as gas-solution absorbers, where the liquid solutions can be varied depending on the experimental objectives. Sample gases are bubbled through various solutions in which gaseous diffusion occurs, generating a sample in a liquid matrix. Figure 2.12 shows an experimental setup with an impinger [67].

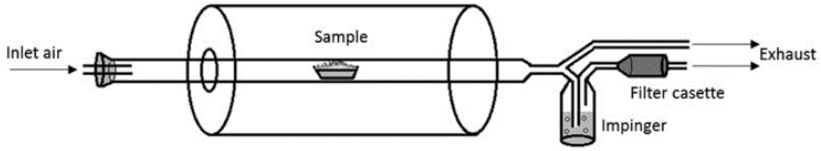

Figure 2.12: An experimental setup featuring an impinger used to investigate the isocyanate composition of smoke. Effluent was passed through an impinger containing dibutyl amine in methylbenzene, the impinger itself was placed in an ice bath. Reproduced from L. Bengtström *et al.*, Stability of Isocyanates Sampled in Fire Smokes [67].

Provided that an appropriate specific chemical solution can be found, impinger solutions enable specific target compounds to be detected and traced. The selected solution must interact preferentially with the species of interest to produce a stable product that can be quantified at a later date. If an appropriate solution cannot be found, multiple solvents can be used in series. The use of three different solvents (tetrachloromethane, ethanol/ bromine and sodium hydroxide) in consecutive impingers has been used to investigate aromatic esters present in fire effluent [68]. However, as the same ester was detected in two consecutive solvents, it is plausible to conclude that some species were passing between all three impingers without being retained. For quantification strategies to be successful, a stable internal standard should be added to the impinger solution prior to the experiment commencing. An appropriate impinger setup can therefore enable quantification of specific gases with a quick and simple experimental setup.

Despite the success of impingers for the investigation of isocyanates, they do not close the combustion mass balance. An impinger solution will be focused on monitoring a particular group of species, potentially missing other products of concern. Furthermore, the concentrations obtained with impingers tend to be lower than other sampling methods. It has been shown that gaseous sampling strategies are more convenient and effective for tracking species than the corresponding impinger setup [69]. It is believed the size and rate of bubbles passing through the impinger solution impacts the rate of gaseous diffusion from the bubbles, impacting the overall species yield.

2.3.3 Solid Sampling

Solid samples offer the greatest flexibility in terms of sample stability, transportation and storage. Solid chars and other fuel residues may remain once a fire has been extinguished. Such solids are worth sampling and analysing, however, gaseous effluent is also possible to be sampled using solid-phase sampling strategies, usually via adsorption/ desorption techniques.

To sample effluent, solid-phase filters, plugs or Tenax tubes may be placed within sampling lines, enabling gaseous species to adsorb to the exposed surfaces. Trapped species can be removed via solvent washing or gentle heating, generating liquids or gases for analysis. This strategy has proven to be effective with semi-volatile analytes generated by the cone

calorimeter being retained on glass wool filters and polyurethane foam (PUF) plugs [22]. However, the majority of volatile products, unless they have a particular affinity for the chosen surface, will simply bypass the trap.

Solid-phase microextraction (SPME) is an alternative sampling strategy that attempts to minimise these losses by conducting the extraction in a closed environment. The technique works on the premise of adsorption and subsequent sample desorption at a later date. As the name suggests, a solid-phase fibre is used to extract, and retain, analytes of interest. The adsorbent fibre is typically attached to a retractable rod positioned towards the end of a syringe.

The extraction process involves a sample being placed within a sealed vial. Volatile species emitted from the sample are allowed to equilibrate in the headspace prior to the syringe entering the vial. Once inserted, the syringe cover is retracted exposing the fibre to the headspace. Volatile components preferentially adsorb to the exposed fibre, being retained for analysis. After a predetermined timeframe has elapsed, the fibre is covered and removed from the vial, being directly transferred to the GC-MS machine (or another appropriate analytical methodology). The desorption process occurs within the GC chamber, re-volatilising the adsorbed species, before transferring them to the column for separation prior to analysis. Figure 2.13 summarises the SPME extraction process [70].

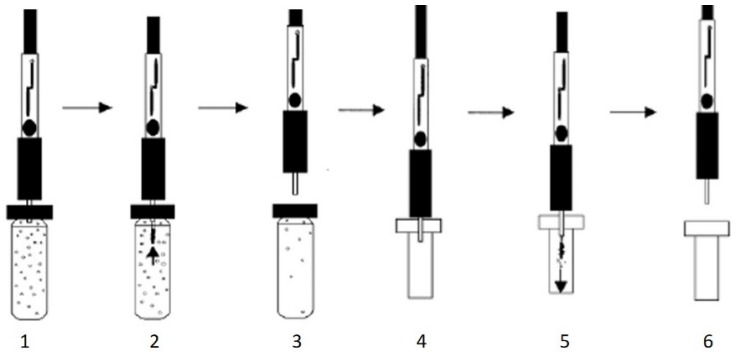

Figure 2.13: The six stages of SPME. 1) The septum on the sample vial is pierced. 2) The SPME fibre is exposed to the volatiles within the vial. 3) The fibre is retracted and the needle withdrawn. 4) The needle is inserted into the GC inlet. 5) The SPME fibre is exposed and desorption occurs. 6) The needle is withdrawn. Reproduced from V. Agotici *et al.*, Solid phase micro extraction and gas chromatography analysis of benzene, toluene, ethyl-benzene and xylene from water [70].

When applying SPME to sample pyrolytic products, the sealed vial must be heated to, and maintained at, a temperature that promotes pyrolysis. Any volatile species generated during extraction will be emitted into a sealed environment, as such the rate of pyrolysis will gradually slow as the headspace becomes saturated with volatile products. The sealed environment retains the heat that would naturally be dissipated when volatile species are evolved, artificially warming the headspace. The greater concentration of species present, alongside the elevated temperatures, may lead to side reactions that would not naturally occur. As such, any species detected in this manner should be verified utilising additional analytical methods.

Quantification via SPME may only be possible if the selected internal standard has a similar affinity for the selected fibre as the target analyte. If the standard has a greater affinity for the fibre than the analyte, reported concentrations will be inflated. As long as the quantification process utilises an appropriate standard alongside a representative temperature, SPME offers a unique insight into pyrolysis processes. The technique has the potential to identify and quantify species on the parts per billion level. However, any species detected should also be confirmed via other analytical procedures coupled to standard methods of effluent generation, verifying that the detected species will actually be generated.

2.3.4 Critical Summary of Sampling Strategies

Each of the sampling approaches covered in this section have their merits and uses depending on the overall sampling setup. A combination of both the manner in which effluent is being generated and the analytical technique being deployed will dictate the appropriate sampling strategy to use. Table 2.4 summarises the advantages and disadvantages of each approach.

Due to the open and turbulent nature of effluent streams, the advantages of solid-phase sampling afforded by SPME are hard to implement when sampling fire effluent. The entrainment of pyrolysis products in air prevents the localised concentration of species building to levels favourable for SPME. As such, an equilibrium between the species adsorbed to the solid in relation to the gas phase is hard to obtain thus, SPME will always be a standalone technique, useful as a predictive tool.

Cryogenic traps enable a larger range of species to be retained when compared to solid-phase traps. These techniques enable low levels of gaseous species to be retained and therefore concentrated above detection thresholds. As long as the limitations surround boiling points are noted, these sampling strategies should be able to help identify additional products of combustion and therefore help to consolidate the combustion mass balance.

By far the easiest sampling strategy, inline gaseous sampling should always be conducted wherever possible. This technique does not tarnish the effluent, enabling it to pass on to a solid or liquid phase trap. If paired with an appropriate analytical technique, inline gaseous sampling can enable real-time data acquisition, which allows combustion phases to be determined. Ultimately, the appropriate sampling strategy will hinge on the selected effluent generating methodology and desired analytical technique. As such, condensing effluent deployed in tandem alongside inline gaseous sampling was identified as the best way to get the most complete picture of fire effluent.

Table 2.4: A comparison of the key advantages and disadvantages offered by a range of fire effluent sampling strategies.

Technique	Advantages	Disadvantages
Inline Gaseous Sampling	• Effluent can be sampled in real-time • No phase changes required, effluent is sampled directly • Effluent not disturbed	• Effluent not retained • Species at low concentrations diluted with air entrainment
Gas Bags	• Entirety of the effluent may be retained • Effluent can be transported for analysis at a later date	• Retained species may react with the bag lining • Effluent escapes over time making concentrations unrepresentative
Ice baths/ Condensers	• A liquid is obtained, which is much easier for transport and further analysis • Different ice baths can be used to target a specific species based the boiling point of the target compound	• The species collected depends on the temperature of the cold trap in relation to their boiling point • Solvent washes likely to be required to remove condensed water
Impinger	• Can be designed to target a specific analyte of interest • Generates a liquid that can analysed at a later date	• Requires a specific chemical solution that preferentially interacts with the analyte of interest • The size and rate of bubble generation impacts diffusion and thus the obtained concentration of analyte
Foam Plugs/ Solid-phase Microextraction	• Solid cartridges/ fibres are easy to transport for analysis • Samples can be obtained before and after an inline sampling technique e.g., to demonstrate certain species have been retained by a cold trap	• Best results obtained when an analyte reaches equilibrium with an exposed fibre which requires a steady and unchanging stream of effluent • Quantification only possible if the selected internal standard has a similar affinity for the selected fibre/ plug as the target analyte

2.4 Analytical Methods of Fire Analysis

Being able to quantify the oxygen concentration in fire effluent is necessary for the calculation of heat release rates via oxygen consumption calorimetry [44]. Molecular oxygen has two unpaired electrons in Π* antibonding orbitals, rendering it paramagnetically active. Thus, paramagnetic cells can distinguish and quantify oxygen even when it is part of a complex matrix. Unfortunately, for the remaining species retained in the effluent, the appropriate analytical techniques required are not usually quite so apparent. Often, a combination of the techniques discussed in this section will be necessary to completely characterise fire effluent.

Once a method of effluent generation and a sampling technique have been finalised, an appropriate analytical technique must be selected to glean meaningful information. The selected analytical techniques must be able to both identify and quantify the species being generated, relating these back to the way the material is burning via the MLR.

2.4.1 Fourier Transformed - Infrared Spectroscopy

One of the most commonly used techniques for the study of fire effluent is Fourier transformed - infrared spectroscopy (FT-IR). This technique involves effluent passing into a gas cell before being subjected to an IR beam. The low energy beam is partially absorbed by molecules with a net dipole moment, triggering vibrational, rotational and translational transitions. Specific functional groups are shown to absorb at specific wavenumbers helping to identify specific species within the effluent. Table 2.5 shows some typical IR absorption frequencies used for speciation [71].

Table 2.5: Table of typical IR absorption frequencies for standard functional groups [71].

Functional Group	Absorption /cm^{-1}	Notes
Alkyl (C-H)	2950 - 2850	Present in most spectra
Alkene (C-H)	3100 - 3010	3000 Indicates unsaturation
Alkene (C=C)	1680 - 1620	
Alkyne (C-H)	3300	
Alkyne (C≡C)	2260 - 2100	
Aromatic (C=C)	1700 - 1500	
Hydroxyl (O-H)	3550 - 3200	Broad peak
Amine (N-H)	3500 - 3300	
Nitrile (C≡N)	2260 - 2220	
Carbonyl (C=O)	1740 - 1690	Prominent peak

If a pure sample is assessed, comprising a single chemical species, FT-IR will provide a unique chemical fingerprint that can be matched against a spectral database to positively identify the unknown species. Unfortunately, this is not often possible when sampling fire effluent as the produced spectra often display overlapping peaks arising from multiple species [66]. Instead, existing studies look for characteristic peaks arising from specific species including CO, CO_2, nitrogen monoxide (NO), HCN, HCl and sulphur dioxide

(SO_2) [72]. Each of these gases has a characteristic IR absorption region, making them readily detectable, the identification of more complex species requires careful spectra interpretation. Figure 2.14 shows the IR spectra for species commonly tracked in fire effluent.

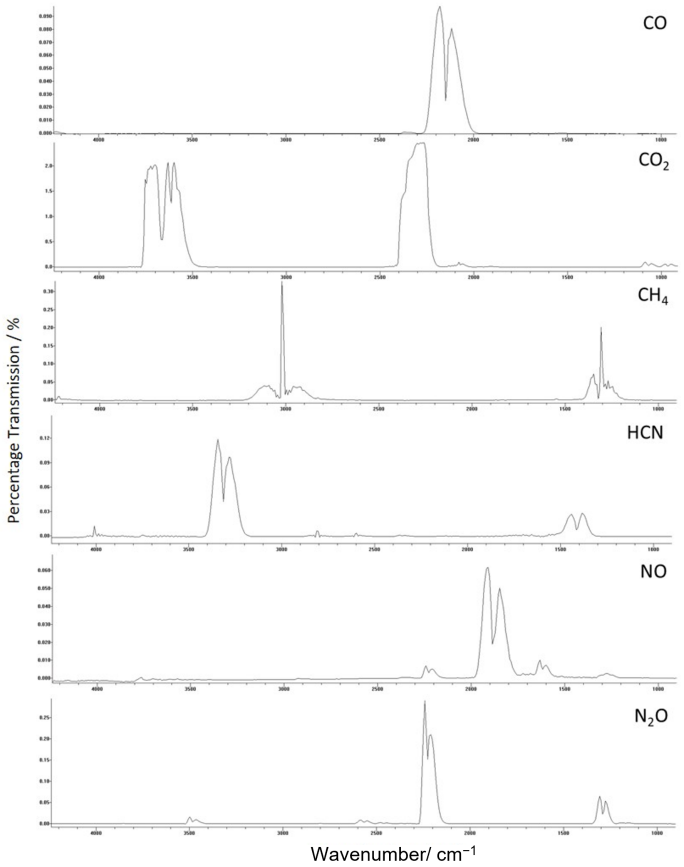

Figure 2.14: The reference FT-IR spectra for six common species tracked in fire effluent (from top to bottom: carbon monoxide, carbon dioxide, methane, hydrogen cyanide, nitrogen monoxide and nitrous oxide). These species typically have sharp IR bands in distinct regions.

Each of the bands shown in Figure 2.14 occupies a unique wavenumber or set of wavenumbers, enabling these species to be individually identified from a mixture of the six gases. The sharp IR absorbances for CO and CO_2 enable FT-IR to track these common combustion products in near real time with a greater certainty. Interpretation of the spectra for species with multiple bands, like HCN, is often more complex as regions overlap with broad bands arising from common species like water, making identification difficult. However, as the functional groups responsible for these absorbances differ between these six species, identification is still possible. It is much more complex distinguishing between two species in the same family, e.g., ethanol and n-propanol, as the majority of the bands will overlap.

When sampling with FT-IR, a pump transfers effluent down a heated sampling line into a gas cell for analysis. The size of the gas cell determines how quickly it can fill and thus the sampling frequency. Smaller cells have a reduced path length but enable a greater sampling frequency. Sampling every three seconds can often provide clearer spectra than six second

sampling intervals, highlighting the importance of optimising the sampling strategy [35]. However, overlapping bands from multiple species with the same functional groups will always remain, rendering FT-IR slightly meaningless for implicit chemical speciation.

As discussed, FT-IR has a key place as an analytical tool when investigating the species emitted from fires. The main advantage being its non-invasive nature, which enables real-time data collection without impacting the experimental conditions [66]. The technique is versatile, enabling the effects of changing combustion conditions to be seen directly on product formation, allowing combustion stages to be deduced whilst identifying the key functional groups present in the effluent [35].

However, FT-IR has limited use a speciation tool when faced with multiple species in a complex matrix. From a chemical perspective, individual molecules cannot always be identified. When deciding on the appropriate optical cell for analysis, a compromise between cell length and sampling time must be made [42].A longer cell length increases the detection threshold for many species, increasing confidence in the analytical readings. However, a longer cell length reduces the frequency of readings due to the increased time required to fill the cell. Therefore, concentration fluctuations for certain species may be missed.

Furthermore, trace levels of interesting species may be overpowered by intense bands from common species like H_2O and CO_2, potentially impacting the quantification of CO_2 in fire effluent. As many species share functional groups, a study cannot be certain that an intense carbonyl band is solely caused by a single species, requiring additional analytical tools to be utilised alongside FT-IR to develop a precise quantification technique.

2.4.2 Nuclear Magnetic Resonance

Nuclear magnetic resonance (NMR) is one of the most powerful chemical speciation techniques available. During analysis a sample is subjected to an intense magnetic field. Spin-active nuclei within the sample can align with (low energy state) or against (high energy state) the external magnetic field. A pulse of radio frequency radiation causes spin active nuclei to excite, transitioning to the higher energy state. As the nuclei relax back to the lower, favourable, energy state they emit radio frequency radiation which is then used to produce an NMR spectrum [73]. Figure 2.15 illustrates the key principles underpinning NMR.

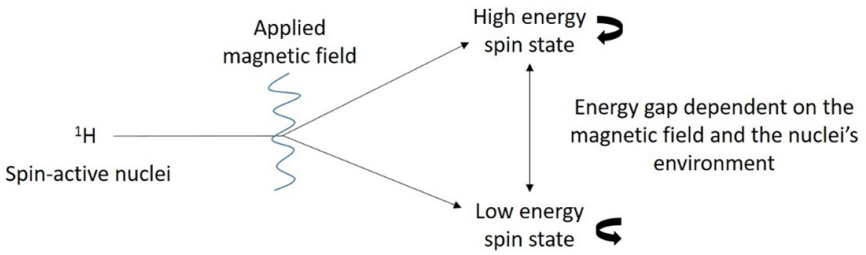

Figure 2.15: A visual representation of the energy levels that an NMR magnet induces for spin active nuclei.

The power of the technique lies with the ability to distinguish between different chemical environments. The energy gap between the spin states is altered by localised electron shielding, meaning each nucleus will have a unique energy emission associated with it - a unique chemical shift. The chemical shift values are indicative of the functional groups present within the molecule. Additionally, the peaks undergo a process known as splitting, revealing information regarding the neighbouring chemical environments. The combination of these features generates a spectrum that enables identification of unknown chemical structures.

Traditionally, NMR requires a pure sample, in the liquid phase, dissolved in a deuterated solvent. These restrictions immediately pose problems for the analysis of unresolved gaseous mixtures and as such the technique is seldom used when investigating fire effluent. There are however, several examples of NMR being successfully implemented in the fire science field. NMR analysis has shown to be a useful technique for the characterisation of young soot particles emitted from ethene inverse diffusion flames [74]. Figure 2.16 displays the obtained spectra, comparing the composition of soot recorded at 6 mm above the flame to that of the exhaust.

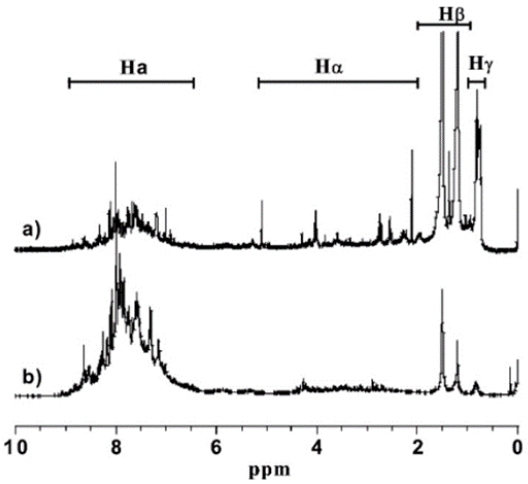

Figure 2.16: ^{1}H NMR spectra for young soot extracted at a) 6 mm and b) the exhaust, above an ethene inverse diffusion flame. The spectra have had four proton environments identified: H_a - aromatic, H_α - neighbouring an aromatic environment, H_β - neighbouring an H_α environment and H_γ - aliphatic. Reproduced from A. Santamaría *et al.*, FT-IR and ^{1}H NMR characterization of the products of an ethylene inverse diffusion flame [74].

The spectra in Figure 2.16 shifted in composition from largely aliphatic unoxidised species to mainly aromatic species as the sampling moved away from the centre of the flame. These NMR spectra were well resolved, enabling the distinction of different environments within the aromatic regions. Di-, tri- and tetra-aromatic rings can be distinguished using the NMR spectra, a level of detail that other analytical techniques struggle to provide. However, significant peak overlap, particularly in the aliphatic region, prevented integration and hence quantification of individual peaks. As a result, NMR is often not an appropriate tool to be used for product yield calculations in the fire science field.

NMR can also be conducted for solid materials; however, the resultant spectrum is often

broad. In a liquid, molecules are free to rotate, occupying a range of orientations. On average these orientations and the resultant internuclear couplings cancel each other out, producing sharp spectra [75]. For a solid sample, molecules are fixed in rigid positions, thus anisotropic spectra are produced. To remove this anisotropic effect, samples can be rotated using magic-angle spinning, evening out the internuclear couplings to produce a usable spectrum. Figure 2.17 depicts this process.

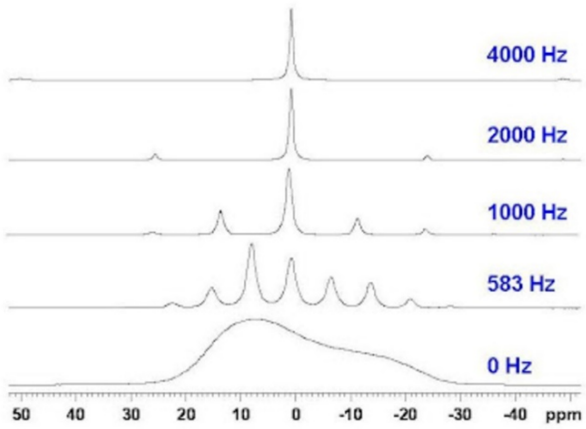

Figure 2.17: ^{31}P Solid-state NMR spectrum for ammonium dihydrogen phosphate recorded under five different sample rotation speeds. The resolution that can be achieved via rotating at the magic-angle enables solid state NMR to be used as an analytical tool. Reproduced from The University of Ottawa NMR Facility Blog: Magic Angle Spinning [76].

Solid-state NMR can be used to analyse the solid chars and the residues that remain after combustion. The combination of ^{29}Si and ^{13}C NMR has been used to determine the impacts of silica gel and potassium carbonate flame retardants on char formation [77]. Each of the ^{13}C NMR char spectra unanimously had only trace aliphatic signals, indicating that the produced char was mainly aromatic. A poor signal to noise ratio prevented integration and therefore quantification of the extent of this aromatic character.

Given the complexity of the sample matrices that fire scenarios generate, NMR is often an inappropriate characterisation technique. The most powerful characterisation tools that NMR enables can only be extensively utilised when a pure sample is analysed. As this segment explains, there are studies that have managed to successfully incorporate the technique, but it often feels forced and unnecessary. If a simpler characterisation option is available, it makes sense to only use NMR as a last resort.

2.4.3 Mass Spectrometry

Mass spectrometry (MS) is a speciation technique used throughout the fire science literature to identify combustion products [56]. Mass spectrometry is an ex-situ analytical technique, requiring a sample to be collected prior to analysis. Without an initial separation, the produced mass spectrum displays a meaningless overlapping combination of multiple

species. For the vast majority of studies, gas chromatography (GC) is coupled to the mass spectrometer, providing this separation. The combination of these techniques is commonly referred to as GC-MS.

A sample, either condensed or taken directly from the effluent line, is injected into a GC machine where the analytes are vaporised. An inert carrier gas is then flowed through the injection port and into the column. Assuming that an appropriate stationary phase has been selected, analytes will have different affinities for the column and will be slowed by differing extents. The analytes subsequently elute with differing retention times ready for MS analysis [78].

The mass spectrometer detects species based on their mass to charge ratios (m/z values). The generation of charged ions from the eluted species requires ionisation of the sample. Electrons are usually accelerated towards analyte molecules, dislodging existing electrons, producing positive ions. This intense electron bombardment can cause bonds within analyte molecules to break, forming fragment ions. Fragment ions and the difference in m/z between these fragments reveals additional structural information.

Electron ionisation, as shown in Equations 2.1 and 2.2, is appropriate for the ionisation of stable volatile species, suitable for the analysis of pyrolysis and combustion products [79]. Electron ionisation is a hard ionisation technique, promoting fragmentation (Equation 2.2), generating multiple fragments (A^+) that yield information on the structure of the compound. The type of ionisation used can be varied depending on the desired extent of fragmentation.

$$M + e^- \rightarrow M^{+\cdot} + 2\ e^- \tag{2.1}$$

$$M + e^- \rightarrow A^+ + M^{\cdot} + 2\ e^- \tag{2.2}$$

The $M^{+\cdot}$ fragment reveals the molecular mass of the analyte ion. The combination of this value with the fragmentation pattern enables the deduction of chemical structure.

There are many advantages to the GC-MS setup that make it appropriate for the analysis of fire effluent. The setup requires gaseous, volatile species, precisely the type of species generated during a fire. As such, the technique is being increasing use throughout the literature to identify species in fire effluent. Table 2.6, summarises GC-MS being used across the literature.

Despite the technique being utilised for the past forty years, Table 2.6, shows that there is no standard extraction procedure for GC-MS. The lack of standardisation stems from the multiple, changeable, variables present when analysing fires. A study monitoring monomer yields from a known polymer may conduct GC-MS directly on the collected gaseous emissions [86]. In this scenario a single species can readily be identified as it should be dominant in the effluent. Contrastingly, a study investigating low-levels of unknown

Table 2.6: A comparison of the GC columns and extraction solvents used for the GC-MS analysis of various combustible materials. Note that TCM indicates the solvent tetrachloromethane while DCM represents dichloromethane. N/A indicates that analysis has been conducted directly on the eluted gases.[66, 68, 80–85]

Year	Material	Extraction Solvent	Column / m x mm
1982	Polyethylene	MeOH	1.8 x 2.0
1985	Polyethylene	N/A	4 x 2.0
1994	Pine	DCM	25 x 0.22
2003	Beechwood	Acetone	60 x 0.25
2004	PMMA	TCM	30 x 0.25
2005	Bisphenol A ether	Acetone	30 x 0.25
2016	Bisphenol A ether	N/A	30 x 0.25
2020	Atmospheric Aerosol	N/A	30 x 0.25

volatiles will likely deploy a cold trap to concentrate analytes prior to analysis [80]. Given the variation in experimental outcome, GC-MS conditions will always be optimised for each specific experimental scenario.

The GC column length has settled at 30 m. A longer column will increase the separation between analyte peaks, at the expense of increasing the analytical run time. It appears that a column length of 30 m enables a high enough resolution to prevent the coelution of common pyrolysis and combustion products. Thus, the use of different heating rates, hold temperatures and extraction solvents should enable GC-MS processes to be optimised for a specific analytical scenario. Early GC-MS work focussed on assessing how the combustion conditions impacted the intensity and the ratio of the peaks being produced in the chromatograms rather than implicitly identifying the species being generated. Figure 2.18 shows how the produced volatiles varied for the combustion of polyamide two combustion chambers: 4.5 m^3 and 650 m^3 [83].

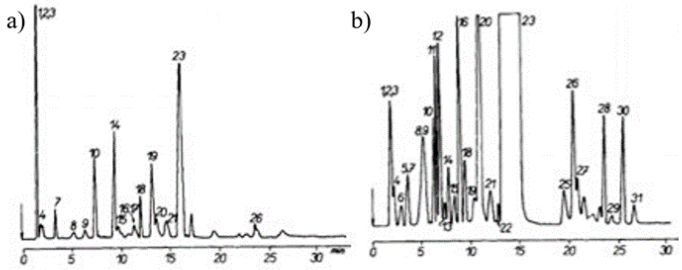

Figure 2.18: Total ion chromatograms showing a comparison of the impact of dilution on the flaming combustion products produced during the combustion of polyamide at 873 K. a) was recorded in a 650 m^3 chamber, while b) was recorded in a 4.5 m^3 chamber. Reproduced from J. Mitera *et al.*, The combustion products of polymeric materials. III: GC–MS Analysis of the combustion products of polyethylene, polypropylene, polystyrene and polyamide [83].

Figure 2.18 shows that a greater signal intensity was observed for the species obtained in the smaller room, illustrating how the combustion conditions have a large impact on relative levels of the volatiles being generated. However, multiple signals overlapped and the burning rates were not presented, a factor likely to have affected both the rate and the type of species being generated. Despite this omission, several of the volatiles produced during the combustion of polyethylene (propene, toluene, butene and benzene) corroborated with species identified by other studies utilising cold traps, providing evidence for the viability of the cold trap methodology [66, 83]. The issues surrounding overlapping species do not detract from the powerful insights that GC-MS provides, just that the apparatus requires appropriate instrument optimisation (column selection, temperature ramp rates, carrier gas selection etc.) and that the spectra require appropriate interpretation.

The analytical field has moved onto utilising tandem MS within its research. Tandem MS involves coupling two mass spectrometers together, separated by a collision cell. Ions can be selected to pass into the collision cell by altering the current supplied along the electrodes across the first mass spectrometer. Once inside the cell, additional fragmentation, via collision-induced dissociation (CID), can be induced enabling a greater degree of specificity. Figure 2.19 displays the four operating modes that tandem MS enables [87].

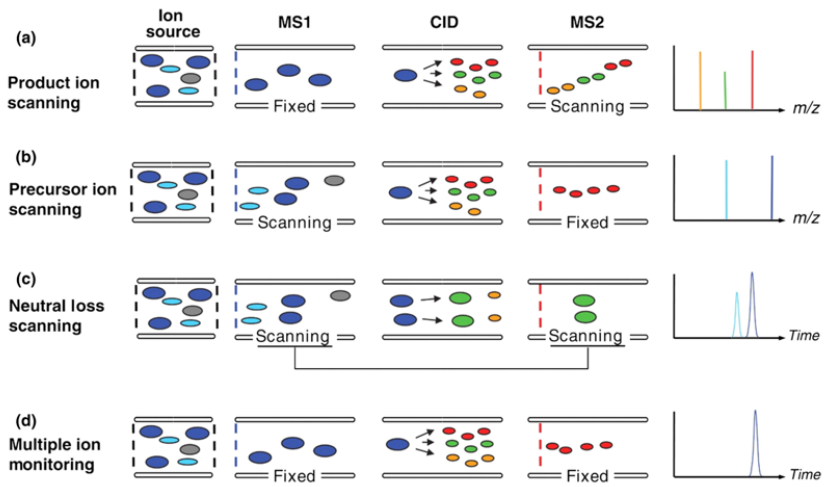

Figure 2.19: The four key tandem MS modes. a) Product ion scanning - A specific precursor ion is selected and fragmented to provide further analytical information. b) Precursor ion scanning - Ions are only detected if they produce a specific target fragment. c) Neutral loss scanning - Ions only appear if a fragment of a specific mass has been lost. d) Multiple ion monitoring - Specific ions can be targeted enabling species with the same m/z to be individually distinguished. Reproduced from S. Maher *et al.*, Colloquium: 100 years of mass spectrometry: Perspectives and future trends [87].

Tandem MS is yet to be fully utilised in the fire science field. At the time of writing, there is a distinct lack of studies utilising any of the four techniques. Precursor ion scanning would appear to be extremely useful for screening novel materials for specific known products of concern, deconvoluting complex spectra, yielding easily interpretable results. Tandem MS has a significant potential to enhance the analysis of fire volatiles.

An alternative means of increasing the speciation power of GC-MS lies with the separation

prior to analysis. Chemical species with similar properties will elute at similar times, creating overlapping responses. This overlap is increasingly noteworthy when multiple materials are involved in the fire. As previously discussed, the GC column can be extended to enhance component separation, however this drastically increases sample runtimes without guaranteeing peak resolution. Multidimensional chromatography (GC × GC-MS) introduces a second GC column, orthogonal to the first, in an attempt to circumnavigate this overlap. Figure 2.20 displays a typical GC × GC-MS setup, detailing the two columns [81].

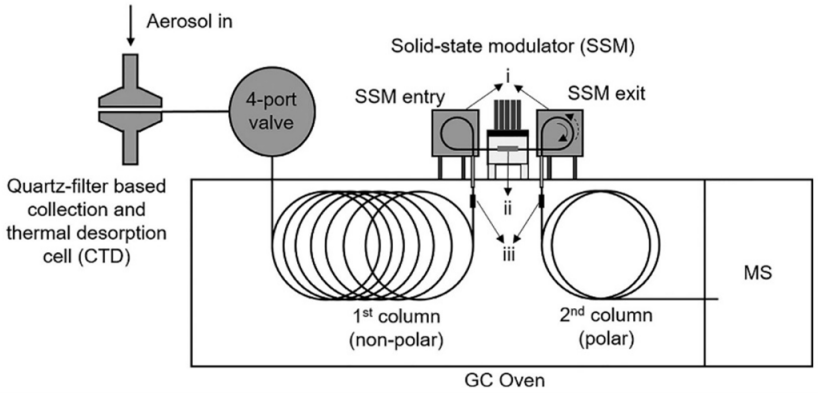

Figure 2.20: A typical GC × GC-MS setup, note that the two columns are of different lengths and have different stationary phase compositions. The solid-state modulator (SSM) connects the two columns, enabling the temperature difference, pressure and appropriate delay to be programmed to prevent overloading the second column. Reproduced from Z. An *et al.*, Comprehensive two-dimensional gas chromatography mass spectrometry with a solid-state thermal modulator for in-situ speciated measurement of organic aerosols [81].

Typically, one column adopts a polar stationary phase with the other, orthogonal, phase being non-polar, separating components based on their polarity and volatility respectively. Without this orthogonality between the columns, the first separation would simply be repeated, failing to yield multidimensional data.

Multidimensional chromatography has been used to demonstrate how increased temperatures cause the composition of pyrolysis products to vary during the pyrolysis of polyurethane and polyisocyanurate (PIR) foams [88]. A correctly optimised GC x GC-MS setup can accurately detect and distinguish species at levels below 1 mg L^{-1}. Such resolution enables trace levels of combustible species to be detected even if the specific molecule cannot be precisely identified.

Multidimensional chromatography appears to have solved the analytical issues that the fire science field faces, it offers a detailed breakdown of effluent composition whilst enabling quantification. The complexity surrounding method optimisation requires analytical parameters being determined for each experiment. Parameters such as column temperature, diameter, length and thickness that are easily fine-tuned in standard GC-MS have consequential effects as illustrated in Figure 2.21 [89].

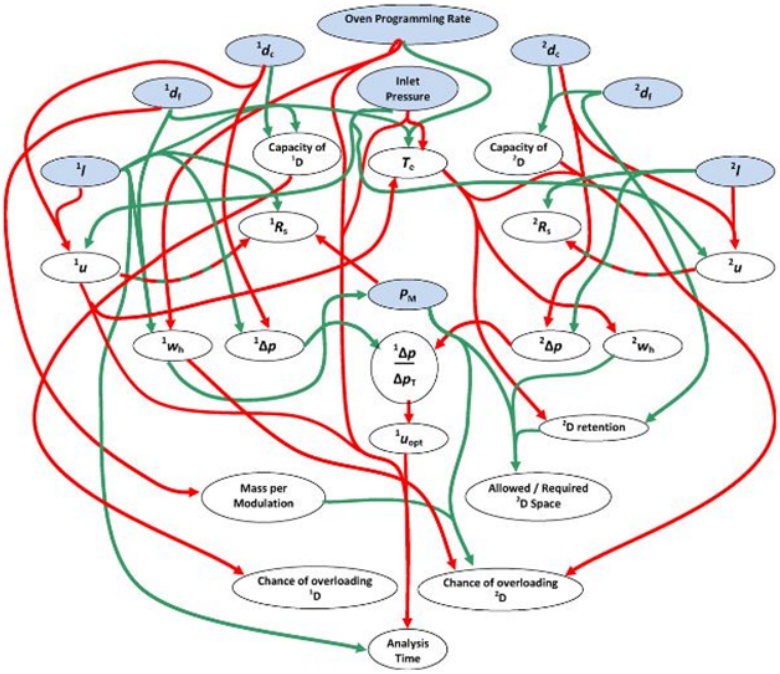

Figure 2.21: The complexity of the interlinking parameters that require optimising for multidimensional chromatography to be successful. Green lines link values that both increase as one is manually increased, red lines indicate the reverse relationship. Symbols: ^{1}de: 1D column diameter, ^{2}de: 2D column diameter, ^{1}l: 1D column length, ^{2}l: 2D column length, Te: elution temperature, ^{1}u: 1D column linear velocity, ^{2}u: 2D column linear velocity, $^1\mathrm{W}_h$: 1D peak width, $^1\mathrm{W}_h$: 2D peak width, $^1\Delta_p$: pressure drop in the 1D, $^1\Delta_p$: pressure drop in the 2D, $^1\Delta_p/\Delta_p T$: pressure drop in the 1D compared to the total pressure drop, $^1\mathrm{R}_S$: 1D resolution, $^2\mathrm{R}_S$: 2D resolution, $^1\mathrm{u}_{opt}$: 1D column optimal linear velocity, P_M: Required 2D space. Reproduced from A. Mostafa *et al.*, Optimization aspects of comprehensive two-dimensional gas chromatography [89].

Additionally, software manipulation involving peak picking and integral selection, must occur after the spectra are recorded, leading to long processing times with no guarantee that the parameters have been optimised. Non-targeted or suboptimal GC x GC-MS can give information on the types of species present, negating the complexity described in Figure 2.21. Non-targeted GC x GC-MS enables more detailed analytical information to be provided, identifying the types of species present in complex mixtures. Such detail is more insightful than that provided by one-dimensional GC-MS. Both non-targeted GC x GC-MS and one-dimensional GC-MS require a degree of optimisation to provide information of use. The appropriateness of each technique will vary with the experimental context.

2.4.4 Matrix-assisted Laser Desorption Ionisation

Analysing the surface of samples either pre- or post-combustion can yield insights into the chemical processes that occur to create volatile species. MS can also be used to identify

these species, provided that the ions can be produced from a solid surface. Matrix-assisted laser desorption ionisation (MALDI) is used to generate ions from the surface of a solid sample, assuming that an appropriate matrix substance has been selected [90].

The species present on a surface tend to have a greater molecular mass than the volatiles that have been emitted during the fire. As such, it is important to minimise fragmentation of these species, thus retaining chemical structure. MALDI is a soft ionisation technique, ions are formed via cation transfer, limiting fragmentation. This soft ionisation stems from the selection of an appropriate matrix. A small volume of the selected matrix solution is added to the investigated surface prior to laser irradiation.

Due to the large excess of the matrix solution, analyte molecules are relatively isolated from one another. Once laser irradiation has commenced, the matrix will absorb the majority of the transferred energy, causing matrix, and analyte, ions to desorb from the surface. When gaseous, cations from the matrix adhere to the analyte molecules, creating detectable positive ions that pass into a spectrometer. Figure 2.22 depicts the process by which MALDI generates these ions.

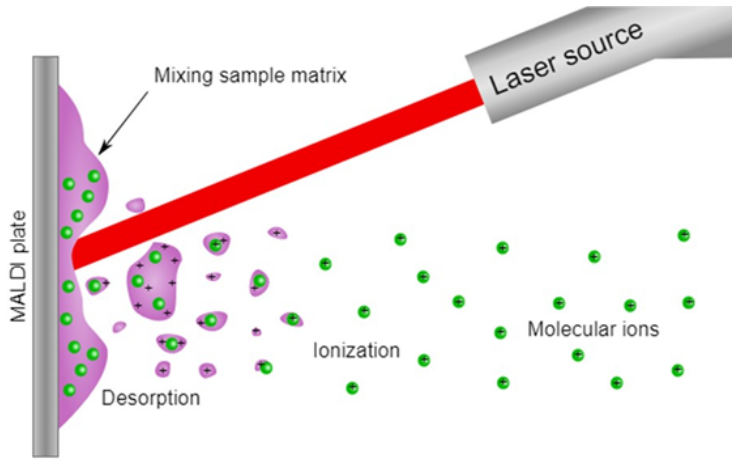

Figure 2.22: The generation of molecular ions from a solid sample using MALDI. Reproduced from F. Hillenkamp *et al.*, MALDI MS: A Practical Guide to Instrumentation, Methods and Applications [91].

MALDI has been used to analyse the surface of polyamide chars with a combination of 2,5-dihydroxybenzoic acid and sodium trifluoroacetate being used as the matrix and cation source [92].Comparison of the surface chars to the original polymers enables insights into the effluent generating processes that occur during combustion. The obtained spectrum depicted three oligomer peaks, one being cyclic. A cyclic oligomer peak in the char suggested that the polyamide underwent several depolymerisation reactions at the surface, with some preferential cyclisation occurring. These results corroborate with char findings analysed via NMR, where the highly aromatic nature of synthetic polymer chars has been shown [77].

MALDI can provide an insight into the complex char structures remaining after flame extinction however, there is no guarantee that the technique will be able to yield results. The appropriate selection of a liquid matrix to be added to a sample surface needs to

solubilise the surface molecules without damaging them. As such, preparatory work must be conducted to determine plausibility. Some surfaces will simply not be able to be sampled in such a manner.

2.4.5 Critical Summary of Analytical Methodologies

Multidimensional chromatography removes several of the problems associated with the chemical analysis of fire effluent. Most notably the technique offers the ability to resolve co-eluting peaks, facilitating additional speciation. However, utilising the technique does generate additional complications. The sheer volume of peaks produced often implies that diastereomers and enantiomers have been separated. Although this separation is useful when honing in on specific species and their subsequent toxicity, the level of detail provided is beyond the requirements for an initial screening. The generation of these additional peaks increases the likelihood of peak misallocation.

Adapting the experimental setup for the specific experimental scenario can also be time-consuming. Both columns need to have their lengths and stationary phases optimised for the species being analysed, tough when the species being detected are largely unknown. If appropriate standards have been run, and time is dedicated to peak allocation, the information gleaned from multidimensional chromatography could enhance our understanding of combustion processes. At the time of writing, there are not nearly enough studies in the literature to fully assess the viability of the technique, but multidimensional chromatography retains the potential to reveal unique pyrolysis and combustion products.

FT-IR offers a means of assessing effluent undisturbed in real time. Despite being useful to identify functional groups, the technique is poor for implicit speciation, particularly when it comes to identifying products generated at low concentrations. As such FT-IR should be used alongside a GC-MS based method, enabling a wider range of compounds to be screened and identified, depending on the extraction technique. A complete summary of the analytical methods discussed in this section is covered in Table 2.7.

Table 2.7: A comparison of the key advantages and disadvantages offered by a range of analytical methodologies.

Technique	Advantages	Disadvantages
FT-IR	• Can identify functional groups • Works in near real-time • Works with gaseous samples • Speciation possible if mixture contains a few known species	• Overlapping bands prevent full speciation for complex mixtures • Similar species with the same functional groups are often masked by band overlap • Not all species are IR active
NMR	• Can provide detailed information on chemical structure • Helpful in identifying where specific functional groups sit in relation to one another in unknown molecules	• Signals often noisy due to multiple species and contaminants – reducing the feasibility of the technique • Requires liquid phase or occasionally solid phase samples • The requirement for deuterated solvents makes sample preparation lengthily and expensive • Samples analysed ex-situ
GC-MS	• Provides full speciation identifying species via database matching • Fragmentation ions enable unknown species (not on the database) to be identified	• Samples often have to be retained and moved to the machine for analysis (usually as liquids) • Optimisation of GC-MS parameters often takes several weeks depending on the sample and its matrix
GC × GC-MS	• Overlapping bands from GC-MS can be separated out into their individual species • Reveals more unique species than any of the other discussed analytical approaches	• Optimisation procedure is lengthily and may require several years • Some analytes still overlap • The level of separation is sometimes too extreme for fire effluent analysis (e.g., separation of enantiomers)
MALDI	• Direct analysis of a sample • Enables MS for a solid surface	• Soft ionisation technique reduces fragmentation and thus makes speciation tougher than GC-MS • Some surfaces cannot be sampled as appropriate matrices do not exist

2.5 Concluding Remarks

Numerous techniques for assessing fire effluent have been discussed throughout this chapter, with the approaches used being tailored to each specific experimental scenario. There exists a variation in both the methodology used to generate the effluent and the analytical techniques selected for the analysis. Figure 2.23 offers a visual representation of the various approaches taken by the studies within this review chapter.

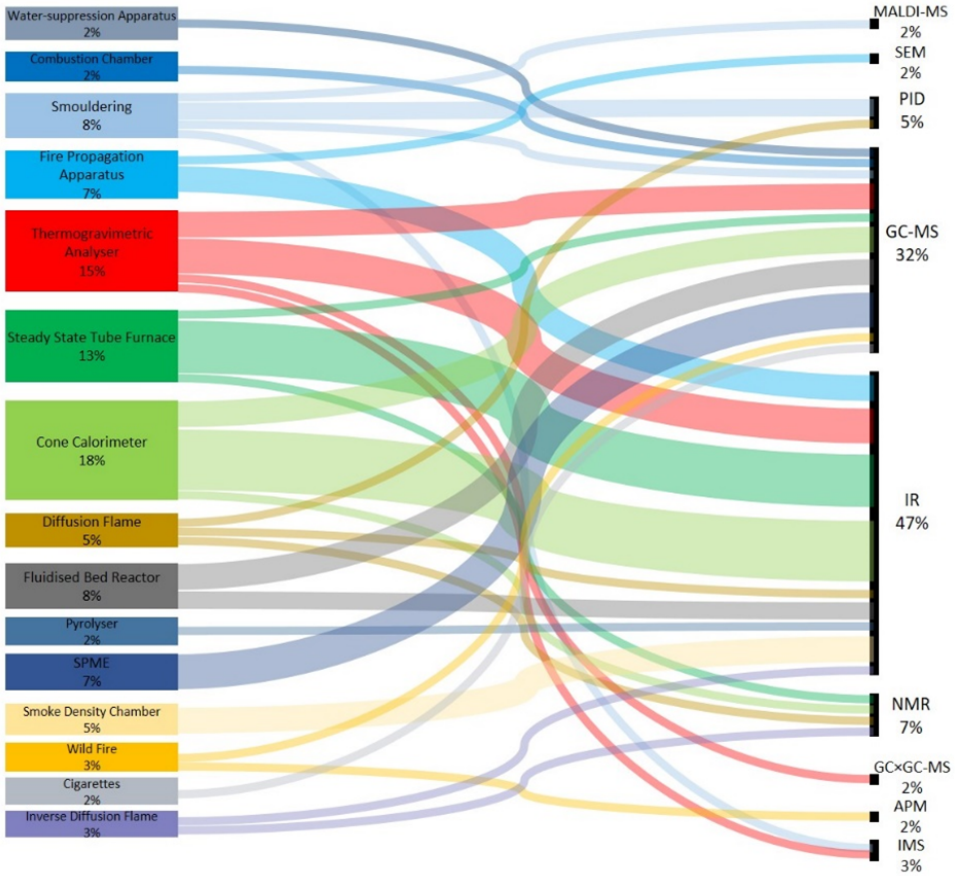

Figure 2.23: A summary of each of the experimental techniques used in the papers discussed throughout this chapter. The column to the left summarises the effluent generating methods, while the right depicts the corresponding analytical techniques used. SEM refers to scanning electron microscopy, PID refers to photoionization detector, IMS refers to Ion-mobility Mass Spectrometry and APM represents aerosol particle mass analyser.

The cone calorimeter is the most readily used effluent generating technique, appearing in 18 % of the studies reviewed here. The apparatus provides a repeatable means of generating effluent, being favoured for its inbuilt spectroscopic analysers, enabling the calculation of heat release rates. Despite the FPA being very similar to the cone calorimeter, there is a marked reduction in its use, with only 7 % of the reviewed papers utilising the technique. If more research groups had access to an FPA, the greater ability to modify and control external variables may increase its prevalence across the literature.

In contrast to the array of effluent generating methods, there is a reduced spread in the techniques used to analyse fire effluent. IR analysis represented nearly half of the analytical techniques used in the reviewed literature. FT-IR can identify specific functional groups present in real time, however overlapping species with similar functional groups are likely to be combined into a single signal. The dependency of the field on IR spectroscopy has facilitated the analysis of traditionally non-condensable species like NO and CO, however careful interpretation of spectra is required to identify more complex species, which is often impossible for complex mixtures.

To achieve implicit characterisation, the produced effluent must be retained, and separated, prior to analysis with a technique like GC-MS. The application of the technique will vary depending on individual experimental setup and the level of analysis required with some successful studies deploying adsorption cartridges for the collection of the effluent [22]. However, a condenser is favourable, retaining both the volatile and semi-volatile species [66]. The species condensed in a cold trap will naturally rise in concentration, increasing the likelihood of detection. Such techniques can be conducted alongside FT-IR analysis, increasing the proportion of speciation of fire effluent. A standardised, yet appropriate, extraction methodology may be impossible to form, thus the use of multiple analytical techniques, whenever possible, will bring us a step closer towards successfully identifying a greater proportion of the species present in fire effluent.

Pyrolysis products are generated prior to the formation of gaseous combustion products, dictating the composition of the fire effluent. To increase our understanding of the combustion process, both the pyrolysis and combustion species need to be analysed and identified. Successful analysis of similar pyrolysis products requires the produced effluent to be collected and separated. It is therefore crucial to cool any effluent in a quick and controlled manner, preventing post-generation oxidation reactions. The FPA is best placed to deliver these requirements, primarily due to the responsiveness of both the lamps and the air inlet, enabling control over the combustion environment. Once generated, effluent can be condensed, with GC-MS analysis occurring before degradation of the sample, via UV or thermal exposure, can begin.

In reality, fires are often much larger than bench-scale apparatuses allow. A larger-scale methodology like the ISO room testing is therefore likely to generate an effluent stream that changes in composition as a fire evolves, thus generating representative species for analysis. Work has been undertaken to link yields of species obtained from cone calorimeter and FPA experiments to larger-scale studies, with some agreement shown for CO and CO_2 [93]. However, future work identifying and tracking more complex species produced during both bench-scale and room-scale studies has been recommended.

If a representative scale has been selected, one that facilitates control over the heating rate whilst allowing observation of the sample, the combination of both FT-IR and GC-MS should therefore be used to investigate the composition of effluent being generated by known materials. Although the limitations of the techniques to identify lightweight species must be noted. The use of a load cell enables the burning behaviour of a sample to be ascertained whilst facilitating the calculation of product yields. The combination of the emissions data, the mass loss rate and the observation of the sample enables fire effluent to be sampled in a meaningful manner.

Chapter 3

Large-scale Evaluation of Effluent Composition

"This fire is out of control."

– Franz Ferdinand
This Fire (Franz Ferdinand, 2004)

This page has been intentionally left blank.

3.1 Representativeness

Most testing scenarios attempt to be representative of the real-world problems that they are designed to mimic. The testing methodology must therefore result in the same outcomes being obtained as those expected to be achieved in the real world. Any deviation from these expectations requires a significant understanding of the problem, enabling the obtained results to be interpreted in a meaningful manner [94]. When applying these principles to the study of fire effluent, large-scale testing initially appears to be the most representative way to replicate real-world fire scenarios.

In an ideal testing scenario, adequate control variables should be established to ensure that any obtained outcomes are repeatable. Increasing the number of control variables results in an improved repeatability, but assumes that these control variables are not relevant to the problem being probed, thus decreasing representativeness [95]. Therefore, a trade-off exists between representativeness and repeatability which must be acknowledged when selecting an appropriate testing method. The factors are inverse of one another, optimising one comes at the expense of the other. Such principles led to the development of the single burning item (SBI) testing procedure; however, the restrictions on the burner size and sample orientation positioned the SBI as a means of assessing flame spread rather than a means of assessing fire effluent.

The other large-scale testing procedure mentioned in the previous chapter was the international organisation for standardisation (ISO) room. The ISO room setup mimics how a fire behaves in a confined room whilst enabling the mass of a sample to be recorded. The upper portion of the compartment will become filled with an oxygen-deficient hot gas layer, and if the flames project into this layer the combustion chemistry is dramatically altered [96]. The ISO room enables these real-world conditions to be imitated, thus, should generate much more representative effluent than comparable bench-scale methodologies.

3.2 ISO Room Testing

To standardise ventilation and compartment feedbacks under large-scale environments, an ISO 9705 room (3.6 m × 2.4 m × 2.4 m) can be used. Through the manipulation of the opening(s) different airflows and thus different ventilation environments can be created as a function of the fire size [97]. The combination of a room constructed to the ISO 9705 dimensions, Figure A.2, alongside testing materials individually was deemed an appropriate strategy to assess combustion emissions at a representative scale.

3.2.1 Material Selection

One of the biggest factors that controls the hazards associated with fire effluent is the starting material. During the Grenfell tower tragedy in 2017, many of the hazardous chemicals in the effluent were believed to have been generated during the combustion of insulation material [17]. Insulation foams are combined with timber battens to insulate internal and external walls. Assessing common construction materials like these would therefore increase the representativity of any obtained data. As a result, three common construction materials were sourced commercially: polyisocyanurate (PIR) insulation foam, phenolic insulation foam and untreated timber (*Pinus sylvestris*). Images of these materials burning are shown in Figures A.3, A.4 and A.5.

Of the synthetic foams, PIR has a slightly more complex structure than phenolic foam due to the increased nitrogen content. Figure 3.1 compares the aromatic structure of a phenolic resin after curing, a key process during the manufacture of phenolic foam, to the nitrogen-based isocyanate linkages present in PIR [98].

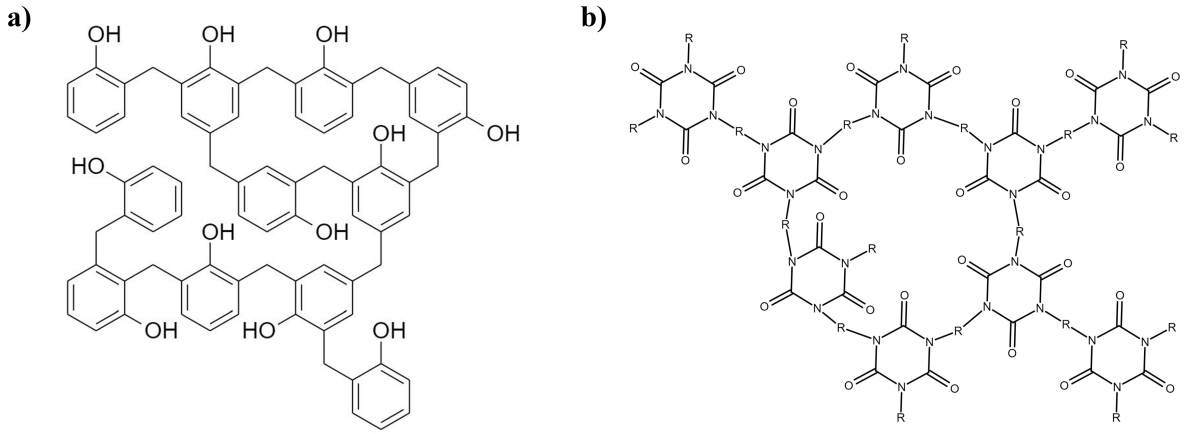

Figure 3.1: a) A cured phenolic resin, a precursor involved in the formation of phenolic insulation foam. b) An example of the structure of polyisocyanurate foam, where R represents a hydrocarbon chain. Note that R is likely to be a long-chain hydrocarbon and may contain aromatic rings [98].

During the manufacture of phenolic foams, substituted phenols are used to form resins. The use of sulphuric acid catalysts during this manufacturing process may result in residual

sulphur making its way into the final product [99, 100]. During flaming combustion, this sulphur may be oxidised to produce sulphur dioxide (SO_2), a species readily traceable in fire effluent. Other products detected in phenolic foam effluent have been reported as carbon monoxide (CO), carbon dioxide (CO_2), phenol (C_6H_5OH) and methane (CH_4) [101].

PIR has a slightly more complex structure than that of phenolic foam, due to the presence of the isocyanate linkages. During pyrolysis, these linkages break down primarily to form hydrogen cyanide (HCN), a known asphyxiant, with elevated temperatures facilitating this dissociation [102]. Despite other asphyxiants like CO also being linked to PIR effluent, it is the nitrogen that enables the formation of this cyanide, leading to the well documented link between PIR and HCN.

The monitoring of SO_2, HCN, CO and CO_2 in real-time via Fourier transformed infrared spectroscopy (FT-IR) will enable differences in the effluent composition between these materials to be assessed. Additional speciation may be obtained via gas chromatography – mass spectrometry (GC-MS) analysis of the effluent, potentially enabling some of the aromatic species produced during the combustion of timber to be identified. By linking the generated species back to the MLR of each material, a modified ISO room setup should allow the effects of ventilation on fire effluent to be documented in a representative manner.

3.2.2 Cribs

Large-scale testing methodologies often opt to use the same mass of each material under investigation. Given the low density of insulation foams compared to other polymeric materials, maintaining the same fuel loading by mass results in the insulation foams inevitably having a much larger surface area than the equivalent mass of a denser fuel like timber. Such discrepancies in surface area and orientation alters the surface energy balance that each fuel experiences, impacting the mass loss rate (MLR) which subsequently alters flame spread rates and large-scale fire dynamics. It was therefore decided to match the geometry of the fuel loading whilst recording the MLR rather than aligning the starting mass of each fuel.

Large-scale repeatable testing of timber has traditionally occurred through the construction of wooden cribs. The stacking of a material in a controlled manner facilitates repeatability whilst enabling control over factors such as the size of a fire and the rate of fire growth [2]. Figure 3.2 shows the three adjustable parameters that enable cribs of single materials to be finetuned to meet specific experimental requirements.

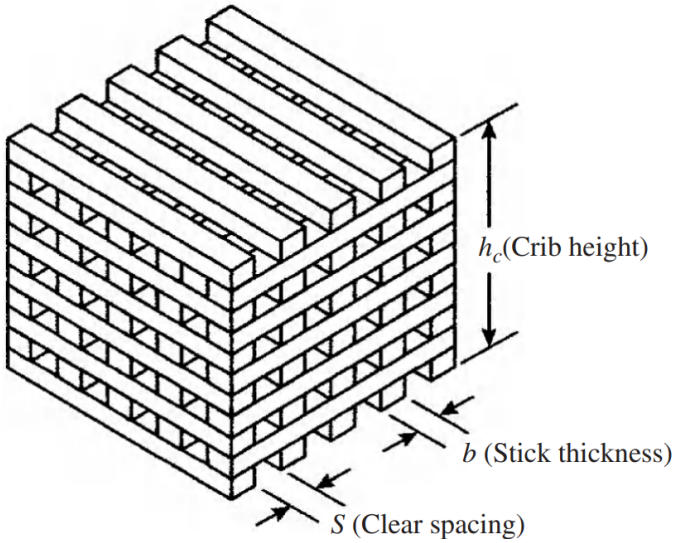

Figure 3.2: The parameters that may be altered when designing a crib. Reproduced from D. Drysdale, An Introduction to Fire Dynamics [2].

Crib dimensions can be manipulated to enable a specific mass of fuel to be present, controlling the expected overall heat release rate (HRR) for an experiment. Careful adjustment of b (stick thickness) and S (clear spacing) can be used to control flame spread, influencing the rate at which the peak HRR will be reached. The simplest way to limit the maximum fire size is to reduce h_c (crib height) based upon the most flammable material under investigation. A reduction in S can be used to facilitate successful ignition, thus finalised crib dimensions can be finetuned to ensure that each investigated material generates a representative fire.

3.2.3 Experimental Setup

The PIR and phenolic foams were cut to form sticks before removal of the aluminium foil facers. The cut sticks were stacked to produce cribs, $b = 0.05$ m, $S = 0.025$ m, $h_c = 0.15$ m, as detailed in Figure 3.3. The timber was sourced pre-cut to these same dimensions and stored within a conditioning room (298 K, 8 hrs), prior to testing commencing.

The cribs were designed with a fuel loading that provided a sufficient fire duration to enable an oxygen-deficient hot gas layer to form within the ISO room. As the combustion behaviour of these materials at this scale is not well understood, preliminary free-burn testing was conducted to identify a range of crib dimensions in which a sufficient volume of effluent would be generated for sampling without causing the compartment to flashover. A square crib design, comprising of three layers was shown to enable each selected material to burn to completion without causing the compartment to flashover.

To enable differing ventilation factors to be tested, the opening to the ISO 9705 room was modified. An obstruction was placed in the doorway located at the centre of one of the

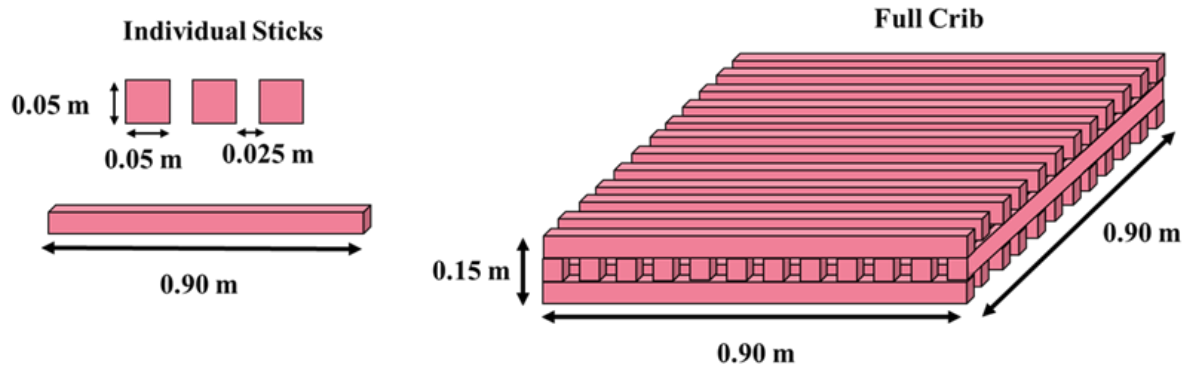

Figure 3.3: The stick dimensions used to form the cribs for each of the investigated construction materials (PIR foam, phenolic foam and timber). Sticks were stacked three layers high, half-spaced, with twelve to a layer. Each crib was homogenous, materials were not mixed.

short walls of the room, which split the large opening into two apertures of equal size. These gaps were designed to allow air to enter from the bottom and combustion products to exit from the top of the opening. The dimensions of the doors and resulting openings are given in Figure 3.4. These corresponded to ventilation factors of 0.08 and 0.22 $m^{5/2}$ for the small and large openings respectively.

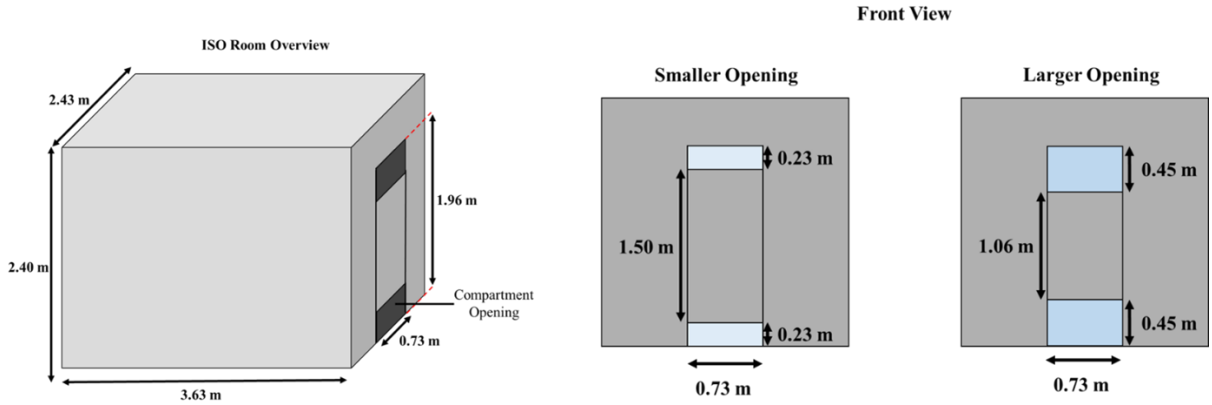

Figure 3.4: The dimensions of the ISO room. The front view includes the two different opening sizes that were used during this chapter. Note that the fully-ventilated experiments occurred outside the ISO room under a 1 MW scale calorimeter with no obstruction to the ventilation.

The fully-ventilated experiments were carried out away from the ISO room under free-burn conditions using a 1 MW scale calorimeter. These conditions enabled a third scenario to be probed in which oxygen could readily diffuse towards each crib fire. For these experiments, the sampling setup was revised to sample effluent from the exhaust duct, but other procedures remained untouched. Figure 3.5 details the overall setup for the restricted ventilation experiments.

Once a crib had been constructed, four cotton wool balls soaked in heptane were placed between the sticks at the front of the crib at the side nearest the opening. A match was used as the ignition source and was dropped onto these cotton wool balls. Once ignited,

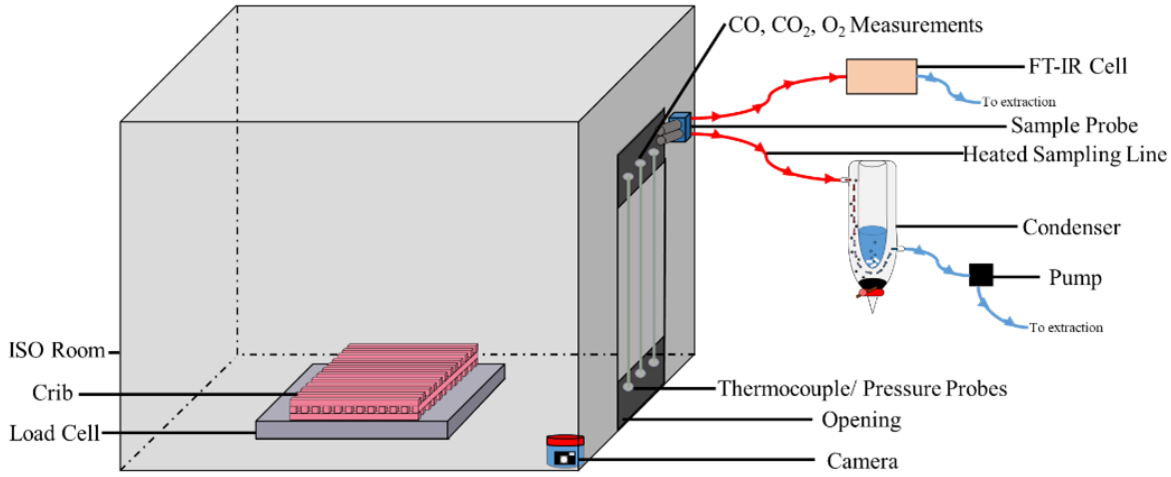

Figure 3.5: The complete experimental setup. A crib was placed on a load cell in the centre of an ISO 9705 room. Air entered the room through the lower opening and exited via the upper opening. Sampling of the effluent exiting the ISO room occurred from the upper opening.

each crib was left to run until burnout was achieved, as determined by an absence of flaming alongside no change in mass. Each experimental run for the smaller openings was replicated in triplicate for both foams, with emission sampling commencing at the point of ignition. The larger opening and fully-ventilated experimental runs were conducted once for each material.

3.2.4 Effluent Sampling

Effluent exiting the compartment from the upper opening was sampled by two separate heated sampling lines. The first sampling line headed to a FT-IR cell (Gasmet, Vantaa, Finland) while the second passed through a condenser (0.2 L s^{-1}) containing a mixture of dry ice and acetone (195 K). Condensed effluent was accumulated over the course of a run to give a crude brown liquid. The glass parts of the sampling lines were cleaned with dichloromethane (CH_2Cl_2) and the remaining parts were cleaned with acetone between runs. FT-IR analysis was conducted using a Gasmet DX4000 portable gas analyser (scanning range 594.4 – 4238.3 cm^{-1}, path length 250 cm, cell temperature 453 K), spectra were analysed utilising the Calcmet software (V2005.100), alongside calibrated reference samples.

CH_2Cl_2 (4 mL) was added to the crude condensed effluent and the two layers were separated. The organic layer was extracted to give a colourless liquid. The resultant solution (∼5 mL) was taken for GC-MS analysis. GC-MS analysis was conducted using a Thermo Trace 1300 GC with an ISQ LT single quadrupole MS (Thermo Fisher Scientific, Massachusetts, USA), in splitless mode equipped with an AI 1310 liquid autosampler (Thermo Fisher Scientific, Massachusetts, USA), using a TraceGOLD TG-5 column (30 m x 0.25 mm x 0.25 µm), held at 308 K for 600 seconds before rising to 553 K at 10 K min^{-1}. This gradual temperature ramp was designed to limit the coelution of similar species. A helium carrier

gas was flowed at 0.8 mL min^{-1}. The MS had a 573 K ion source temperature and was operated in positive electron ionisation mode, scanning m/z 40 – 400. The organic portion of the effluent condensate was analysed.

For the experiments conducted in the ISO room, independent measurements of CO, CO_2 and oxygen (O_2) were performed using the Transportable Analyser for Calorimetry Outside (TACO). The TACO, an IR analyser, was operated as per existing literature [103]. These data were used in conjunction with the flows measured in the upper opening to calculate the heat release rate (HRR) according to Janssens [44].

3.3 Burning Behaviour

This section details the means by which the data generated by the instrumentation in the compartment can be used to comment on the burning behaviour of the investigated materials.

3.3.1 Smoke Layer Interaction

Cameras situated within the compartment enclosure recorded each experiment in full, enabling differences in the burning behaviour to be noted between the fuels. Still images taken from these cameras are annotated in Figure 3.6 for the small opening experiments for each of the investigated materials. Each series of images shows a warm smoke layer building within the compartment. The extent of each smoke layer/ flame interaction was hard to determine due to the combination of the sooty compartment walls and the extreme camera angles. Despite these challenges, the moment that the flames first interacted with the smoke layer was noted for each experiment. To account for the differing masses of the fuels used to construct the cribs, visual observations were made based upon the normalised mass of remaining fuel.

As shown by Figure 3.6, each fuel initially burned with an unobstructed luminous flame. A small volume of smoke was generated but could efficiently leave the compartment through the upper opening. As the flames began to develop across each crib, the proportion of fuel involved with the fire rose, causing an increase in the volume of smoke being produced. For the PIR and phenolic foams, the rate of effluent generation exceeded the flowrate out of the compartment resulting in the formation of a thick black smoke layer. This layer was observed to form within the compartment when 90 % of the mass of the PIR and phenolic foam cribs remained. Such observations outline the importance of large-scale testing as these smoke layer interactions are not observed using existing bench-scale methodologies.

The smoke layer continued to build over the course of an experimental run, descending towards both the PIR and phenolic foam cribs. By the time 60 % of each of these fuels remained, the smoke layer had quenched parts of the upper flame envelope, significantly decreasing the combustion efficiency. These quenching interactions increased the $CO:CO_2$ ratio from 0.05 to 0.11 for PIR, demonstrating the decreased ease of oxidation once the flame envelope had been disrupted by the warm effluent layer building in the compartment. It was observed that flames for the timber experiments did not interact with the smoke layer to the same extent as the PIR or phenolic foam experiments. Thus, the different materials generated differing environments which were intrinsically linked to the properties of the material being burned.

Both cribs constructed from insulation foams continued to burn under the descending smoke layer, albeit with a visibly decreased flame length, until burnout was achieved. This glowing can be observed in Figure 3.6 when 30 % of mass remained. The contrast between the luminous fully-developed flames present during the combustion of the timber cribs at 30 % remaining mass and the dull glow of the PIR and phenolic cribs with the same percentage of fuel remaining reinforced the differences in combustion efficiency. Upon

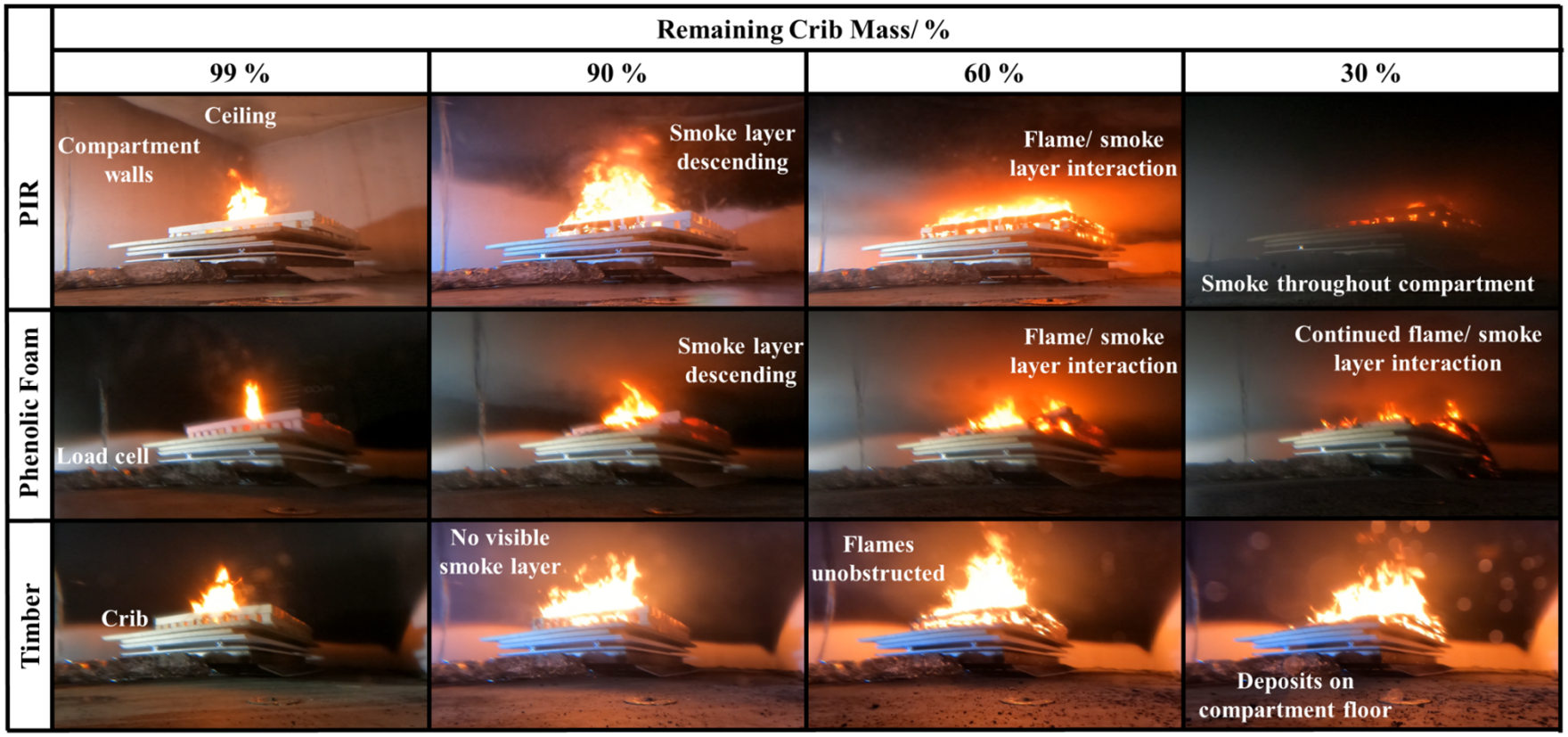

Figure 3.6: Still images taken at four normalised mass intervals (99 %, 90 %, 60 % and 30 %) during the combustion of PIR, phenolic foam and timber cribs within an ISO room with a small compartment opening. A smoke layer was initially formed and descended onto the PIR and phenolic foam cribs, quenching the flames. This quenching interaction was absent during the timber experiments.

completion of an experiment, charred PIR and phenolic foam remnants remained but the majority of the fuel had been consumed, suggesting that the descending smoke layer did not extinguish the fire. These differences in the combustion conditions must be applied to any interpretation of effluent composition.

3.3.2 Mass Loss Rate

Considering the observed differences in the flame length caused by the smoke layer/ flame interactions, MLRs were calculated to determine whether the rate of pyrolysis differed between the screened materials. MLRs were plotted as they reflect the pyrolysis rate, accounting for the generation of the gaseous fuel which includes species that were not oxidised during combustion. Figure 3.7 compares the calculated MLRs obtained across each of the investigated materials.

Data were smoothed using the Gaussian Smoothing Operator in MATLAB (R2021b). Based on the size of the selected filter, the smoothing operator applied a weighted average around each data point, using weights derived from a Gaussian distribution. Such smoothing reduced the noise in the data. Unsmoothed data for Figure 3.7 is presented in Figure A.1 in the appendix.

Despite the different ventilation factors, the MLRs remained very similar for each type of material burned in the compartment. Each of the cribs exhibited peak-decay behaviour with the ventilation having little, if any, influence on both the time taken to reach a peak MLR and the value of this peak MLR. This rise and fall relationship alongside an absence of a steady period suggested that the burning behaviour was changeable throughout each experiment, with heat feedback cycles causing the MLR to peak and fall. As the warm upper smoke layer formed within the ISO room for the insulation foams, the thermal feedback interaction between the smoke layer and the surface of the crib caused the MLR to increase, providing more fuel for oxidative processes. These feedback cycles contributed towards the increase in MLR as the fire began to develop. Despite these escalations, the data were repeatable for the small openings for both foams, enhancing the confidence in the design and construction of the cribs.

The PIR experiments all peaked in unison showing little if any discrepancy between the fully-ventilated conditions and the experiments conducted in an ISO room. This suggested that the build-up of the smoke layer only had a marginal effect on the combustion behaviour exhibited by the PIR, as the rapid heat release from the material itself dominated the heat transfer. For the phenolic foam, the fully-ventilated conditions led to a peak MLR approximately 200 seconds earlier than the experiments conducted in the ISO room. However, a similar magnitude of peak MLR ($\sim$6 g s^{-1}) and similar burn duration prevented this discrepancy being attributed to the absence of the smoke layer. Despite the differing ventilation conditions, the similarity in recorded MLR for experiments conducted with the same material suggested similar burning behaviours.

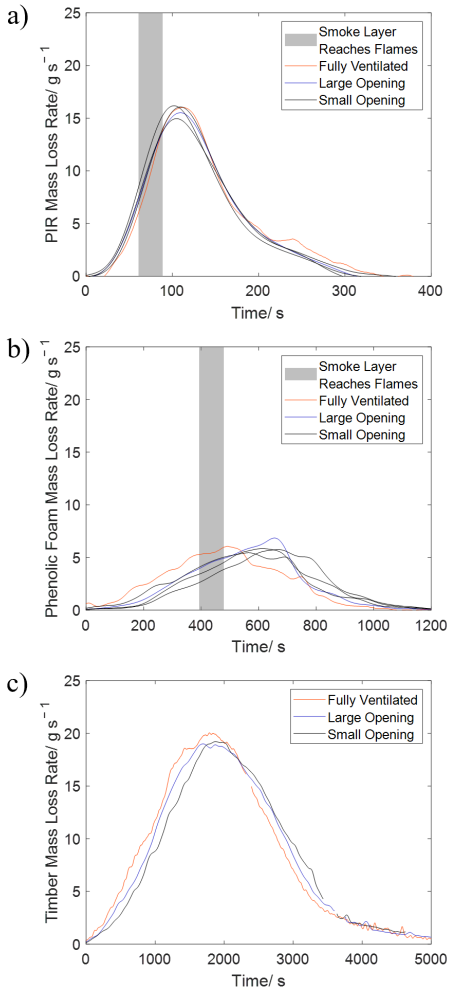

Figure 3.7: The calculated mass loss rates (MLRs) for each of the materials investigated during the crib experiments: a) PIR, b) Phenolic foam and c) Timber. Note that the highlighted smoke layer region does not apply to the fully-ventilated experiments. This data has been smoothed (Gaussian filter, 50 periods). The timber runs were smoothed over 300 periods and have had spikes in the MLR afforded by sticks tumbling from the load cell removed.

3.3.3 Heat Release Rate

The heat release rate (HRR) calculated during the combustion of a given material can be obtained using oxygen consumption calorimetry. This technique works on the principle that 13.1 MJ of energy is released per kilogram of oxygen (O_2) consumed during combustion [12]. Through the comparison of the mass flow rate of air entering and exiting the ISO room compartment, the extent of oxygen consumption and hence the HRR for each crib fire could be calculated. These calculations assumed that air comprises of only O_2, CO_2, CO and nitrogen (N_2) and that each of these gases behaves as an ideal gas. In reality these assumptions will warrant minor deviations from the calculated HRRs, however the results obtained utilising this methodology provided a comparable means of assessing each of the experiments.

The HRR for each of these fuels determined the energy available to drive processes within the compartment. Given the similarities between the MLRs obtained for the same fuel under differing ventilation factors, any difference in the HRR would suggest that differing combustion processes were being favoured. By reducing the availability of oxygen within the compartment, via the restricted opening, it was expected that the HRR would vary across the screened ventilation conditions. Figure 3.8 summarises the HRRs obtained for each of the investigated materials.

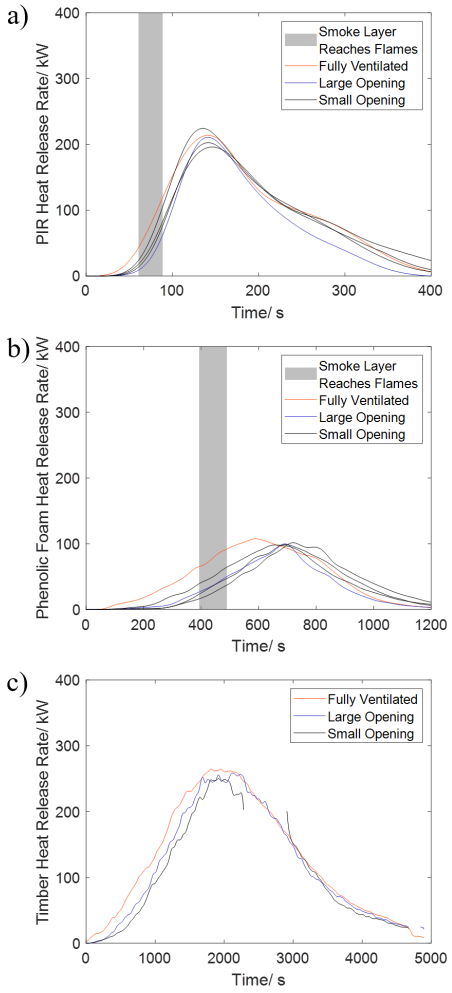

Figure 3.8: The calculated heat release rates (HRRs) for each of the materials investigated in this study: a) PIR, b) Phenolic foam and c) Timber. Note that the highlighted smoke layer region does not apply to the fully-ventilated experiments and that the absence of data between 2400 and 2900 seconds on the small opening timber run occurred due to equipment shut off. This data has been smoothed (Gaussian filter, 100 periods).

The variation of opening size in the ISO rooms resulted in a minimal impact in the HRR results, as is consistent with the MLR. This similarity suggested that for the conditions examined, the size of the opening had a minimal influence on the burning behaviour, where the crib fire remained fuel controlled. Considering Figures 3.8a and 3.8b, during the

period prior to the smoke layer reaching the cribs, the large opening enabled an initially greater HRR. Once the smoke layer developed, it restricted the combustion of the PIR and phenolic foam cribs and the HRR values realigned.

A smoke layer was not observed during the combustion of the timber cribs in Figure 3.8c, thus both the HRR and the MLR across the varied ventilation conditions appeared to rise and fall in unison. The small opening run had a slightly lower peak heat release rate, 251 kW, and reached this peak after around 2000 seconds. The slightly later peak and a gentler decay in HRR for this experiment may have arisen from the restricted ventilation, which limited the degree of complete combustion. However, as the MLRs, and hence pyrolysis rates, displayed limited variation under the differing ventilation conditions, it may also be concluded that each experiment was slightly over-ventilated, arising, in part, due to the increased timeframes associated with the timber experiments.

The presence of a smoke layer, arising as a function of changing the compartment opening, affected combustion processes. The smoke layer at least in part restricted the peak HRR for both of the investigated insulation foams, resulting in differing combustion efficiencies and hence differing effluent compositions. Through the adjustment of the ventilation, these large-scale experiments changed the combustion mechanics and not just the differing oxygen environments under investigation.

3.3.4 Enclosure Environment

To vary the oxygen availability during each experiment, the ventilation factor was adjusted, enabling the effect of oxygen on large-scale fires to be understood. To confirm that the oxygen environment within the ISO room did indeed vary, oxygen concentrations were monitored and are shown in Figure 3.9.

As Figure 3.9 shows, the smaller opening rendered the lowest oxidative environment across all of the investigated materials. The percentage of oxygen available for the larger opening experiments fell between the small opening and the fully-ventilated experiments, indicating that a range of differing oxidative conditions had successfully been achieved. However, when differing materials with the same imposed ventilation conditions were compared, large differences in the environment being assessed became apparent. For example, the small opening during the timber experiments dropped to 15 % O_2, 3 % lower than the equivalent small opening environment achieved during the combustion of the phenolic foam. It is likely that the combination of the differing HRRs, MLRs and other enclosure conditions like temperature and volumetric flows defined the oxidative environment, factors that cannot be ignored at a large-scale.

Features like the build-up of a smoke layer afforded by the ISO room resulted in several parameters other than the oxygen composition inadvertently varying. To assess the influence of these changes, local conditions within the ISO rooms were monitored. As it was not possible to generate measurements of the local flow conditions near the flame, which would have resulted in significant disruption to combustion behaviour, temperatures recorded within the compartment were used alongside external volumetric flows to describe the conditions within the ISO room. These flows are detailed in Figure 3.10.

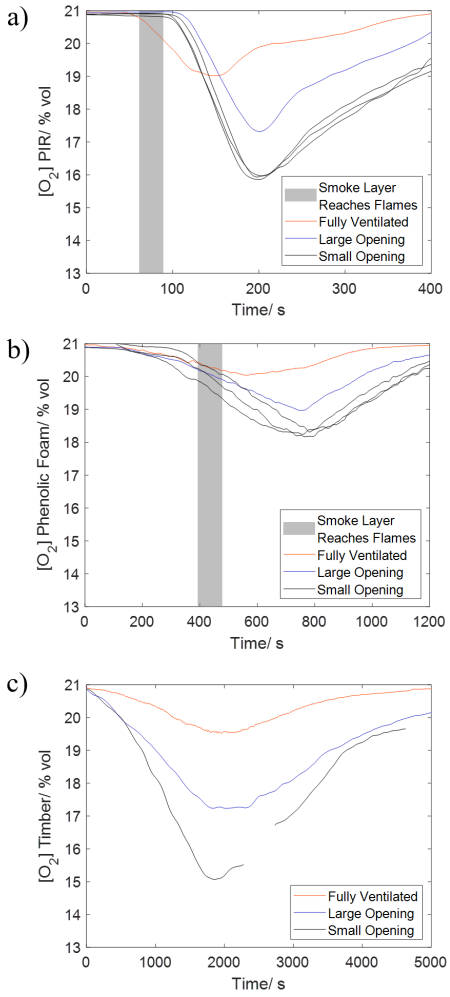

Figure 3.9: The percentage by volume of oxygen (O_2) measured in the effluent for each of the materials investigated in this study: a) PIR, b) Phenolic foam and c) Timber. Note that the highlighted smoke layer region does not apply to the fully ventilated experiments and that the absence of data between 2400 and 2900 seconds for the small opening timber run occurred due to equipment shut off. This data has been smoothed (Gaussian filter, 20 periods).

Pressure probes situated in the centre of the upper and lower openings measured the volumetric flows into and out of the compartment. The larger opening size increased both the airflow into the ISO room for each of the investigated materials. The magnitudes of the flows correlated with the timing of the peak HRRs, with the largest influx of air into the ISO room aligning with these peaks.

The volumetric flows across the compartments varied as a function of opening size. The increased flow out of the compartment for the larger opening experiments is likely to have affected flame spread rates over the cribs. Changes in this flame spread rate will have altered the mixing of fuel and oxygen within the compartment, affecting the rate at which combustion reactions could occur and thus dictating the generation of certain species. The differing flow environments caused by the differing openings highlighted another changeable variable that could not be independently controlled at this larger scale.

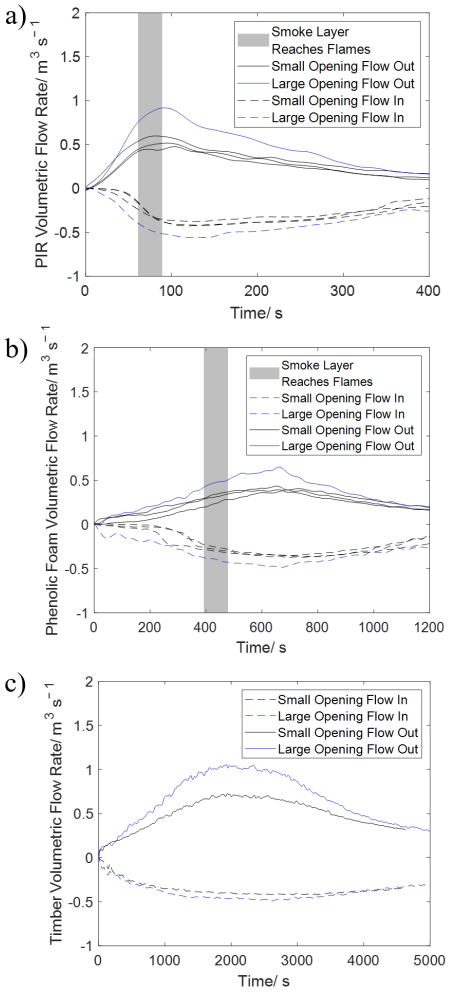

Figure 3.10: The flows into and out of the ISO room measured for each of the materials investigated in this study: a) PIR, b) Phenolic foam and c) Timber. This data has been smoothed (Gaussian filter, 30 periods).

The variance between the opening sizes in the ISO rooms resulted in differing flow rates observed within the opening, with the larger opening having a lower velocity. This variance resulted in a greater volumetric flow rate due to the greater area over which the effluent was exhausting. The greater flow rate for the larger opening experiments was coupled with a lesser reduction of oxygen concentrations, which resulted in a similar HRR to the smaller opening size. This is consistent with the observed MLR behaviours, where the burning rate was found to be similar for both the small and large opening ISO room configurations.

The increased airflows recorded during the experiments conducted with the larger opening were predicted to decrease effluent temperatures within the compartment, these are recorded in Figure 3.11. Temperature within the compartment is another variable that is challenging to independently control at a large scale whilst facilitating an increased oxygen flow into the compartment.

The PIR effluent peaked with a maximum temperature ∼500 K, approximately 100 K

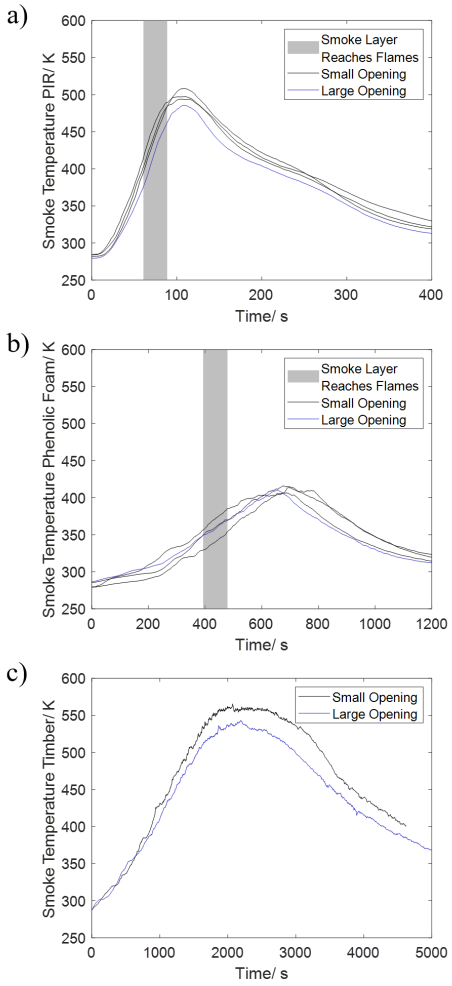

Figure 3.11: The temperature of the effluent exiting the ISO room enclosure for each of the materials investigated in this study: a) PIR, b) Phenolic foam and c) Timber. This data has been smoothed (Gaussian filter, 20 periods).

higher than that recorded for the phenolic foam. This increased temperature correlated with an enhanced airflow into the compartment, leading to an increased combustion efficiency for the PIR. This relationship was also shown during the timber experiments with temperatures exceeding 500 K for a longer duration than the PIR. The increased combustion efficiency afforded by these higher temperatures is likely to have altered the effluent composition, enhancing the proportion of complete combustion products produced by these materials.

Despite these observations, when considering the effluent temperatures recorded for a material in isolation, a similar maximum value was obtained. These findings suggested that ventilation had a minimal effect on the temperature, at least in comparison to the impact arising from the differing chemical composition of the investigated materials.

The variation in the airflows across the cribs highlighted some of the variables that were changing beyond the intended independent variable: the oxygen composition. The HRR

was selected as a proxy to incorporate these changeable variables into a single parameter as the flow rate, temperature and effluent composition are all accounted for when calculating the HRR.

3.4 Emissions

Based on the differing combustion behaviour, indicated by the differing HRRs, differing combustion chemistry was predicted to have occurred. The composition of the effluent being generated was investigated to determine whether changes in the types of chemical species being generated could be detected.

3.4.1 GC-MS

Chemical species were monitored in near real time by FT-IR, with the identities of certain molecules within the effluent being confirmed by complementary GC-MS analysis. Despite the additional speciation afforded by GC-MS, several species had similar retention times, therefore, the GC separation was unable to distinguish, and subsequently identify, every unique species within the effluent. Despite these challenges, Table 3.1 summarises the most prominent species identified through the GC-MS analysis of PIR effluent. Tables A.1 and A.2 contain the results obtained for the other investigated materials and can be found in Appendix A alongside the full total ion chromatograms (TICs), Figures A.6–A.8, for each of these materials.

The GC-MS analysis of the effluent enabled species beyond the standard spectroscopic and paramagnetic analysis of CO, CO_2 and O_2 to be identified. Despite some overlapping peaks being seen in the TICs, several aromatic species were observed in the effluent for each of the materials investigated. The PIR experiments contained 1-naphthyl isocyanide in the effluent, a HCN precursor, aligning with the species reported in literature [102]. As the condensed effluent was collected over the entirety of an experiment, the relative proportions of the species identified by GC-MS varied, suggesting that the differing combustion processes occurred to varying extents over the course of an experiment. It was therefore necessary to use a near real-time analytical technique to track changes in the effluent composition over the course of each experiment.

Table 3.1: The most prominent species identified via GC-MS in PIR effluent collected under three differing ventilation conditions.

Opening	Small 1	Small 2	Small 3	Large	Fully-ventilated
Species detected in descending order of abundance	Benzyl 4-acetylbenzoate	Methylbenzene	Methylbenzene	2,4-bis(1,1-dimethylethyl)-phenol	Benzyl 4-acetylbenzoate
	1,4-Dimethylbenzene	Benzonitrile	Benzyl 4-acetylbenzoate	α,α-Dimethyl-benzenemethanol	1-Naphthyl isocyanide
	Methylbenzene	1-Naphthyl isocyanide	1-Naphthyl isocyanide	-	1,4-Dimethylbenzene
	1-Naphthyl isocyanide	-	-	-	Methylbenzene
	Benzonitrile	-	-	-	α,α-Dimethyl-benzenemethanol

3.4.2 Species Yields

To enable meaningful comparisons to be drawn from the collected data, the yields of the chemical species tracked via FT-IR were quantified relative to the MLR. By default, species assessed via FT-IR were reported in parts per million (ppm), where the readings occurred every three seconds, Equation 3.1 summaries this relationship. To enable useful comparisons of the species being generated during the burning of the cribs, the data required presenting in the form of yields (g g^{-1}).

$$\text{ppm} = \frac{1\,\mu\text{mol (gas)}}{1\,\text{mol (air)}} \tag{3.1}$$

The ideal gas law states that under any given pressure (P), whilst at any given temperature (T), n moles of an ideal gas will always occupy the same volume (V), as illustrated by Equation 3.2. This law holds true, over multiple species, using the molar gas constant (R) and assuming that the gases are ideal. The gaseous species sampled by FT-IR consisted of small pyrolysis and combustion products. Once entrained in air, the small size of these species made them unlikely to interact and as such were assumed to behave in a near ideal manner.

$$P\,(\text{Pa}) \times V\,(\text{m}^3) = n\,(\text{mol}) \times R\,(\text{J K}^{-1}\,\text{mol}^{-1}) \times T\,(\text{K}) \tag{3.2}$$

Throughout the experiments conducted in this chapter, pressure and temperature readings from the effluent stream were acquired. Utilising these values alongside a rearrangement of Equation 3.2 enabled Equation 3.3, for molar volume (V_m), to be formed.

$$V_m\,\left(\text{m}^3\,\text{mol}^{-1}\right) = \frac{V\,(\text{m}^3)}{n\,(\text{mol})} = \frac{R\,\left(\text{J K}^{-1}\,\text{mol}^{-1}\right) \times T\,(\text{K})}{P\,(\text{Pa})} \tag{3.3}$$

To obtain the concentration of each species being monitored, ppm values needed to be converted into masses. A density term (ρ) was introduced to describe the relationship between the mass and volume of a gas. Equation 3.4 describes this density term, with Equation 3.5 showing the relationship between mass and molar mass (M_r).

$$\rho\,(\text{g m}^{-3}) = \frac{m\,(\text{g})}{V\,(\text{m}^3)} \tag{3.4}$$

$$m\,(\text{g}) = n\,(\text{mol}) \times M_r\,(\text{g mol}^{-1}) \tag{3.5}$$

The substitution of Equations 3.2 and 3.5 into Equation 3.4 generated Equation 3.6.

$$\rho\,(\text{g m}^{-3}) = \frac{n\,(\text{mol}) \times M_r\,(\text{g mol}^{-1}) \times P\,(\text{Pa})}{n\,(\text{mol}) \times R\,(\text{J K}^{-1}\ \text{mol}^{-1}) \times T\,(\text{K})} = \frac{M_r\,(\text{g mol}^{-1}) \times P\,(\text{Pa})}{R\,(\text{J K}^{-1}\ \text{mol}^{-1}) \times T\,(\text{K})} \tag{3.6}$$

Equation 3.3 was substituted into Equation 3.6 forming Equation 3.7. At this point the dimensionless ppm reading was converted into a decimal, via division by 1000000, before being added into Equation 3.7 to form Equation 3.8, enabling the calculation of the density of each species of interest.

$$\rho\,(\text{g m}^{-3}) = \frac{M_r\,(\text{g mol}^{-1})}{V_m\,(\text{m}^3\ \text{mol}^{-1})} \tag{3.7}$$

$$\rho\,(\text{g m}^{-3}) = \frac{\text{ppm (decimalised)} \times M_r\,(\text{g mol}^{-1})}{V_m\,(\text{m}^3\ \text{mol}^{-1})} \tag{3.8}$$

Having calculated the density of the species of interest via Equation 3.8, the flowrates reported in Figure 3.10 were used to calculate the mass flow for the species of interest via Equation 3.9.

$$\text{Mass Flow}\,(\text{g s}^{-1}) = \rho\,(\text{g m}^{-3}) \times \text{Flow Rate}\,(\text{m}^3\ \text{s}^{-1}) \tag{3.9}$$

Finally, to enable the mass flow rate data to be comparable, the data had to be linked to the rate of fuel generation. Through the division of the MLR, whilst accounting for the area of the sample, a yield could be obtained. This calculation is outlined in Equation 3.10.

$$\text{Yield}\,(\text{g g}^{-1}) = \frac{\text{Mass Flow}\,(\text{g s}^{-1})}{\text{MLR}\,(\text{g s}^{-1}\ \text{m}^{-2}) \times \text{Sample Area}\,(\text{m}^2)} \tag{3.10}$$

These calculations are much more reliable when the rate of pyrolysis is occurring at a steady state and relies heavily on the assumption that the gases being generated behave in an ideal manner. In reality there will be slight variations from the calculated values; however, the yields enabled comparisons to be made between the crib experiments conducted using the same material.

3.4.3 Hydrogen Cyanide

As detailed in Section 3.3.4, the differing conditions that were established during each experiment varied with the type of material being burned. As such, any comparison between different materials, even with the same opening factor, did not imply that the same compartment conditions had been attained. Therefore, comparisons between the differing ventilation conditions and thus the impact of heat and mass transfer on fire processes, could only be made between experiments utilising the same material.

Given the differing conditions, plotting species yields against time failed to account for the differing environments that each experiment encompassed. As the HRR obtained for each experiment was intrinsically linked to the combined impacts of the smoke layer, volumetric flows, temperature differentials and oxygen concentrations, the effect of HRR on species yields was deemed an appropriate approximation to enable a more meaningful analysis of the data. To avoid noise introduced by numerical differentiation, data were only plotted for the first 90 % of the mass loss for each fuel. To further improve the interpretation of the data, plots were plotted as individual markers, enabling potential outliers to be readily identified.

As the GC-MS results indicated that HCN precursors were being generated during the combustion of the PIR, HCN emissions were monitored for each of the cribs. Figure 3.12 details the HCN yields as a function of the HRR for each of the investigated materials.

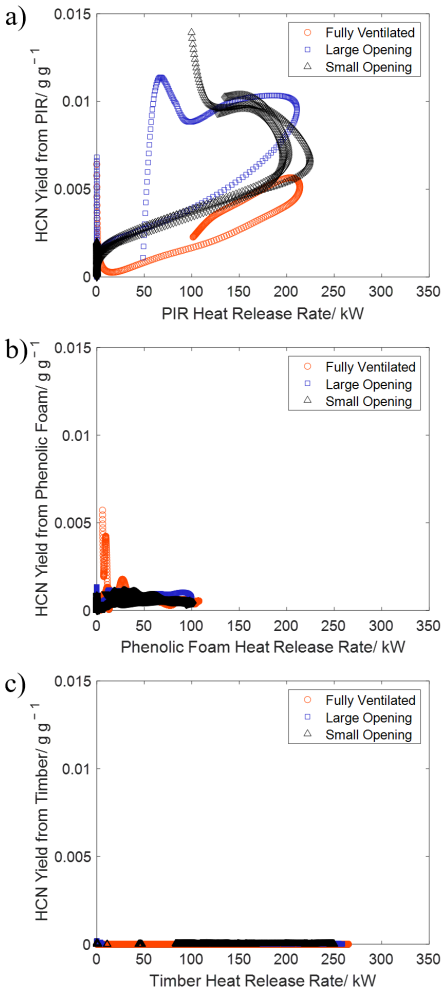

Figure 3.12: The HCN yields measured in the effluent for each of the materials investigated in this study plotted as a function of the obtained HRRs: a) PIR, b) Phenolic foam and c) Timber. This data has been smoothed (Gaussian filter, 60 periods).

The highest HCN yields were associated with the PIR cribs, with two prominent regions being identified. The first occurred at low HRRs, below 10 kW, indicating that HCN was

generated during pyrolysis, prior to flaming combusting becoming established. The second prominent region of an escalated cyanide yield occurred just below the peak HRR of each PIR crib. In these regions, HCN yields initially increased with a rising HRR, eventually plateauing just after the fire peaked in size.

The under-ventilated conditions established within the ISO room caused the HCN yield from the PIR to peak at 0.013 g g^{-1}, around twice the value of the ∼0.005 g g^{-1} recorded for PIR cribs burnt in ISO 9705 rooms in existing literature [104]. Inversely, the fully-ventilated PIR crib peaked at 0.006 g g^{-1}, around half the value of the ∼0.012 g g^{-1} previously reported in literature. These differences are likely to have arisen from the combination of differing crib dimensions and the reduced ability to control external variables like airflow rates and compartment temperatures. Such combined effects resulted in differing MLRs, thus accounting for the observed minor discrepancies.

Comparing the PIR experiments, a larger peak HRR resulted in a lower peak HCN yield. Such observations suggested that increased oxidative conditions reduced the overall proportion of HCN in the effluent during large-scale testing. However, it is hard to explicitly decouple a single variable from the multiple factors that each contributed towards the HRR.

No significant HCN was detected during the phenolic foam or the timber experiments. The yield of 0.0013 g g^{-1} for the larger opening at the peak HRR for the phenolic foam matched small-scale literature values around this limit of detection, approximately 0.001 g g^{-1} [16]. These comparisons may not be representative due to the different scales being assessed; however, the agreement that phenolic foam was not a major generator of HCN emissions correlated. A small HCN yield was detected during pyrolysis under the fully-ventilated conditions, Chapter 5 will probe the pyrolysis products generated by phenolic foam to ascertain the source of these species.

3.4.4 Carbon Monoxide

As detailed in Chapter 1, a second asphyxiant often screened for in fire effluent is CO. The generation of CO indicates that incomplete combustion processes have begun to occur, thus its presence signified a reduction in combustion efficiency. In an attempt to account for the multiple changeable variables, as with the HCN, the CO yields in Figure 3.13 have been plotted against the obtained HRRs.

Both insulation foams generated a much larger peak CO yield than the timber, reinforcing the notion that the timber crib experiments were somewhat all over-ventilated. Each timber experiment showed an increased CO yield after the HRR had peaked. Such increased yields aligned with the observed smouldering phase for the timber cribs after flaming combustion had ceased. Despite these similarities between the timber experiments, the small opening experiment resulted in the greatest CO yield. During this experiment, the radiation from the compartment walls enabled inefficient smouldering processes to occur more readily than under the other two investigated conditions, both of which had greater airflows cooling the timber cribs. Additionally, it is likely that the reduced oxygen availability prevented complete combustion process occurring, resulting in a rise in the CO yield.

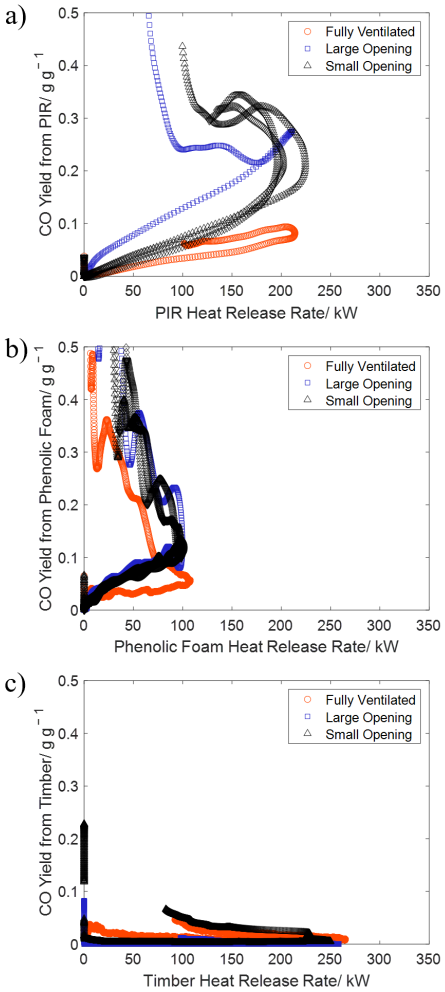

Figure 3.13: The CO yields measured in the effluent for each of the materials investigated in this study plotted as a function of the obtained HRRs: a) PIR, b) Phenolic foam and c) Timber. This data has been smoothed (Gaussian filter, 60 periods).

However, given that several factors varied during these experiments, a clear link between effluent composition and oxidative conditions cannot be made until the changeable MLR is decoupled from the oxidative environment.

For each of the phenolic foam experiments, the CO yield peaked at around 180 kW. As per Figure 3.8, this HRR was sustained during the later stages of an experiment. These findings correlated with the onset of char formation, with charred sticks being oxidised during the later stages of an experiment. Similar observations have been made in literature with the char oxidation of phenolic foam being a significant source of CO during small-scale testing [105]. The fully-ventilated experiment had a lower CO yield during this char oxidation phase. It is likely that the increased oxidative conditions facilitated an increase in the oxidation of CO into CO_2, however supplementary work controlling additional external variables would be required to confirm this relationship.

Like the phenolic foam, a greater peak HRR resulted in a lower CO yield for the PIR,

suggesting that combustion efficiency decreased within the ISO room. However, unlike the phenolic foam, the CO yield for PIR seemed to somewhat stabilise once the HRR had peaked. The PIR sticks formed a char during combustion. This char formed a protective layer around each PIR stick, which is known to preserve an internal layer of intact foam [106]. This preservation correlated with the increased mass of PIR, relative to the phenolic foam, remaining at the end of an experiment. These results indicate that the char formed during the PIR experiments was more resistant to subsequent oxidation reactions than the phenolic foam char. However, it is noted that each material behaved in a slightly different manner, thus, generated a unique set of experimental conditions.

3.4.5 Sulphur Dioxide

As shown in Figure 3.14, the emission of SO_2 was only notable for the phenolic foam experiments with yields ranging between 0.05 g g^{-1} and 0.19 g g^{-1}. These yields are larger than the small-scale yields reported in literature, $\sim$0.03 g g^{-1} but establish SO_2 as an emission associated with phenolic foam [107]. Only trace yields of SO_2 were detected during the PIR and timber experiments.

The four FT-IR absorption bands associated with SO_2, 1350, 1035-1260, 1290-1450 and 2500 cm^{-1} align with the bands produced for many phenolic compounds [108]. As shown in Table A.1, the GC-MS analysis of phenolic foam effluent detected 2,4-bis(1,1-dimethylethyl)-phenol and 2-methylphenol thus, it is plausible that the combined presence of these phenolic species alongside water vapour caused an unintended SO_2 signal. The reported SO_2 yield remained fairly constant no matter the HRR, suggesting that the species responsible was being liberated from the highly aromatic structure of the foam at a similar rate throughout an experiment. Such complexities highlight the issues faced when analysing a complex mixture of species in real time and reinforce the need for multiple analytical techniques as described in Chapter 2.

Once generated, the SO_2 yield remained fairly constant, suggesting that the highly aromatic structure of the phenolic foam enabled sulphur and/or various phenols to be liberated at a similar rate throughout an experiment regardless of the investigated conditions. The constant liberation of SO_2 and/or various phenols, independent of changes in the MLR and HRR, indicated that SO_2 and/or various phenols were generated during pyrolysis, flaming combustion and smouldering combustion to relatively equal extents. The detection of SO_2 during phenolic foam combustion could contribute towards the fire retardancy of the material and thus may explain the lower peak HRR observed when compared to the PIR [109].

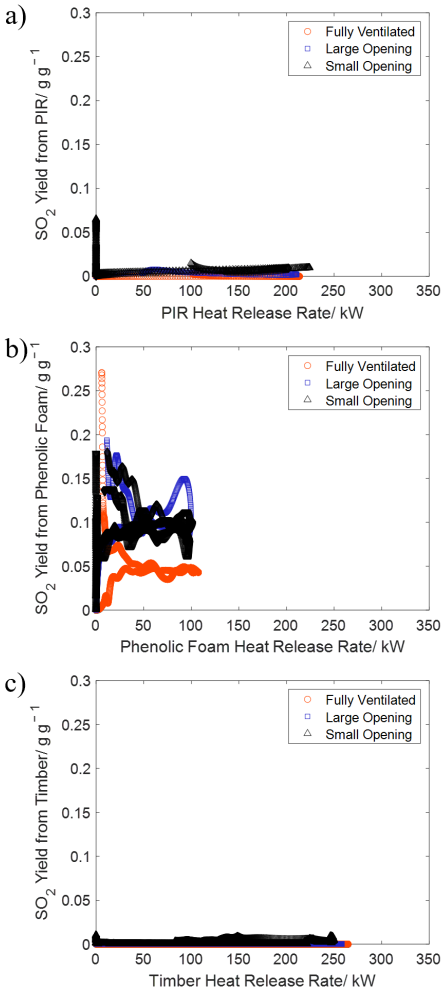

Figure 3.14: The SO_2 yields measured in the effluent for each of the materials investigated in this study plotted as a function of the obtained HRRs: a) PIR, b) Phenolic foam and c) Timber. This data has been smoothed (Gaussian filter, 60 periods).

3.5 Conclusions

The work presented in this chapter aimed to identify, track, and quantify the volatile species produced during the large-scale combustion of cribs comprising different insulation materials: PIR, phenolic foam and timber. Given the amount of analytical information collected during large-scale testing, the manner in which this data is interpreted and thus applied to real-world fire behaviour influences fire safety strategies. Therefore, the volume of heat and mass transfer data being generated from the range of differing outputs requires collation and interpretation in a meaningful way. Large-scale testing enables hazards associated with materials to be identified in a representative manner. Yet, the variability stemming from the reduced ability to control external variables restricts the usefulness of the generated datasets in terms of universal applicability.

Through the use of pressure probes, thermocouples, heated sample lines, cameras and load

cells the external conditions during large-scale fire tests were successfully monitored with a great level of detail. Species identified in the effluent were compared to assess whether the impacts of ventilation at large-scale could be decoupled from the burning of the crib, the thermal environment and the fluid flows in the vicinity of the flames. Whilst emissions data for a range of species was gathered, interpretation of this data needed to consider that the flow of oxidiser could not be independently adjusted without introducing extra variables like a smoke layer. While these data sets were successfully obtained, the variables that were responsible for differences in effluent composition could not be decoupled from one another.

Representative data was obtained as room-scale interactions between the flames and a smoke layer could be generated in a repeatable manner. However, it was the interpretation of the data, particularly the emissions data, that could not be conducted due to the coupling between the MLR and the oxygen demand, preventing the impacts of oxygen on heat and mass transfer during fires from being independently ascertained. Therefore, an experimental methodology at a reduced scale, which enables an increased ability to simultaneously control numerous experimental variables, was considered the next logical step to develop an enhanced means of analysing fire effluent.

This page has been intentionally left blank.

Chapter 4

Improving the Measurement of Pyrolysis Products

"We rarely see the warning signs in the air we breathe."

– Maxïmo Park
Books from Boxes (Our Earthly Pleasures, 2007)

This page has been intentionally left blank.

4.1 Simplifying the Problem

As discussed in the previous chapter, altering a single variable during large-scale fire testing often induces changes in several other variables. Such effects prevent the impacts of heat and mass transfer during fires being linked to the single variable under investigation. In order to explicitly enable one variable to be altered whilst maintaining constant experimental parameters, three key simplifications to the work in Chapter 3 were proposed:

1. Simplify the scale.
2. Simplify the materials.
3. Simplify the process.

The first simplification, the scale, ties back to the information presented in Chapter 2. Several bench-scale effluent generating methodologies exist, enabling an easier management over the external conditions compared to large-scale work. Depending on the apparatus, manipulation of the flowrates, heat fluxes and oxidative conditions can all occur in a near real-time manner, helping to control the test conditions. Thus, the use of a bench-scale methodology was considered to improve the control over the changeable variables present during the analysis of fire effluent.

Simplifying the material refers to the low-density insulation foams trialled in Chapter 3 and the complex variety of aromatic products detected in the effluent via gas chromatography – mass spectrometry (GC-MS). Selecting alternative, simple, synthetic polymeric materials that break down to produce a smaller range of known pyrolysis products will reduce the complexity of the effluent, enabling links between starting materials and combustion processes to be more easily identified.

By focusing on the link between solid and gas phase processes, the final simplification, simplifying the process, notes a shift of focus away from combustion and onto the initial pyrolysis process. Before introducing the complexity of the differing extents of oxidation that occur during combustion, the identity of the gas phase fuel must be known. The study of pyrolysis can therefore provide information on when a flammable mixture may be generated, increasing our understanding of phenomena such as flame spread and ignition [110].

4.1.1 Simplifying the Scale

As discussed in detail during Chapter 2, bench-scale flammability apparatuses, such as the Fire Propagation Apparatus (FPA), can be used to collect emissions data under differing thermal and oxidative conditions [111]. Preliminary work utilising such methodologies have identified the potential to scale recorded emission yields to larger and more complex fire scenarios [93].

The standard means of controlling the FPA, ASTM E2058-19, like many bench-scale

apparatuses requires the use of a constant heat flux. To assess the suitability of such a methodology to investigate heat and mass transfer processes, a heat flux of 35 kW m^{-2} was selected to initially assess opaque black sheets of PMMA (100 mm × 100 mm × 5 mm, 55.94 g). Samples of PMMA were placed onto a pedestal connected to a load cell situated within the combustion chamber of the FPA. A quartz tube (435 mm high, outer diameter 174 mm, inner diameter 164 mm) was placed over the sample. Initial experiments were completed with and without a pilot flame (60 % air, 40 % ethylene), to enable a comparison between pyrolysis and flaming combustion behaviour. These initial experiments were conducted in triplicate and the obtained mass loss rates (MLRs) and heat release rates (HRRs) are shown in Figure 4.1.

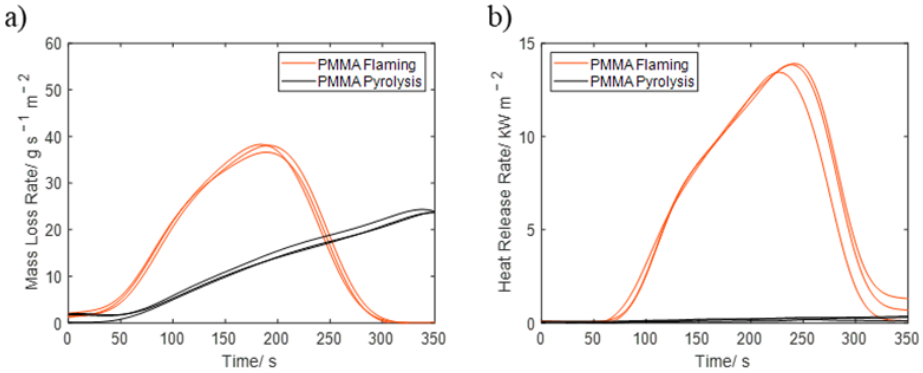

Figure 4.1: a) The mass loss rates (MLRs) and b) The heat release rates (HRRs) obtained when PMMA was subjected to a 35 kW m^{-2} heat flux with and without a pilot flame using the standard means of controlling the FPA, ASTM E2058-19.

Figure 4.1a shows that using the FPA with a constant heat flux, as per the standard, results in the MLR changing throughout an experiment. For the experiments that occurred without a pilot flame, the MLR gradually increased over the course of the sampling period. As the surface of the sample heated up during these pyrolysis experiments, heat transfer into the sample established thermal gradients throughout the solid PMMA, enabling different pyrolysis mechanisms to occur. Such gradients are dependent on the physical and geometric properties of the sample with both factors impacting the heat transfer into the sample and the resultant mass transfer of pyrolysis products out of the sample.

Across the depth of the sample, differing concentration gradients of diffused species like oxygen and produced species originating from PMMA (monomers/ dimers) will be present, depending on the heat transfer to the sample. Such gradients will impact the rate at which pyrolysis products are liberated from the surface of the PMMA, thus contribute, in part, to the MLR of the sample. These thermal gradients are not present in the smaller samples used during TGA analysis; thus, it is plausible that differences in effluent composition exist between studies conducted with microscale samples compared to those conducted with comparatively larger bench-scale methodologies. Furthermore, as the thermal gradients within the samples varied throughout the experiments following ASTM E2058-19, it was therefore likely that the effluent composition was also varying with time.

When a pilot flame was present during the experiments presented in Figure 1, the ignition of a sample caused an uncontrolled escalation in the MLR. As the flame established itself

over the surface of the polymer the MLR continued to increase, albeit at a slower rate, before burnout led to a rapid decline in MLR at ∼t = 220 s. The standard means of controlling the FPA cannot control or maintain a steady pyrolysis rate. Either the presence of a pilot flame enables ignition and the MLR gradually rises until burnout or the entire sample is slowly warmed when a pilot is not present. The extent of these heat feedback cycles is driven by the oxidative environment, where processes like smouldering and flaming combustion generate additional heat under an abundance of oxygen. Thus, the unmodified FPA is unable to facilitate the independent assessment of the effect of oxidiser on effluent composition.

As the pyrolysis rate dictates the availability of the gaseous fuel, an increased MLR enabled more fuel to be available for oxidative processes. During the flaming combustion experiments, this effect established positive heat feedback cycles, causing the MLR to rise dramatically. Around the peak MLR, flames could be seen above the quartz tube, as per Figure 4.2, indicating that not all the species being produced during pyrolysis were being fully oxidised. This incomplete oxidation suggested that the effluent had become fuel-rich, resulting in a reduction in combustion efficacy. After the flames were observed above the quartz tube, the MLR for the flaming combustion experiments rapidly declined, with the flames eventually quenching. These uncontrolled oxidative processes prevented a steady effluent stream from being generated, necessary for representative emissions sampling.

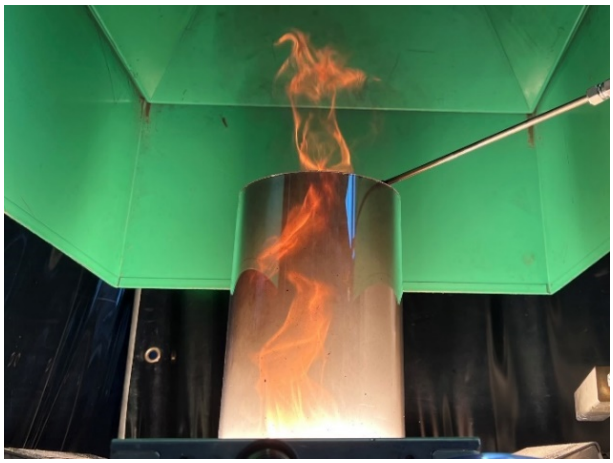

Figure 4.2: The oxidation of species beyond the quartz tube in the FPA. Such external flames are often uncontrollable and suggest that the effluent comprises of a significant proportion of unburnt species.

The observation of flames above the quartz tube in Figure 4.2 correlated with the peak HRR in Figure 4.1b. As with the MLR, the HRR for the flaming combustion experiments did not stabilise, gradually rising to a peak. The pyrolysis experiments did not result in oxygen being consumed, thus, these experiments all had a HRR of effectively 0 kW m^{-2}. Overall, these results highlight the main challenge with the standard means of controlling the FPA: it cannot generate a constant, unchanging, effluent stream for analysis. To enable such analysis, the pyrolysis rate must be controlled and a steady MLR must be achieved. A steady state pyrolysis rate would also allow sampling techniques to be deployed over longer timeframes, increasing the range of analytical techniques that could be used for

effluent analysis. It was therefore proposed that the FPA should be modified to enable a greater degree of control over the heat and mass transfer processes occurring during fire scenarios.

4.1.2 Simplifying the Materials

Unbranched, straight-chain polymers are chemically simplistic materials, often used to produce plastics with predictable properties and behaviours. These polymers consist of one or two monomer units bound in a repetitive structure. The simplest of these materials are linked through a central backbone, where the π-bonds only feature in specific locations on the monomer, enabling a greater degree of control over the polymerisation process.

The synthetic polymer polymethylmethacrylate (PMMA) has been studied extensively across the fire literature. PMMA is a simple material that burns well, thus, was selected for analysis. This polymer, commonly referred to as acrylic, consists of a single monomer species, methyl methacrylate (MMA), bound in a repetitive straight-chain structure. The lack of both cross-linking and monomer variation within PMMA, enables predictable pyrolysis pathways and thus results in the accurate estimation of effluent composition. When subjected to an escalated heat flux, initially monomers are lost from the end of the PMMA polymer chain in a predictable manner via a process called chain-end scission [112]. A plausible mechanism for this process is outlined in Figure 4.3.

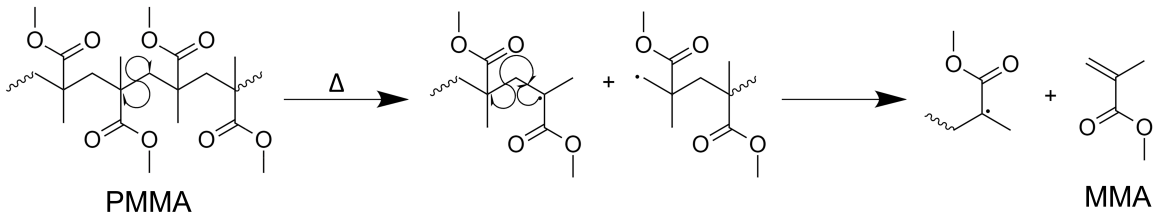

Figure 4.3: An example of an initial scission mechanism during the thermal degradation of the polymer PMMA to form the monomer MMA. The initial cleavage generates two unstable radical species, enabling further decomposition [112]. Additional scission is hypothesised to happen preferentially from the end of the polymer chain.

As a sample heats up, internal thermal gradients are established throughout the sample. Under these elevated thermal conditions, PMMA chains situated near the surface of the plastic are more likely to split at random intervals, random scission, producing a mixture of monomers and oligomers. As a result of the thermal gradient, a lower temperature environment is therefore established deep within the sample, away from the surface of the PMMA. These slightly lower temperatures will preferentially favour chain-end scission, resulting in the predictable generation of single MMA monomers. The simplistic pyrolysis products produced by PMMA, alongside the potential for minor, yet traceable, variation, rendered it a good material to investigate how heat transfer within a sample directly impacts mass transfer processes.

Polystyrene (PS) is another example of a simple straight-chain synthetic polymer comprising

of a single monomer species: styrene. Unlike PMMA, the pyrolysis of PS is slightly more complex; random scission predominates, resulting in the generation of a mixture of monomers, dimers and trimers [18]. Despite this reduced predictability, the pyrolysis of PS has been linked to the local oxygen availability, with the activation energy to trigger pyrolysis being 75 kJ mol^{-1} higher under inert environments [113]. As monomer formation from PS is known to vary with oxidative conditions, it was therefore concluded that PS would also be a suitable material to investigate mass transfer in fire effluent.

Both PS and PMMA have been shown to form their respective monomers when subjected to external heat fluxes. Knowing the identities of the species that were likely to be generated in the effluent enabled analytical techniques to be selected to target the identification of these specific monomer species. Additionally, timber was selected as a material for investigation as its charring properties were predicted to facilitate control over the MLR.

4.1.3 Simplifying the Processes

Prior to oxidation by a flame, a fuel must transition from the condensed (solid/ liquid) phase into the gas phase. This process can occur via sublimation or evaporation but most commonly as a result of chemical bonds cleaving during a series of reactions collectively termed pyrolysis processes. As these processes generate the volatile species that eventually interact with the flame, it is imperative that pyrolysis products are explicitly identified and quantified whenever possible.

If a species has not been identified after pyrolysis, it becomes challenging to identify it post oxidation, having already passed through the flame envelope. As the composition of the effluent is constantly changing based upon the pyrolysis rate and the position of the flame, care must be taken when interpreting analytical data. The measurement of product yields may not relate to the conditions at the sample surface as external variables alongside the sampling time are likely to have caused the fire dynamics to change since the measurement began. Removing the flame and creating a constant effluent stream to identify the initial pyrolysis products being generated was deemed an appropriate strategy to initially simplify these complex processes.

Removing the ignition source used in Chapter 3 alongside maintaining a MLR below the auto ignition threshold for the selected simplistic materials ensured that only non-flaming processes could occur. In the case of the synthetic materials, their simplistic structures enabled pyrolysis to be the dominant process under investigation.

4.2 Modifying the FPA

The controllable tungsten lamps of the FPA enable the supplied heat flux to be modified as a function of time. When considered alongside the ability to monitor the MLR in real time and the ability to observe a sample throughout an experiment, the FPA had the potential to be modified to control the MLR of a sample.

4.2.1 PID Controllers

Obtaining a constant MLR during combustion indicates that the pyrolysis rate has stabilised under the imposed environmental conditions. When this occurs, the controlled MLR prevents positive feedback cycles from causing the HRR to fluctuate; enabling the effects of the remaining environmental factors, specifically the oxygen concentration, on the effluent to be assessed.

Decoupling the MLR from the oxygen composition in this manner requires a methodology to be able to respond directly to changes in the heat feedback cycles, preventing the MLR from escalating uncontrollably. The benefits of the FPA, identified in Chapter 2, extended beyond the presence of a load cell and the generation of an undisturbed effluent flow, as the lamps may be altered throughout an experimental run to simulate a changing combustion environment. Once the voltage supplied to the lamps is modified, the change in the heat flux experienced by the sample is near instantaneous due to the shorter cooling period associated with the lamps versus a more traditional heater element. The linking of the lamp outputs to the mass loss reading from the load cell therefore offers a means of adapting the FPA to facilitate a steady state MLR.

To enable a controlled MLR during pyrolysis, the standard FPA experimental procedure (ASTM E2058-19) was modified to include a proportional integral derivative (PID) controller. The PID controller facilitated an automatic adjustment of the voltage sent to the FPA lamps based upon the live mass readings received from the inbuilt load cell [114]. The differing voltages received by the lamps resulted in differing heat fluxes being supplied to the sample, enabling the MLR to be controlled as a function of sample mass.

PID controllers drive a system towards a target value via control loops. Each iteration accounts for the difference between the calculated MLR and the desired MLR with an error, $e(t)$, using the function $u(t)$ to cumulatively represent these errors. Equation 4.1 summarises this relationship.

$$u(t) = K_p e(t) + K_i \int_0^t e(t')\,dt' + K_d \frac{de(t)}{dt} \tag{4.1}$$

Each of the three adjustable coefficients in Equation 4.1 were altered to control the overall output voltage sent to the FPA lamps. The proportional term, K_p, represented the error based upon the difference between the current and target mass values, with the integral

term, K_i, accounting for the sum of any error from the proportional term. The final term, the derivative term, K_d, was used to slow the rate at which the overall correction factor was applied.

Preliminary experimental work was conducted to optimise the coefficients for K_p, K_i and K_d. Coefficients were chosen based on the time taken to reach the desired MLR with the aim to decrease the oscillations occurring, hence stabilising the MLR. Figure 4.4 shows how an early iteration of the PID controller repeatedly ended up momentarily enabling and disabling the lamps, causing oscillations in the calculated MLR. Such a controller was deemed unresponsive and the error coefficients were adjusted to eventually stabilise the MLR at the target value.

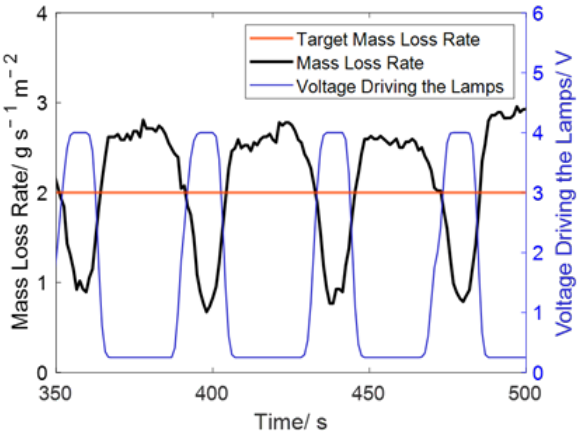

Figure 4.4: An early iteration of the FPA PID controller. Here the PID controller was being optimised for a 2 g s^{-1} m^{-2} mass loss rate. The values 5, 0.015 and 4 were selected for K_p, K_i and K_d respectively. Note that the lamps fluctuated between full power (4 V) and off (0.5 V).

The response time of the lamps granted by the PID control parameters in Figure 4.4 prevented the MLR from being adjusted in real time. The large overshoot beyond the target MLR resulted in the lamps switching off whilst the controller waited for the MLR to decrease back towards the target value. This delay caused oscillations in the MLR as the PID controller once again overshot the target MLR during the decline, resulting in a delay before the lamps were switched back on. The following iteration of the PID controller reduced the value of K_p in an attempt to mitigate this response. Figure 4.5 details four additional iterations of the controller, highlighting the complex effect of changing specific parameters.

As shown across Figure 4.5, decreasing the value of K_p below five did reduce the extent of the oscillations in the MLR. Within each figure, the voltage driving the lamps stayed within the active range (0.5 to 4 V) over the whole controlled MLR period, although it did max out briefly in Figure 4.5a, demonstrating that the lamps were making minor adjustments to maintain the controlled MLR. Decreasing K_i between Figures 4.5b and 4.5c decreased the overall importance of any error associated with the K_p term. As the K_p term had been optimised first, adjusting for any error associated with it was now of a reduced importance, therefore, decreasing K_i yielded a smoother MLR. Further iterations

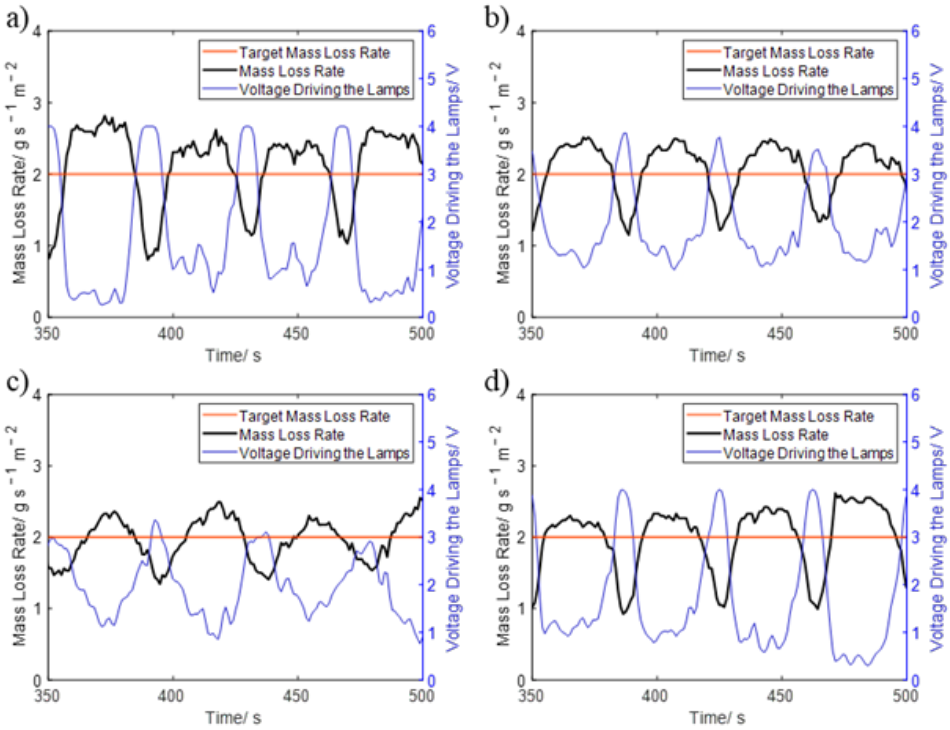

Figure 4.5: Four intermediate versions of the PID controller used to control the FPA lamps. The parameters for each of the plots are as follows: a) $K_p = 3$, $K_i = 0.015$ and $K_d = 4$, b) $K_p = 2$, $K_i = 0.015$ and $K_d = 4$, c) $K_p = 2$, $K_i = 0.01$ and $K_d = 4$ and d) $K_p = 2.5$, $K_i = 0.01$ and $K_d = 4$.

altered the K_d term, which increased the response of the controller to resist rapid changes in the MLR. The results obtained from the finalised PID controller are shown in Figure 4.6.

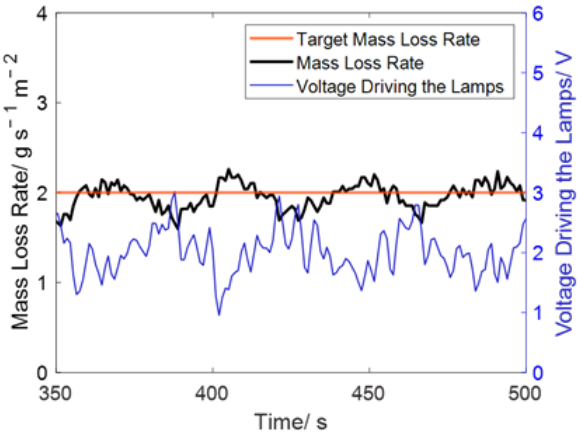

Figure 4.6: The final iteration of the PID controller with the parameters $K_p = 2$, $K_i = 0.01$ and $K_d = 8$, optimised for a 2 g s^{-1} m^{-2} mass loss rate.

The low degree of fluctuation in the voltage driving the lamps demonstrated that the

controller had been progressed to retain a greater level of control throughout an experiment. There was still room to further develop and optimise the controller, as evidenced by the minor fluctuations in MLR, however these parameters were adequate to determine whether the controlled MLR provided by the FPA could provide an additional insight into pyrolysis processes. A similar iterative process was needed to be conducted to determine the parameters for differing target MLRs.

The effectiveness of the applied parameters was determined based on the time taken to reach a steady state, the extent of the oscillation whilst at this steady state and the range of voltages sent to the lamps. After preliminary experimental work involving over forty iterations, the values 2, 0.01 and 8 were selected for K_p, K_i and K_d respectively. These values were found to enable a controlled MLR of 2 ± 0.52 g s^{-1} m^{-2} and were verified for a range of materials including PMMA and PS. The error was determined through the calculation of the standard error of the mean.

4.3 Controlled Mass Loss Rate Experiments

The materials selected to assess whether the FPA could be successfully used to control the MLR were chosen based upon their physical properties. In addition to the non-charring PMMA samples used during the ASTM E2058-19 experiments, melting PS beads (contained in a circular foil dish, 100 mm in diameter, 5 mm in depth, 31.32 g) and charring timber (*Picea abies*, 100 mm × 100 mm × 20 mm, 128.69 g) samples were obtained. These three differing responses to an imposed heat flux were deemed an appropriate range of properties to assess the developed methodology.

4.3.1 Methodology

Each sample, with the rear surface covered in foil, was individually placed onto a load cell situated within the housing of the FPA. A quartz tube (435 mm high, outer diameter 174 mm, inner diameter 164 mm) was placed over the sample and the FPA lamps were set to gradually increase the heat flux provided to the sample (0.02 kW m^{-2} s^{-1}, 60 s). After 60 seconds the PID controller was initiated enabling the supplied heat flux to be varied by altering the voltage sent to the lamps. The PID controller was set to enable a controlled MLR of 2 g s^{-1} m^{-2} over a set time period (800 s). An oxidiser flow (100 L s^{-1}, 0 %, 10 %, or 21 % oxygen with the balance being nitrogen) was maintained throughout each experiment, preventing the localised accumulation of pyrolysis gases. After the MLR had stabilised (200 s), each experiment was triplicated. 200 seconds was selected as it was found to enable each of the materials to reach the desired mass loss rate with minimal mass fluctuations.

To assess the composition of the effluent generated during the controlled MLR experiments, two separate analytical techniques were simultaneously used. In addition to the exhaust duct, two different heated sampling lines (453 K), situated above the quartz tube, withdrew effluent. The first line passed effluent into a Fourier-transform infrared spectroscopy (FT-IR) cell (Gasmet, Vantaa, Finland) while the second passed the gases through a condenser (dry ice/ acetone, 195 K). Effluent was condensed to yield a crude colourless liquid, containing species with boiling points above 195 K. Figures 4.7 and B.2 detail the complete experimental setup.

The near real-time temporal measurements facilitated by the FT-IR enabled the effluent to be sampled every four seconds, however, only predetermined species could be monitored based upon comparisons to the predefined reference spectra. FT-IR analysis was conducted using a Gasmet DX4000 portable gas analyser. Produced IR spectra were analysed using the supplied software (Calcmet V2005.100, Gasmet Technologies Ltd., Vantaa Finland) alongside calibrated reference samples. Each spectrum was analysed across a spectral range (595 – 4240 cm^{-1}) with the resolution (8 cm^{-1}) achieved via a thermoelectrically cooled MCT detector coupled with an antireflection (ZnSe) beamsplitter. Gas samples were filtered (particulate, 2 µm) before entering the sample cell (0.4 L, 453 K). The path length (250 cm) proved adequate to maintain the sampling frequency.

To complement the FT-IR analysis, a second sampling line passing to a condenser, con-

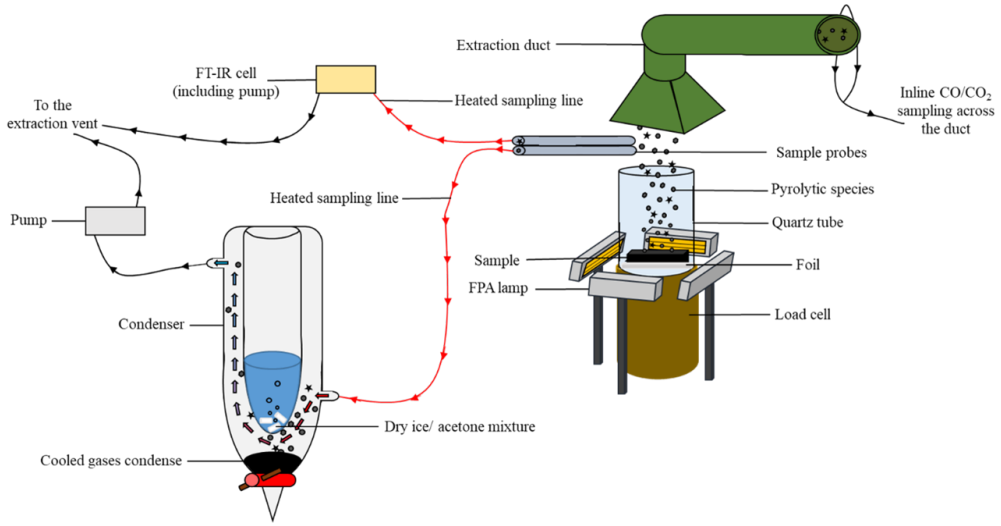

Figure 4.7: The modified FPA experimental setup. Two separate heated sampling lines in addition to the extraction duct sampled effluent generated by the modified FPA apparatus. Condensed effluent was subsequently extracted for GC-MS analysis.

densed species out of the gaseous phase, ahead of ex-situ GC-MS analysis. Upon completion of an experiment, the crude condensate was washed with dichloromethane (DCM, 3.25 mL) to remove condensed water. The organic layer (∼4 mL) was retained for GC-MS analysis. GC-MS analysis was carried out using a Thermo Trace 1300 GC with an ISQ LT single quadrupole MS (Thermo Fisher Scientific, Massachusetts, USA), in splitless mode equipped with an AI 1310 liquid autosampler (Thermo Fisher Scientific, Massachusetts, USA), using a TraceGOLD TG-5 column (30m × 0.25mm × 0.25 µm), held at 308 K for 600 s before rising to 553 K at 273 K min^{-1}. A helium carrier gas was flowed at 0.8 mL min^{-1}. The MS had a 573 K ion source temperature and was operated in positive electron ionisation mode, scanning m/z 40 – 400.

4.3.2 Mass Loss Rate

Once the PID controller initiated, each material had its MLR stabilised by the modified means of controlling the FPA at 2 ± 0.52 g s^{-1} m^{-2}. This reported error (± 0.52 g s^{-1} m^{-2}) was the largest error determined during one PS experiment, obtained through the calculation of the standard error of the mean. The average errors of 0.13, 0.20 and 0.09 ± 0.52 g s^{-1} m^{-2} were obtained for PMMA, PS and timber when averaged across all of the investigated oxidative conditions.

These results are shown in Figure 4.8, with the reported error reflecting the slight material fluctuations. The error reported for the PS runs was calculated from 220 seconds onwards as some samples were still in the process of melting. The error also omits the anomalous peak MLR of 3.48 g s^{-1} m^{-2} that occurred during one of the PMMA trials. It is hypothesised that this peak occurred as a result of mass falling from the load cell rather than a sudden increase in the rate of pyrolysis.

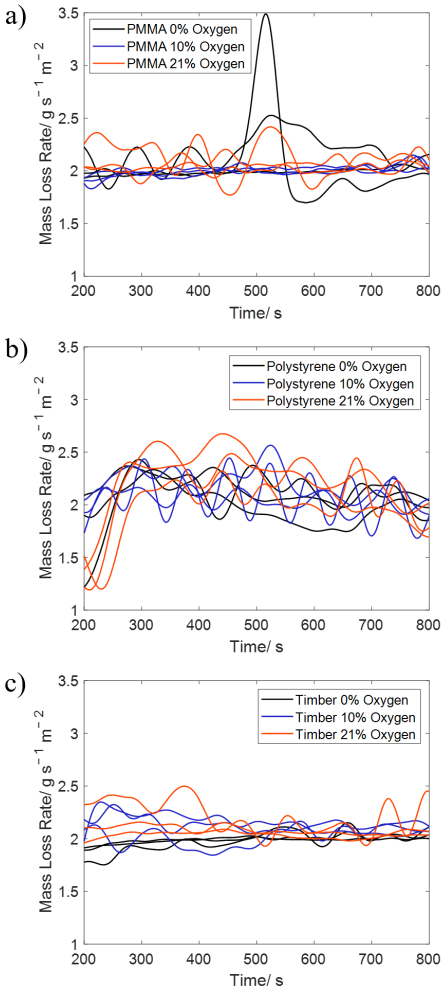

Figure 4.8: Smoothed (Gaussian filter, 80 periods) mass loss rate (MLR) data for a) PMMA, b) polystyrene and c) timber samples under each of the three investigated oxygen environments (0 %, 10 % and 21 % O_2).

Differing material properties resulted in differing responses to the PID controller, explaining the observed variation between the melting/ non-charring synthetic polymers and a charring sample like timber. Once the PS had melted, bubbles formed on the surface of both the PS and PMMA. When these bubbles burst, pyrolysis gases were released, resulting in brief periods of an escalated MLR. These periods of discrete mass loss could not be managed by the PID controller resulting in slight fluctuations in the set MLR.

Comparing the MLR of the PMMA samples pyrolyzed in Figure 4.8a to Figure 4.1a, it can be concluded that the modified FPA had successfully altered the MLR obtained under standard FPA procedures. Rather than having an increasing MLR controlled by internal heat transfer, the stabilised MLR, and by extension pyrolysis rate, was predicted to enable a stable composition of effluent for analytical sampling. As such, the species generated via the alternative means of controlling the FPA were assessed to determine whether mass transfer processes could be investigated utilising this approach.

4.3.3 GC-MS Analysis

As shown in Figure 4.8, the MLRs for each of the investigated materials were constant, relative to slight fluctuations, over the course of each experiment. It was therefore assumed that the effluent collected by the condenser during each steady period reflected the average effluent composition produced over the entirety of each experiment. Thus, quantification via GC-MS could be obtained by dividing any total species yields by the total mass lost from the sample over the steady period.

This GC-MS data was quantified via calibration against responses from known reference compounds. Pure samples ($\geq$99 %) of 2-methoxyphenol and the monomers MMA and styrene and were diluted in DCM to form five different solutions with concentrations ranging from 0.01 – 0.25 mol dm^{-3}. The resultant calibration curves, shown in Figure B.1, enabled peak areas to be converted into product concentrations and subsequently species yields.

For each of the investigated materials, total ion chromatograms (TICs) were obtained. Each peak within each TIC had a mass spectrum recorded, enabling speciation via database matching. Any species with a match greater than 40 % has been included at the top of each of the TICs shown in Figures 4.9, B.3 and B.4 alongside the relevant retention time (RT). The TIC for PMMA is shown here, further TICs can be found in Appendix B.

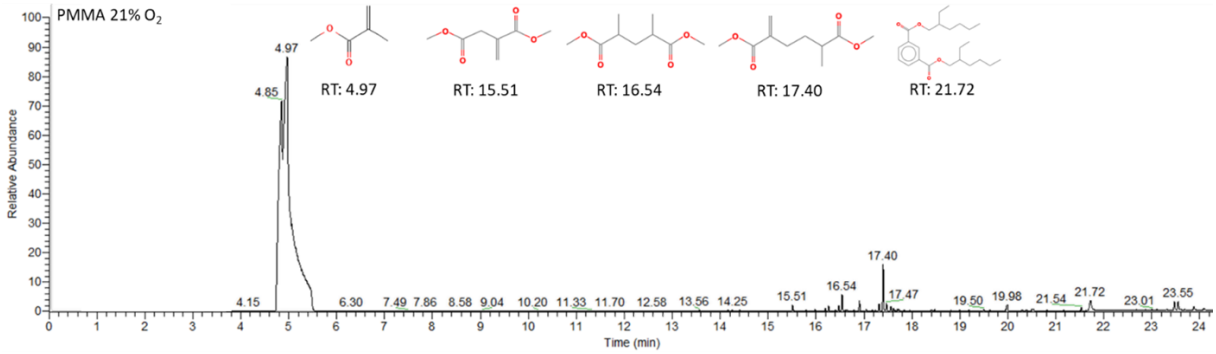

Figure 4.9: The total ion chromatogram (TIC) obtained during the pyrolysis of PMMA under 21 % oxygen. The dominant peak eluting at 4.97 minutes was identified as the monomer MMA.

MMA, styrene and 2-methoxyphenol were identified as major constituents of the effluent condensed out during the pyrolysis of PMMA, PS and timber respectively. Once a peak in Figures 4.9, B.3 and B.4 had been selected, its identity was confirmed through the analysis of the MS fragmentation pattern and the area under the peak was integrated. These peak areas were subsequently quantified via external standards (Figure B.1 in the appendix) and the obtained concentrations are shown in Figure 4.10.

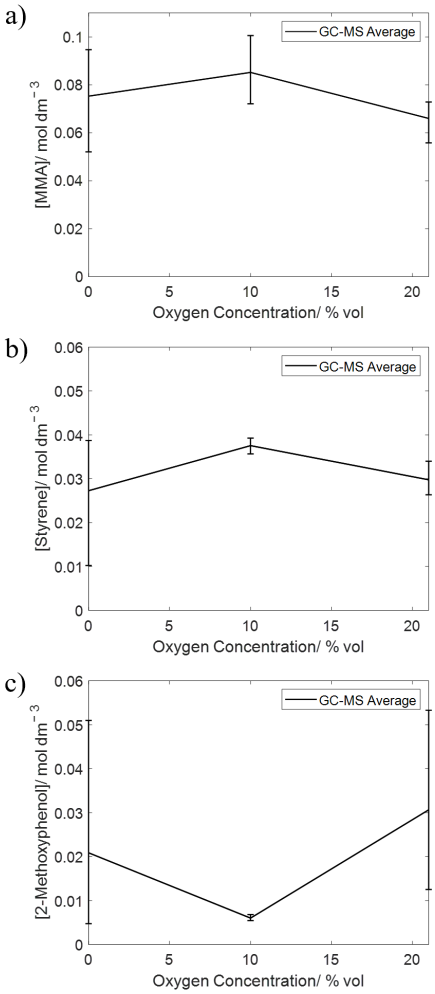

Figure 4.10: The average concentrations of a) MMA, b) styrene and c) 2-methoxyphenol recorded via GC-MS, obtained during the pyrolysis of PMMA, polystyrene and timber under three different oxygen environments (0 %, 10 % and 21 % O_2).

Comparing the three species in Figure 4.10 suggested that the formation of MMA from PMMA was the most favourable pyrolysis process. However, yields had to be obtained to account for the differing molar masses of the species being recorded to enable meaningful comparisons to occur. To calculate the density of the species, Equation 4.2 was initially used.

$$\rho\,(\mathrm{g\,dm^{-3}}) = C\,(\mathrm{mol\,dm^{-3}}) \times M_r\,(\mathrm{g\,mol^{-1}}) \tag{4.2}$$

As summarised by Equation 4.3, the calculated densities were converted into masses via multiplication by the added volume of DCM (0.325 $\mathrm{dm^3}$).

$$\text{Mass (g)} = \rho\,(\mathrm{g\,dm^{-3}}) \times V\,(\mathrm{dm^3}) \tag{4.3}$$

The obtained masses were divided by the total sample mass loss over the course of a run during the timeframe that the condenser sampling line was switched on (600 s), enabling the calculation of each product yield (g g^{-1}). Equation 4.4 summarises this calculation.

$$\text{Yield (g g}^{-1}) = \frac{\text{Mass (g)}}{\text{Sample Mass Loss (g)}} \tag{4.4}$$

4.3.4 FT-IR Analysis

As discussed in Chapter 2, FT-IR analysis works on the principle of identifying species based upon the absorption bands present in the effluent. An example of an FT-IR spectrum obtained during the PMMA experiments is shown in Figure 4.11. This figure shows three dominant bands, 1152 cm^{-1}, 1355 cm^{-1} and 1750 cm^{-1}, amongst some other, less unique, alkyl bands.

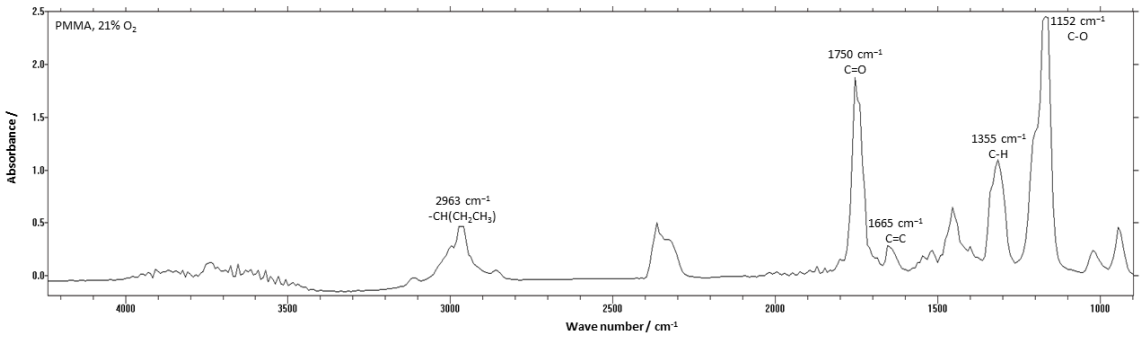

Figure 4.11: An FT-IR spectrum obtained during pyrolysis of PMMA. Prominent bands have been allocated to alkyl, carbonyl and alkene stretching and bending modes.

Focusing on the bands at 1152 cm^{-1} and 1750 cm^{-1}, suggested that a species with an ester linkage was highly prevalent in the effluent. Comparisons between Figure 4.11 and spectra obtained during synthesis of PMMA suggested a strong resemblance to the MMA spectrum [115, 116]. It was likely that the bands in Figure 4.11 were triggered by MMA, or a similar oligomer with the same ester linkages. Consulting the TIC in Figure 4.9, it could be seen that the prominent peak eluting after ∼4.9 minutes had ions present at 101, 69 and 41 m/z, corresponding to the fragmentation pattern and molecular mass of the monomer MMA [116]. Two independent techniques (GC-MS and FT-IR) both identifying MMA as the main pyrolysis product reinforced the interpretation of the FT-IR spectra. However, the TIC enabled some secondary products, at much lower concentrations, including dimethyl 2-methyl-5-methyleneadipate (RT 17.4 in Figure 4.9) to be identified. This species, formed by linking two MMA molecules has been shown to form during the polymerisation of MMA, further cementing the MMA peak assignment [117].

The majority of the species identified via GC-MS had similar functional groups to MMA and as such would be expected to contribute towards the signal recorded by the FT-IR. However, the GC-MS confirmed that on average the main pyrolysis product, MMA, accounted for

99.1 % of the species extracted from the effluent. This value could subsequently be used to adjust the yields recorded by the FT-IR, accounting for the contribution to the signal provided by the oligomers.

A full description of the calculations used to obtain species yields from FT-IR data is outlined in Chapter 3, Equations 3.1 to 3.10. A broadly similar approach was utilised here however it became necessary to calculate the flowrate of air through the experimental setup and through the sampling lines as this was now a control variable. Equation 4.5 details the calculation of this flowrate, which enabled the mass flow for the species of interest to be obtained.

$$\text{Flow Rate } (\text{m}^3\ \text{s}^{-1}) = 100\,\text{L}\,\text{min}^{-1} = \frac{100\,\text{L}}{60\,\text{s}} = 1.67 \times 10^{-3}\,\text{m}^3\,\text{s}^{-1} \tag{4.5}$$

A summary of the overall yield calculations based on mass flows ($\dot{m}$) is given in Equations 4.6 and 4.7. For these equations $\dot{V}$ was the volumetric flow rate, R represented the molar gas constant, M_r referred to the molecular weight of the species being monitored, T was the temperature of the effluent stream and P_{atm} referred to atmospheric pressure.

$$\dot{m}_{\text{Species}} = \frac{\dot{V}[\text{Species}]P_{\text{atm}}M_r}{RT} \tag{4.6}$$

$$\text{Yield}_{\text{Species}} = \frac{\dot{m}_{\text{Species}}}{\text{MLR}} \tag{4.7}$$

4.3.5 Effluent Composition

Assessing whether a stable stream of pyrolysis products was generated by the modified means of controlling the FPA required multiple analytical approaches. Both techniques, the FT-IR and the GC-MS analysis, had their own specific merits and flaws. The enhanced speciation provided by the GC-MS analysis was somewhat limited by lack of temporal measurements. While in contrast, the FT-IR enabled the effluent composition to be probed in near real-time, however the analysis failed to accurately distinguish between signals produced by similar species. Combining the different techniques reduced their individual limitations, enabling a greater understanding of mass transfer processes occurring during fires.

The overlapping bands produced by similar compounds was most noteworthy during the analysis of the aromatic species generated during the pyrolysis of the timber and the PS. For PS, the GC-MS analysis presented in Figure B.3, was found to contain a high proportion of styrene, methylstyrene and methylbenzene. Figure 4.12 shows FT-IR reference spectra for these and similar compounds, highlighting their similarity [118].

Each of the species in Figure 4.12 had bands present in three distinct regions, $\sim$3000 cm^{-1}, denoting an aromatic C-H stretch, $\sim$1500 cm^{-1}, indicative of aromatic C-C stretching and

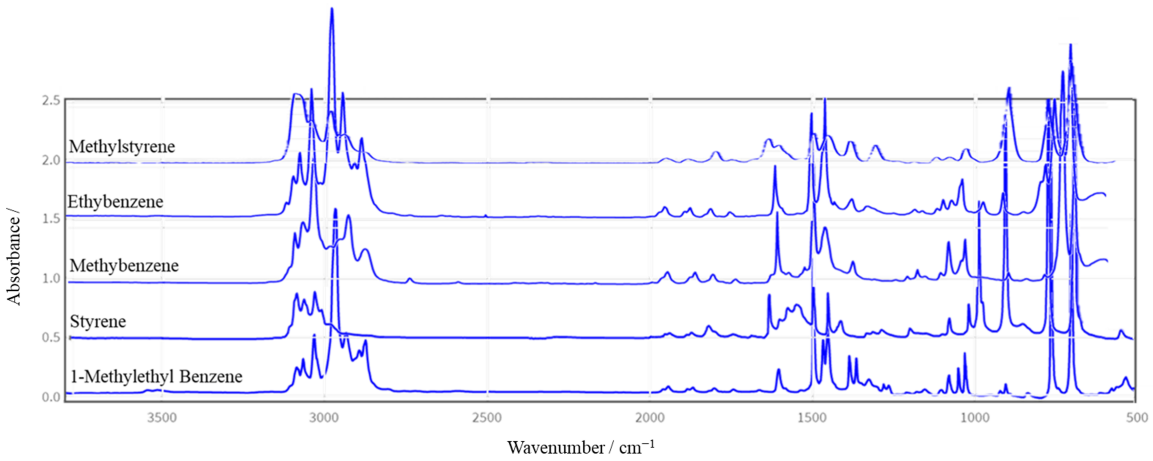

Figure 4.12: A comparison between reference IR spectra for methylstyrene, ethylbenzene, methylbenzene, styrene and 1-methylethly benzene, modified from Linstrom *et al.*, NIST Chemistry WebBook [118]. These species were all identified via the GC-MS analysis of the effluent condensed during the pyrolysis of polystyrene. Note the considerable band overlap between spectra.

$\sim$750 cm^{-1}, corresponding to aliphatic C-H bending. Comparing these absorbances to a spectrum obtained during the pyrolysis of PS, Figure 4.13, suggested that one or perhaps several of these species were present in the PS effluent.

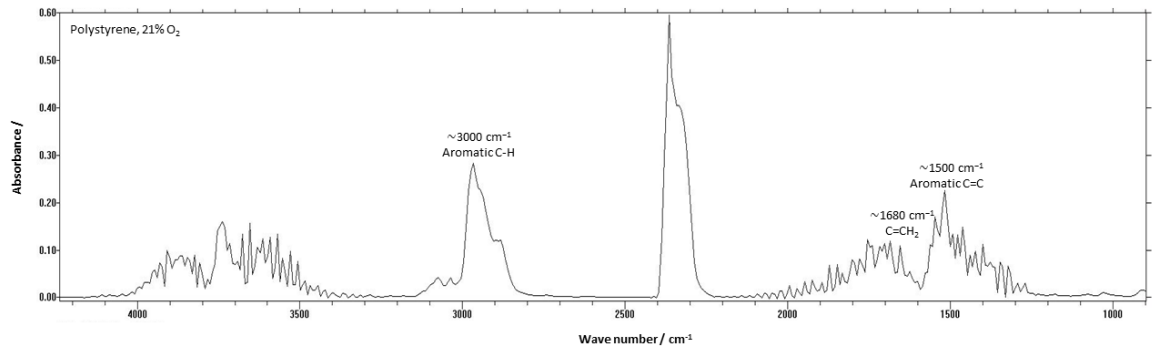

Figure 4.13: An example of an annotated FT-IR spectrum produced during PS pyrolysis. Prominent absorption bands have been allocated to aromatic stretching and bending modes.

Comparing Figure 4.13 to the reference spectra in Figure 4.12, the limited speciation afforded by the FT-IR became apparent. As styrene, methylstyrene and methylbenzene all generated a band in each of the three annotated regions, the FT-IR was unable to distinguish between these similar species within the effluent. To mitigate for this limited speciation, the ratio of these species in the effluent was determined using the GC-MS data. The FT-IR readings for these styrene related species were subsequently summed to represent the total signal being produced by mono-substituted aromatic compounds. The

combined FT-IR signal was then adjusted based upon the GC-MS product ratios. The percentage by area for styrene, averaging at 48.8 %, from the GC-MS peaks was used to 'correct' the FT-IR readings, which enabled the styrene yield to be estimated.

A similar situation occurred when analysing the FT-IR spectra generated by the PMMA, where MMA and several of the oligomers are likely to have generated overlapping bands. Unlike the PS, these signals were much easier to separate because of the dominance of the MMA monomer identified via GC-MS, suggesting that 99.1 % of the signal corresponded to MMA. Figure 4.14 shows the adjusted FT-IR yields obtained for MMA, styrene and 2-methoxyphenol compared to the GC-MS yields for these species.

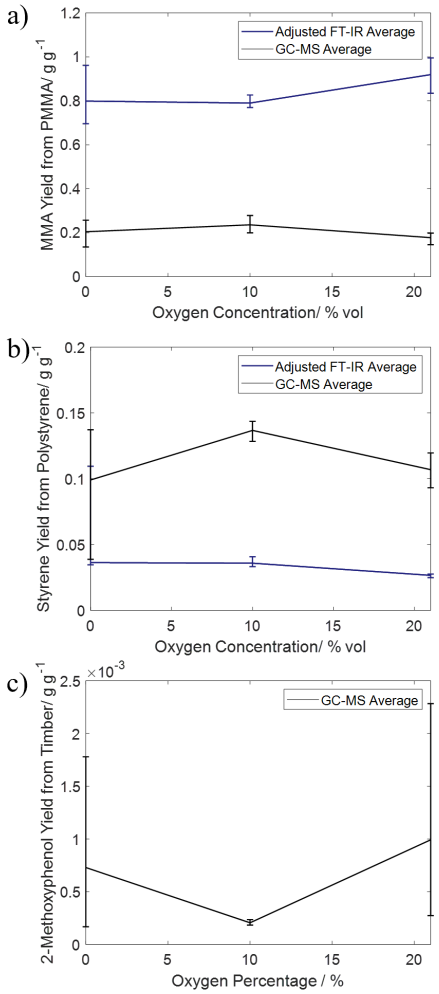

Figure 4.14: The GC-MS yields of a) MMA b) styrene and c) 2-methoxyphenol compared to the corresponding adjusted FT-IR yields obtained during the pyrolysis of PMMA, PS and timber.

Assessing the adjusted FT-IR plots, Figure 4.14a shows that PMMA effluent comprised mainly of MMA. The adjusted yields sat between 0.8 and 1 g g^{-1}, suggesting that the pyrolysis of PMMA was largely unaffected by the oxidative conditions. Figure 4.14b indicates that styrene formed large component of PS effluent, but several other species

must also have been generated to account for the ∼0.9 g g^{-1} of missing mass. For the PS, the adjusted yields appear to have underestimated the styrene yield, highlighting the complexities associated with interpreting the FT-IR spectra of complex mixtures.

Due to a greater variety of volatile species being generated, the band overlap problem was found to be much more of an issue when analysing the effluent produced by organic polymers like the timber. During the pyrolysis of timber, the significant band overlap prevented the FT-IR analysis from detecting 2-methoxyphenol or a similar aromatic ether. As such, an adjusted FT-IR yield could not be presented for 2-methoxyphenol, but the GC-MS yield has been included for completeness in Figure 4.14c. As the GC-MS data appeared to underestimate the yield of MMA, at least in comparison to the FT-IR data, it is likely that the GC-MS yield of 2-methoxyphenol alone was inadequate to obtain a complete picture of the timber effluent.

To account for this issue, a simple short-chain hydrocarbon, methane (CH_4), was selected to represent pyrolysis of the timber sample. Although it is likely that several other species were being generated, methane was predicted to be released when the aliphatic chains within the wood structure broke down. Using the temporal data from the adjusted FT-IR results, Figure 4.15 displays the near real-time yields of MMA, ethylbenzene and methane obtained from the pyrolysis of PMMA, PS and timber respectively.

Figure 4.15a showed a steady MMA yield of ∼0.9 g g^{-1}, suggesting that the methodology did successfully generate a constant effluent stream, thus performed as an improved means of assessing effluent composition. The occasional peaks above 1 g g^{-1}, have arisen from FT-IR band overlap where non-condensed species may have interfered with the signal interpretation. These fluctuations suggest room for method refinement, perhaps utilising cooler refrigerants (e.g., liquid nitrogen) to enhance the insight into pyrolysis and hence the adjustment process. On average, the yields indicate that MMA comprised ∼84 % of the effluent, mirroring values obtained in literature, thus highlighting the potential of the proposed methodology [119].

In the absence of a strong FT-IR styrene signal, methylbenzene was selected to represent the aromatic species obtained during the pyrolysis of polystyrene, shown in Figure 4.15b. Styrene and methylbenzene are both mono-substituted aromatic rings, differing in mass by one carbon atom and their FT-IR spectra overlap significantly. Methylbenzene yields started to stabilise once the PS had completely melted, displaying a slight oxygen dependency. It is likely that styrene would follow a similar relationship to the recorded methylbenzene trend, reflecting the literature, although further work alongside alternative reference spectra would be required [113].

From Figure 4.15c, it can be seen that ambient oxidative conditions resulted in an increased methane yield during the pyrolysis of timber. This increased production of short-chain volatile species hinted that a high temperature process was occurring alongside pyrolysis. The increased methane yields correlated with the observation of ash formation on the timber char, suggesting that oxidation of the char had begun to occur. It is worth noting that the high degree of fluctuation associated with the methane yield could arise from C–H bonds in other compounds overlapping with the methane FT-IR signal. This process warranted further investigation.

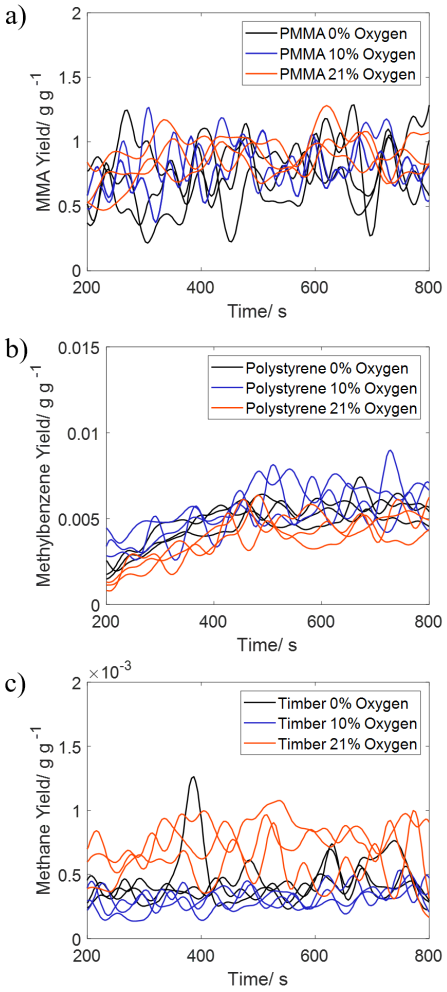

Figure 4.15: The adjusted temporal FT-IR yields of a) MMA, b) methylbenzene and c) methane obtained during the pyrolysis of PMMA, PS and timber under differing oxidative conditions. This data has been smoothed (Gaussian filter, 15 periods).

4.4 Heat Flux Data

Another advantage of the modified means of controlling the FPA concerns the ability to record the voltages being sent by the PID controller to the lamps. By calibrating the voltages sent to the lamps with a heat flux gauge, the heat flux supplied by the lamps to establish the controlled MLR can be obtained. Assessing these heat fluxes, both the PMMA and the PS required similar inputs across the range of investigated pyrolysis atmospheres to maintain the set MLR. However, as Figure 4.16 details, the timber required a lower heat flux under ambient oxidative conditions to sustain the target MLR.

Across all three investigated atmospheres, the supplied heat flux remained below the critical value for flaming combustion, 40 kW m^{-2} [120]. As per the initial objectives, simplifying the problem, staying below this level prevented flaming combustion occurring, enabling investigation into the mass transfer processes prior to oxidation via a flame. There was

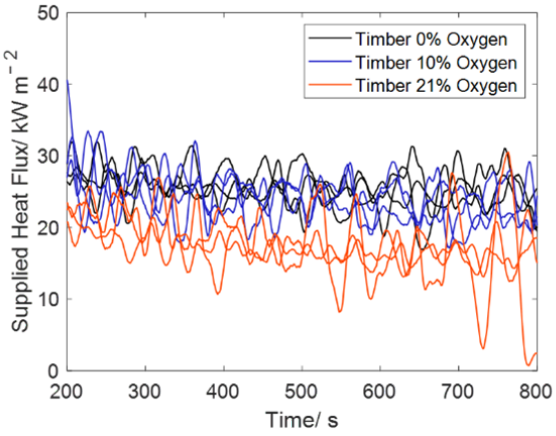

Figure 4.16: The heat flux supplied by the FPA to maintain a steady state MLR during the pyrolysis of timber. The data has been smoothed (Gaussian filter, 20 periods).

however a difference, ∼10 kW m^{-2}, between the heat flux supplied under 21 % oxygen to the other two investigated atmospheres. This difference correlated with the observation of white flecks of ash on the char layer. Figure 4.17 shows an image taken from a timber sample where the char was formed in an inert environment, resulting in the absence of any ash formation.

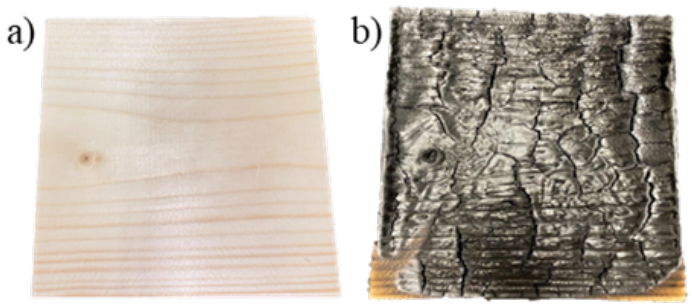

Figure 4.17: The images of timber a) before and b) after an FPA experiment under a constant heat flux at 0 % oxygen. Note the absence of ash on the surface of the timber.

This combination of factors led to the conclusion that additional energy was being supplied to the timber via char oxidation, a process detailed in existing literature [121]. This secondary energy supply required oxygen to oxidise the char, thus was unavailable under inert conditions, hence explaining the higher heat fluxes required for the lower oxidative environments in Figure 4.16. As the timber char oxidised, the exothermic production of carbon monoxide (CO) and carbon dioxide (CO_2) resulted in external mass loss and internal heat transfer. This oxidative process resulted in a lower average incident heat flux being required to maintain the same MLR. These results suggested that char oxidation impacted the pyrolysis processes occurring in timber, with the additional heat generated by char oxidation likely to drive additional pyrolysis [122, 123].

4.5 Reviewing the Approach

Overall, the methodology successfully controlled the MLR for selected simple polymers, generating representative effluent streams. The combination of analytical techniques enabled a deeper interpretation of fire effluent with corroboration between the analytical techniques confirming peak identities. GC-MS analysis enabled the FT-IR signals associated with MMA to be broken down into a ratio of monomers and dimers, improving the accuracy of the effluent analysis.

The direct link between sample mass loss and effluent analysis afforded by the proposed methodology has facilitated insights into the pyrolysis processes, enabling the impact of oxygen to be quantified. The comparison of the heat fluxes required to sustain timber char formation revealed that an additional $\sim$10 kW m^{-2}, heat flux was required to sustain charring under non-ambient atmospheres. These findings could be used to quantify processes like char oxidation for many materials. This methodology has improved our understanding of the pyrolysis process through the quantification of timber char oxidising alongside the measurement of chemical species from controlled and representative effluent streams.

The modified means of controlling the FPA occupies a gap in the existing line-up of bench-scale effluent generating methodologies. Such an approach allows a real-time steady state mass loss measurement to be obtained whilst observing a sample throughout an experiment. These steady mass readings add value to species generation data as they enable the pyrolysis rate to be monitored and controlled generating a steady stream of emissions. On balance, the modification of the FPA occupies a niche in the field and as demonstrated in this chapter can function well when monitoring the pyrolysis products generated by a range of simple materials.

Simplifying the problem presented in Chapter 3 has enabled an effluent sampling methodology to be successfully developed where the oxidative conditions are effectively decoupled from the MLR. Such a decoupling has enabled secondary processes like char oxidation to be quantified during the timber experiments. Building on these successes, the next steps involve utilising the technique to look at charring materials and the impact of flaming combustion on heat and mass transfer processes.

As the methodology enables the supplied heat flux to be recorded, processes like char oxidation, observed during the timber experiments, could potentially be quantified in differing, more complex, materials. Using the methodology to identify and quantify the onset of charring processes will enhance our understanding of mass transfer during fires. Furthermore, being able to control flaming combustion with the FPA would enable the independent assessment of oxygen composition to be explored in greater detail, fully considering the impacts of flame geometry on heat and mass transfer processes. These two topics will form the basis of the discussion during Chapters 5 and 6.

Chapter 5

Investigating Charring Materials

"Burning through the shadow on the ground."

– The Pigeon Detectives
Munro (Broken Glances, 2017)

This page has been intentionally left blank.

5.1 Material Complexity

During Chapter 4 it was established that an alternative means of controlling the Fire Propagation Apparatus (FPA) could be successfully used to adjust the mass loss rate (MLR) of a sample. The automatic adjustment of the MLR via a proportional integral derivative (PID) controller could be used to assess the impact of oxidiser availability on the heat and mass transfer processes occurring during pyrolysis. The alternative means of controlling the FPA generated a controlled stream of pyrolysis products, independent of the oxidiser flow, allowing mass transfer processes to be investigated. As the heat flux supplied to maintain a controlled MLR was recorded, heat transfer processes were also probed with the technique. Despite this progress, the development of the methodology during the thesis thus far has been restricted to simple synthetic polymers rather than the more complex materials and products often encountered in the real world. By assessing the heat flux supplied during the controlled pyrolysis of more complex materials, the transition from pyrolysis into differing combustion regimes may be quantified.

To assess whether the developed methodology would still be appropriate to investigate more complex materials, the insulation foams investigated in Chapter 3, polyisocyanurate (PIR) and phenolic foam, were selected. The pores within these insulation foams contain chemically bound oxygen trapped within the aerated structure of each material. This secondary source of oxygen was predicted to increase the range of chemically processes available to the foams when subjected to a controlled heat flux. Additionally, during Chapter 3 these foams were shown to produce a complex mixture of indistinguishable aromatic products whilst charring to differing extents. As the decoupling of the oxidative conditions from the MLR successfully enabled char formation to be investigated during the pyrolysis of timber in Chapter 4, the charring behaviours exhibited by these foams were selected to further assess the developed methodology.

5.2 The Modified Means of Controlling the FPA

The modified means of controlling the FPA was used as discussed during Chapter 4. This section therefore outlines any deviations from the previously presented methodology.

5.2.1 Adapting the Methodology

Two commercially sourced thermoset polymeric insulation foams, PIR and phenolic foam, had their foil facers removed before being cut into uniform samples (80 mm × 80 mm × 50 mm). These samples were placed onto the pedestal connected to a load cell in the centre of the FPA. A quartz tube (435 mm high, outer diameter 174 mm, inner diameter 164 mm) was placed around the sample. Depending on the experiment, a composition of oxidiser, 0, 10 or 20.9 % oxygen, with the balance being nitrogen, was flowed, at 100 L s^{-1}, through the test chamber. The FPA lamps were controlled by a PID controller, K_p = 5, K_i = 0.015 and K_d = 4, to achieve a MLR of 1 ± 0.44 g s^{-1} m^{-1}.

After 200 seconds had elapsed, accounting for initial fluctuations in the MLR as the PID adjusted the lamps, a controlled period was observed for 400 seconds. During this time physical changes to the foams were observed despite the MLR remaining under control. Effluent was sampled throughout each experiment via Fourier-transform infrared spectroscopy (FT-IR) using a heated sampling line (453 K) with the effluent passing into a gas cell for analysis. Each foam was tested under each of the oxidative atmospheres in triplicate as per the methodology outlined in Chapter 4.

5.2.2 Selecting a Target Mass Loss Rate

The two synthetic insulation foams, PIR and phenolic foam, were observed to exhibit slightly differing behaviours when subjected to escalated heat fluxes during initial experiments(Chapter 3), mirroring literature [105]. The PIR tended to expand while the phenolic foam preferentially cracked before both foams formed a char layer. The low densities of the foams, 26.3 and 37.3 kg m^{-3} for the PIR and phenolic foam respectively, resulted in 0.0013 and 0.0019 kg of starting material when using standard 100 mm × 100 mm × 5 mm samples. These low starting masses were insufficient to generate pyrolysis products consistently over an extended sampling duration; thus, samples were increased in thickness to 50 mm, providing additional mass.

Lightweight materials proved to be a challenge for the developed methodology as they required a low MLR to facilitate an enhanced timeframe for emission analysis, whilst preventing the samples from being burned out instantaneously. These lower MLRs were more difficult to control due to the operational limits of the load cell. Figure 5.1 shows some still images taken from an early experiment where PIR was investigated with the MLR set to 2 g s^{-1} m^{-2}. The figure highlights the main issue presented during the testing of these materials: the rapid expansion of the foam following the formation of a crack. Surface cracks would often subsequently expand, pushing material towards the sides of the

FPA, usually resulting in the load cell momentarily recording an incorrect mass loss. This, in turn, caused the PID controller to fluctuate the voltage driving the lamps between 0.5 and 4 V, ultimately leading to ignition.

To prevent the autoignition of samples via the process outlined in Figure 5.1, two adjustments were made. Cracks that formed along the side of a sample were thought to have arisen due to excessive surface swelling. To reduce this swelling, the sample surface area was reduced to 80 mm × 80 mm and a lower MLR was selected, 1 g s^{-1} m^{-2}. Such adaptations enabled effluent to be sampled over the course of an experiment whilst controlling the MLR of each sample.

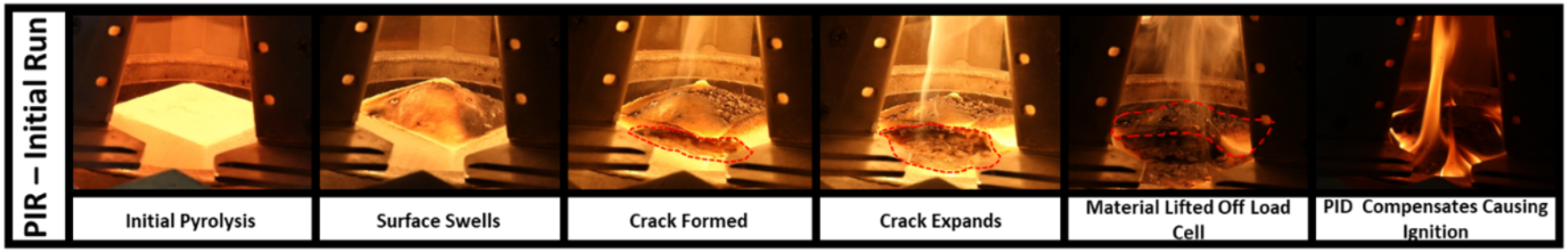

Figure 5.1: An early PIR experiment with the MLR set to 2 g s^{-1} m^{-2}. The sample initially cracked before expanding and opening up. This process lifted the surface of the sample from the load cell resulting in the PID controller switching the FPA lamps to full, causing ignition.

5.2.3 Finalising the Methodology

Figures 5.2a and 5.2b show the MLRs obtained for each insulation foam when using the standard means of operating the FPA, ASTM E2058-19, with a set heat flux of 35 kW m^{-2} [111]. Both figures highlight the extent of the variation in the pyrolysis rate using this standard methodology where an initial rise in MLR was observed before a gradual decline and, in the case of the PIR, an eventual plateau.

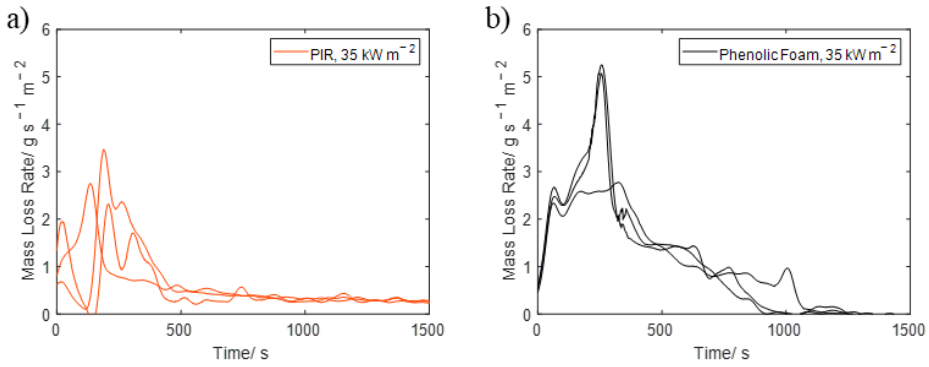

Figure 5.2: The mass loss rates obtained when a) PIR and b) phenolic foam were subjected to a 35 kW m^{-2} heat flux using the standard means of controlling the FPA, ASTM E2058-19. This data has been smoothed (Gaussian filter, 80 periods).

When subjected to a set heat flux, the PIR, Figure 5.2a, had an initial period of elevated mass loss before a surface char was formed, protecting the remnants of the foam from secondary fluctuations in MLR. From this point onwards the PIR sample was not observed to change. The remnants of mass loss during the later stages of these experiments appeared to be dependent on the applied external heat flux rather than any oxidative processes. At these late stages in each experiment, the PIR residues were being warmed by the lamps without causing further decompositional processes to occur.

The greater MLRs initially reached in Figure 5.2b resulted in additional mass being lost from the phenolic foam sample over a reduced timeframe. This in turn meant there was less mass to lose at later experimental stages, resulting in the mass loss ceasing at t = ~1100. The phenolic foam samples visibly decreased in size throughout each experiment until the sample appeared to be completely consumed. The standard means of operating the FPA prompted differing responses in the MLRs, and hence the pyrolysis rates, of these investigated insulation foams.

To rectify for these differing MLR behaviours, the modified means of controlling the FPA was used to control the MLR of each insulation foam. Accounting for the low density of the foams, a controlled MLR was obtained across each of the three investigated oxidative conditions as outlined in Figure 5.3. The controlled MLR approach showed a high degree of quantitative and qualitative repeatability across the investigated experiments.

During each controlled MLR experiment the surface of the PIR was observed to brown, before eventually cracking and swelling, while the phenolic foam crackled and popped throughout. This initial swelling seen during the PIR experiments, prior to cracking,

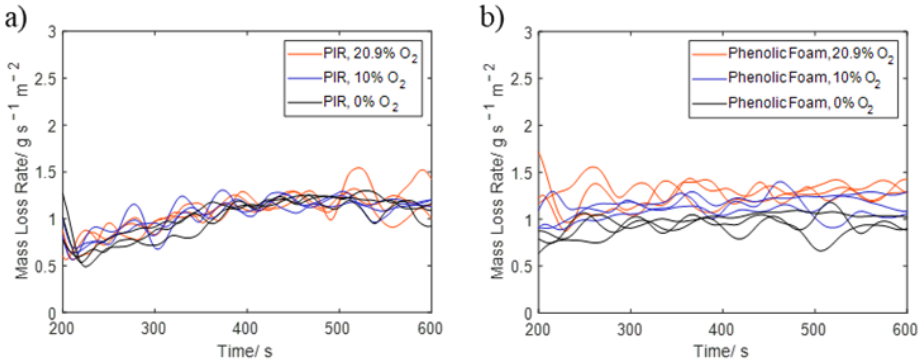

Figure 5.3: The controlled mass loss rates obtained during the pyrolysis of a) PIR and b) phenolic foam under three different oxidative conditions (0, 10 and 20.9 % O_2). This data has been smoothed (Gaussian filter, 80 periods).

retained a proportion of the pyrolysis gases, resulting in the slight delay to reach the set MLR seen in Figure 5.3a. These heterogeneity issues combined with the close proximity to the lower sensitivity limit of the load cell made it challenging to establish controlled MLRs for these materials.

Once a means of releasing the pyrolysis gases became established, the decreased likelihood of rapid foam expansion, resulted in a controlled MLR for the PIR. In contrast, the erratic nature of the popping during the phenolic foam experiments caused larger deviations from the set MLR seen in Figure 5.3b throughout each experiment. Overall, the comparison between Figures 5.2 and 5.3 indicated that the MLR was successfully managed by the modified means of controlling the FPA, thus a steady effluent stream was expected to be generated.

5.3 Secondary Processes

As the phenolic foam samples in Figure 5.2b left only a trace residual mass, it was hypothesised that processes in addition to pyrolysis were responsible for material decomposition.

5.3.1 Observations

Approximately halfway through the controlled MLR period, around 400 seconds, the surface of both foams was observed to become completely charred. As each experiment continued, cracks began to appear within the charred surfaces. The visual extent of this blackening and cracking varied with the type of insulation material and the applied oxidative environment. A summary of these observations is presented for both foams in Figure 5.4.

Despite the FPA maintaining a controlled MLR, these visual changes alluded to processes in addition to pyrolysis occurring. Once a char layer had formed, it was predicted that despite the controlled MLR, the composition of the emissions would vary to accommodate the new protective layer [124]. As such, the composition of the effluent was assessed across each experimental period to determine whether changes in composition could be linked to the observations in Figure 5.4.

5.3.2 Effluent Composition

To further investigate the differing processes that were occurring, differences in the effluent composition were monitored over the course of the controlled MLR. As carbon monoxide (CO) is a common species detected during several distinct processes including pyrolysis, charring and smouldering, the analysis of the effluent was focused on assessing changes associated with its yield [125]. When considering CO generation during these experiments, both the PIR and the phenolic foams exhibited an oxygen dependency, with only trace yields of CO being generated under inert conditions. Figure 5.5 details the CO yields obtained under the differing conditions investigated for both foams.

The CO yields obtained for the PIR in Figure 5.5a gradually rose to ∼0.4 g g^{-1}, aligning with similar values reported in Chapter 1 [16, 102]. A sharp increase in the CO yield became more pronounced from t = ∼400 s, correlating with the observation of a complete char layer being formed in Figure 5.4. This sharp rise in CO, compounded with an absence under inert atmospheres suggested that char oxidation was the process responsible for the generation of the additional CO [126]. The subsequent rise in CO, beyond t = ∼350 s, suggested that oxidative processes were gradually becoming more prevalent until the PIR experiments were stopped at t = 600 s.

Char oxidation primarily affected the phenolic foam at oxygen environment greater than 0 %, as evidenced by the elevated CO yields across a much greater timespan in Figure 5.5b. The plateau from t = ∼400 s, showed char oxidation had stabilised at a set rate, marking the transition away from a pyrolysis dominated regime [106]. An absence of CO generation

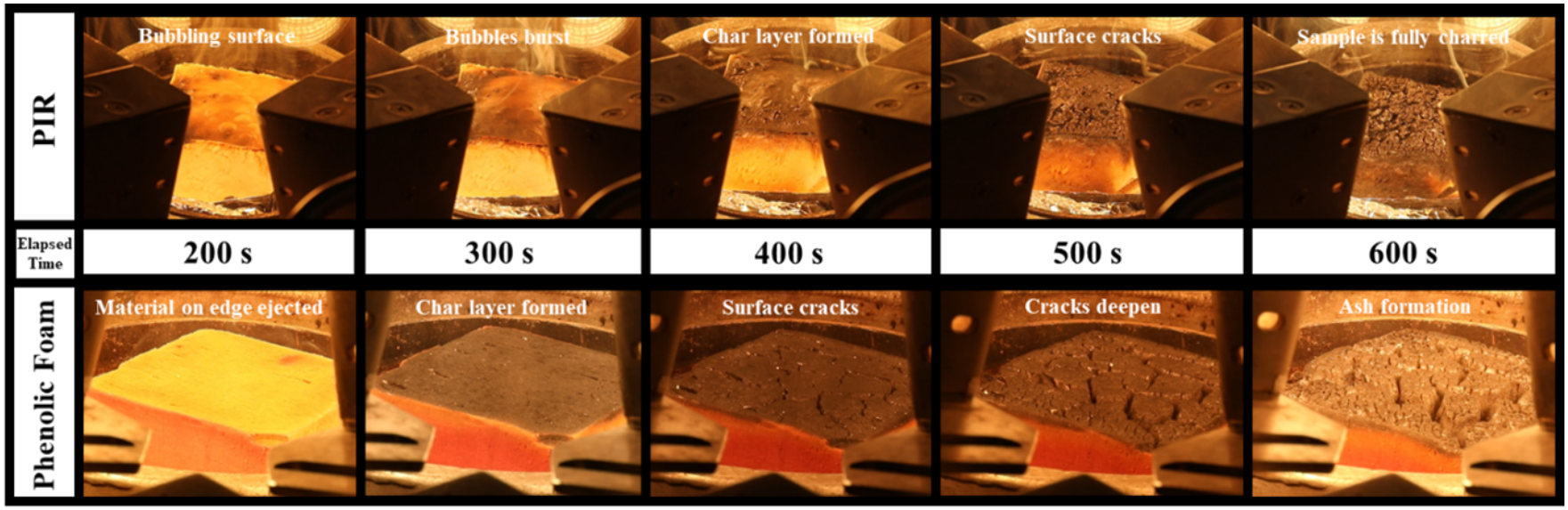

Figure 5.4: Video still images taken during the controlled MLR of PIR and phenolic foam, at 10 % oxygen. For the PIR, a browning is shown between t = 200 and 300 s, before a blackening at t = 400 s and crack formation from t = 500 s. A similar process was observed for the phenolic foam but happened approximately 100 seconds earlier.

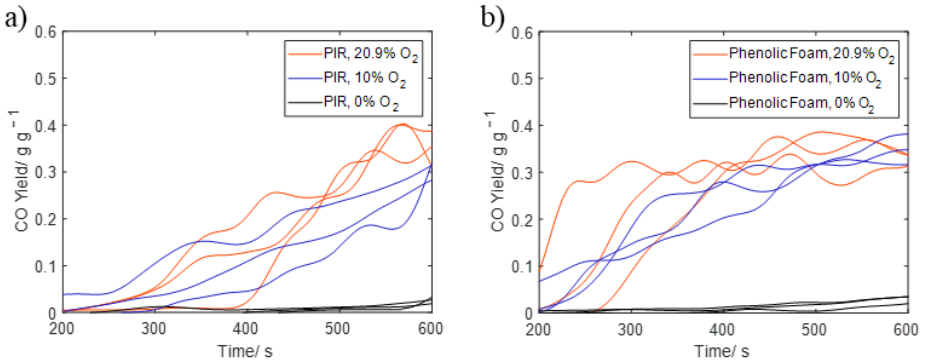

Figure 5.5: The carbon monoxide yields obtained across the controlled mass loss periods for a) PIR and b) phenolic foam under three different oxidative environments.

under inert conditions implied that oxidative processes were prevalent alongside pyrolysis between t = ∼200 s and ∼300 s, a period prior to visible char formation. Therefore, it was hypothesised that CO was both a pyrolysis and a char oxidation product for the phenolic foam. As a result, CO is harder to use to identify differing decompositional processes for this material. Furthermore, it could be concluded that CO is not a major component of the pyrolysis gases for either of these foams, rather, it is a product indicative of oxidative processes. Such results explain the discrepancy in existing literature when comparing the CO yields obtained for these insulation foams under differing ventilation conditions as illustrated in Figure 1.3 [15–17].

Another asphyxiant associated with the effluent generated by these foams is hydrogen cyanide (HCN), discussed in Chapter 3. The detection of HCN was material specific, only being prominent in the PIR effluent outlined in Figures 5.6a and 5.6b.

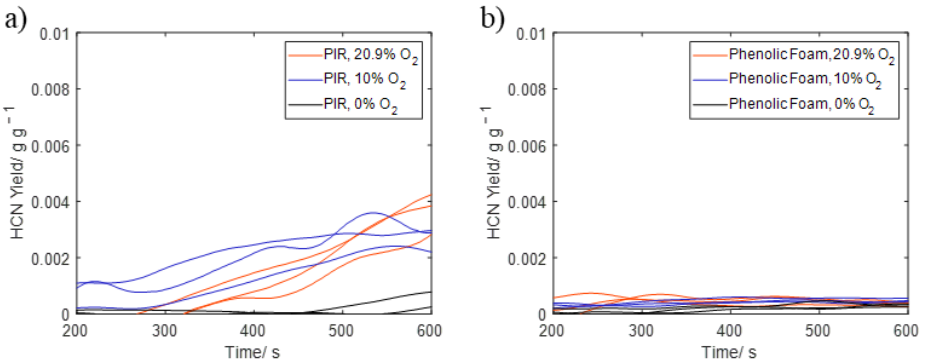

Figure 5.6: The hydrogen cyanide (HCN) yields obtained across the controlled mass loss periods for a) PIR and b) phenolic foam under three different oxidative environments.

A similar pattern to the CO yields was observed when assessing the HCN yields from PIR. Unlike CO, HCN is not an oxidation product, rather it is predominantly a pyrolysis product, yet the yields in Figure 5.6a showed a clear oxygen dependency. This result was contrary to existing literature in which increased HCN yields correlated with low oxygen environments [15–17]. It is hypothesised that some oxygen is required for HCN to be generated. Oxygen may be required to stabilise an immediate species during the formation

of HCN, with the air pockets within these insulation foams potentially providing this small source of oxygen. The environmental conditions that promote HCN formation are plausibly between the tested conditions, 0 and 10 % O_2, however further research should be conducted to determine the specific value.

A comparable lack of HCN generation observed during the pyrolysis of phenolic foam correlated with the differing chemical structures of the insulation foams, with the isocyanate groups in PIR being the plausible source of the HCN. Having the CO yields for PIR mirrored by a pyrolysis product highlights the complexity of the competing processes occurring, demonstrating the significant overlap between pyrolysis dominated and oxidation dominant regimes.

5.3.3 Quantifying the Extent of Oxidation

The modified means of controlling the FPA was able to deal with the physical changes arising from char oxidation by maintaining the set MLR over the entire 600 second experimental period. To further characterise char formation, the heat fluxes supplied to maintain the set MLRs were calculated in the manner outlined during Chapter 4 for the charring timber samples. The heat fluxes supplied to each of the insulation foams are presented in Figure 5.7.

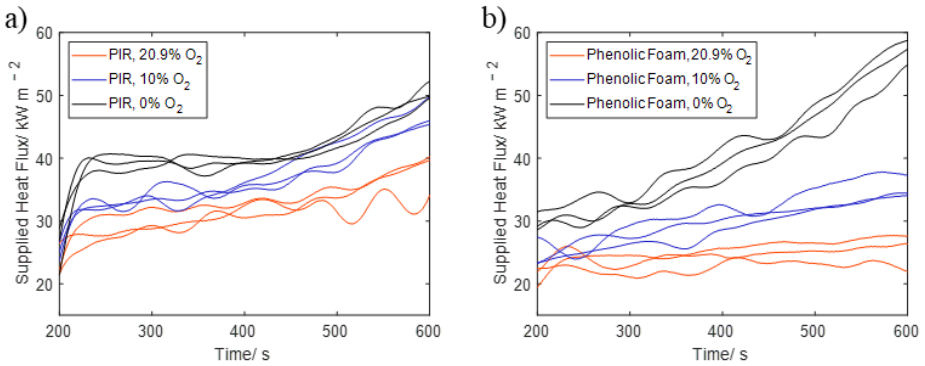

Figure 5.7: The heat fluxes supplied by the FPA to maintain the controlled MLR of 1 ± 0.44 g s^{-1} m^{-2} throughout an experiment for a) PIR and b) phenolic foam.

For both insulation foams, higher heat fluxes were supplied to the samples under lower oxygen environments to sustain the same MLR. These results indicated that oxidative processes were occurring throughout the entire duration of each experiment, contributing energy towards the overall surface energy balance.

After approximately 400 seconds, for each of the PIR experiments in Figure 5.7a, the heat flux required to maintain the desired MLR increased. This rise in supplied heat flux coincided with the observation that the surface of the sample had fully charred, as per Figure 5.4. The additional energy required to maintain the controlled MLR suggested that either the heat of vaporization for the fuel (L_v) or the heat losses ($\dot{Q}''_L$) from the surface of the PIR had increased. An increase in L_v may have occurred due to changes in the pyrolysis processes arising from the formation of a chemically complex char layer,

while $\dot{Q}''_L$ could have increased as a result of the elevated surface temperatures [48]. The increased dependence of the supplied heat flux on the oxygen environment suggested that the oxidative processes became more dominant beyond 400 seconds. As each experiment continued beyond 500 seconds, cracks within the char became more pronounced, enabling oxygen to move deeper into the foam, heightening this oxygen dependency.

The heat flux supplied to the phenolic foam in Figure 5.7b plateaued for the experiments conducted under ambient oxidative conditions (20.9 % oxygen) but gradually rose for the other two investigated atmospheres. The inert conditions, 0 % oxygen, required on average 16.11 kW m^{-2} of additional energy to maintain the same MLR as the ambient experiments. This worked out at approximately 28 % of the total heat flux contribution, corroborating with the magnitude of the heat flux contributions from char oxidation obtained during timber studies [123]. This differing behaviour under oxygenated environments, alongside the observation of white flecks on the phenolic foam char in Figure 5.8, indicated that char oxidation was a much more dominant process for the phenolic foam from an earlier stage.

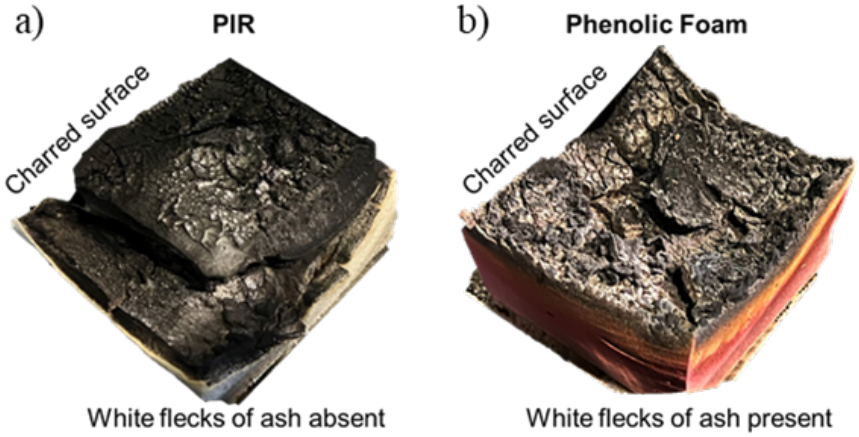

Figure 5.8: Still images taken at the end of a 600 second experiment under ambient oxygen conditions for a) PIR and b) phenolic foam. The phenolic foam sample had white flecks of ash forming on the charred surface, evidence of char oxidation.

Calculating the difference between the averaged supplied heat fluxes for the 0 % and the 20.9 % oxygen experiments across both foams enabled the heat flux contribution from char oxidation to be quantified. Across the controlled MLR period, on average PIR had a 61 W contribution from char oxidation, roughly half of the contribution from the phenolic foam at 103 W. It is likely that this additional energy input under oxidative conditions explains why a greater proportion of phenolic foam mass is lost under ambient environments, compared to inert environments, in literature [127].

Evidence from the analysis of the emissions and the visual observations suggested that char oxidation was most prevalent during the later stages of an experiment. Shifting the focus onto the last 100 seconds of an experiment, Figure 5.9 shows the average heat fluxes obtained towards the end of the controlled MLR period for both insulation foams (between t = 500 s and t = 600 s). The calculated heat release from char oxidation subtracted the heat flux supplied by the FPA at 0 % oxygen; conditions deemed to prevent char oxidation processes. A full set of tabulated data is presented in Tables C.1 and C.2 in Appendix C.

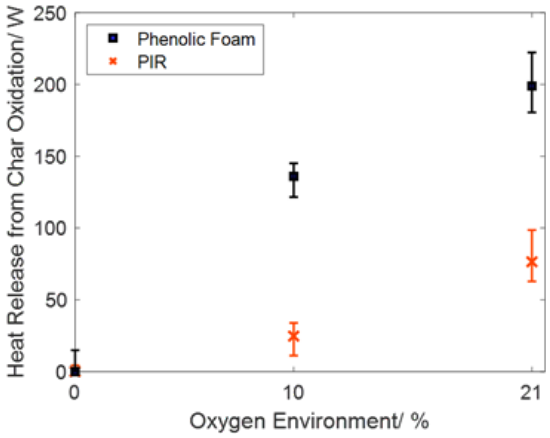

Figure 5.9: The average calculated heat released from char oxidation for PIR and phenolic foam collected under three differing ventilation conditions during the final 100 seconds of each experiment.

As shown by Figure 5.9, increasing the oxidative environment facilitated an increase in char oxidation. The heat release from char oxidation for the phenolic foam rose to 199 W, exceeding the 77 W contribution detected during the later stages of the PIR experiments. Additionally, the char oxidation from the phenolic foam under 10 % oxygen resulted in a greater heat release than the char oxidation occurring under ambient conditions for the PIR, highlighting the ease at which the phenolic foam char could be oxidised.

These results highlight and quantify the complex behaviour of both PIR and phenolic foam under oxidative conditions, findings that build upon observations made under previous techniques [128]. Despite this work requiring more intermediate oxidative environments to confirm the precise trends presented in Figure 5.9, it is apparent that char oxidation is a phenomenon that can be adequately quantified by the modified means of controlling the FPA.

5.4 Critical Summary

The revised means of controlling the FPA was successfully used to manage the pyrolysis and char oxidation of two insulation foams via the implementation of a controlled MLR. The heat flux supplied by the FPA to maintain the set MLR exhibited an increased energy demand after ∼350 seconds, correlating with a visual darkening of the surface of the foam and a rise in the obtained CO yields. The combination of these factors indicated that an initial pyrolysis regime was transitioning into a period of charring, including the development of char oxidation partway through the controlled MLR period. These results demonstrate that care must be taken when generating a representative effluent stream for sampling as processes are changeable during a period of controlled MLR, particularly true for charring materials.

The developed FPA methodology was able to successfully identify the transition to an oxidative regime via a combination of emissions analysis and monitoring changes in the supplied heat flux. Calculation of the heat release contribution from char oxidation, afforded by maintaining a controlled MLR, enabled an insight into the complex behaviours exhibited by these insulation foams. The char generated by phenolic foam was found to oxidise to a much greater extent than that of the PIR, with a difference of 122 W being recorded between the foams under ambient environments with the MLR set at 1 ± 0.44 g s^{-1} m^{-2}. These results show that the methodology can successfully quantify the heat transfer processes occurring during fire scenarios.

Throughout this chapter char oxidation, alongside pyrolysis, has been shown to contribute species towards the total effluent composition obtained during the investigation of insulation foams. The extent of this oxidation has been revealed to vary based upon the type of material under investigation and the oxidative environment. The modified means of controlling the FPA has been demonstrated to enable an insight into the processes beyond pyrolysis, therefore the next logical progression is to assess whether a flame and thus a constant burning rate, can be maintained by the methodology.

This page has been intentionally left blank.

Chapter 6

Assessing the Impact of Flame Geometry on Effluent Composition

"We're all gonna fade or burn out bright."

– The Sherlocks
On the Run (World I Understand, 2022)

This page has been intentionally left blank.

6.1 Adjusting for Flaming Combustion

During this thesis the modified means of controlling the Fire Propagation Apparatus (FPA) has successfully been demonstrated to decouple the mass loss rate (MLR) of a sample from the flow of oxidiser, enabling the impacts of oxygen on heat and mass transfer processes to be investigated. Previous chapters have identified the specific composition of chemical species generated during the pyrolysis of synthetic polymers alongside quantifying the heat transfer contribution from the oxidation of insulation foam chars. Encouraged by these initial results, the methodology was now developed enough to increase the complexity of the probed problem, enabling the assessment of flaming combustion under a fixed MLR.

The addition of a flame to the experimental scenario complicated the steady state process. To sustain a flame throughout an experiment the MLR had to be maintained above the burning rate, providing a steady stream of gaseous fuel molecules to prevent the flame from being quenched. Successful control over flaming combustion using this approach, and hence the stabilisation of the flame, facilitated by the modified means of controlling the FPA, enabled the effect of oxidiser on flame geometry to be probed.

During the previous chapter, polyisocyanurate (PIR) and phenolic foams were shown to exhibit complex burning behaviours. The air pockets within the structure of these materials were hypothesised to enable oxygen to be introduced midway through an experiment. To avoid potential inhomogeneities, the flaming combustion work initially focused on simple straight-chain synthetic polymers. Polymethylmethacrylate (PMMA) and polyoxymethylene (POM) are examples of such materials, comprising of a single monomer species. Due to their high oxygen composition by mass, these simple thermoplastics both burn readily, each sustaining a flame.

The use of simple plastics enabled pyrolysis products and therefore their oxidised combustion products to be predicted, allowing the deployed analytical techniques to be tuned to identify specific chemical species. This method development enabled the effect of oxidative conditions on the shape of diffusion flames to be investigated, determining the impact of diffusion flame geometry on overall effluent composition.

6.2 Combustion Chemistry

Flaming combustion requires a fuel and an oxidiser to be present in a flammable ratio alongside an initial heat source. Depending on the phase of the fuel, gaseous or condensed (solid/ liquid), the geometry of the established flame will vary. Gas-phase fuels like methane or propane, are usually premixed with an oxidiser, resulting in well-defined flame geometries where the fuel:oxidiser ratio is controlled. The control afforded by gaseous premixed flames typically results in mixtures designed to favour complete combustion, often yielding clean, blue flames [129]. The fire effluent generated during the combustion of these gaseous fuels may be assessed using a co-flow burner, an experimental arrangement where the flows of both a gaseous fuel and an oxidiser can be independently controlled [25].

For solid fuels, the pyrolysis rate varies as a function of multiple factors including the external heat flux and any heat feedback provided by the flame; collectively summarised by the surface energy balance. Unfortunately, when studying combustible solids and other condensed-phase fuels, as the pyrolysis rate dictates the gaseous fuel flow rate, a co-flow burner cannot control the rate of fuel injection into the flame. Once a flame has become established, a rise in the abundance of an oxidiser is likely to increase the completeness of the combustion, which in turn causes an increase in the heat flux supplied to the surface of the sample, thus increasing the pyrolysis rate. The combination of these effects results in a strong coupling between the oxidiser and the fuel flow rate. To study the impact of the fuel:oxidiser ratio on the burning of solid fuels, it is therefore necessary to be able to independently control the pyrolysis rate, regardless of the oxygen environment. Such control during flaming combustion will increase our understanding of the composition of fire effluent, enabling insights into the solid and gas-phase processes of burning.

6.2.1 Diffusion Flames

Laminar diffusion flames occur at the interface where a stream of gaseous fuel meets an oxidiser. For condensed-phase fuels, the stream of gaseous fuel molecules is generated by pyrolysis, a process driven by the extent of heat transfer to the sample. If large enough, the overall heat transfer to a sample will enable pyrolysis processes to occur, causing condensed-phase fuels to gasify, releasing a mixture of combustible gases. Buoyancy effects ensure that the generated gases become entrained in air, providing the oxygen necessary for combustion. As positive feedback cycles cause a fire to increase in size, the flow velocity increases, gradually transitioning into turbulence. The transport of both the fuel and the oxidiser towards the flame is influenced by a combination of this heat feedback, buoyancy and turbulence, with the coupling between these phenomena determining the feasible regions for the flame to become established.

The geometry of the flame determines the type of combustion chemistry possible, ranging from stoichiometric (complete) combustion to flame quenching. Stoichiometric combustion assumes infinitely fast chemistry in the abundance of oxidiser, while the conditions approaching quenching result in incomplete combustion processes [130]. To date, the structures of laminar flames originating from gas-phase fuels have been studied and

described by literature in detail [131]. However, these descriptions have not been made for the burning of solid-phase fuels or for turbulent flows, both of which are relevant to genuine fire scenarios.

The Burke-Schumann development described the impacts of oxidiser flow on the shape and geometry of laminar diffusion flames generated by gas-phase fuels [25]. This development theorised that due to the infinitely fast combustion chemistry, relative to the diffusion of molecules, a fuel and oxidiser cannot coexist beyond the thin flame envelope. It was therefore proposed that the diffusion between the gaseous fuel and the air, containing the oxidiser, within a co-flow burner was the dominant contributor to flame geometry, greater than any contribution arising from differing velocities between the streams [26]. The shape and geometry of the diffusion flame was subsequently defined by the region in which the fuel and oxidiser were consumed by the combustion reactions. Following this work, flame shapes arising from gas-phased fuel sources were accurately predicted utilising the Burke-Schumann development, aligning well with experimental results [27].

The co-diffusion of both the fuel and oxidiser towards the flame was found to have the primary influence on the geometry of a diffusion flame although the fuel:oxidiser ratio was also known to play an important role. When this ratio is small, the flame is over-ventilated and the Burke-Schumann framework predicts complete combustion, consisting of a closed flame envelope, generating primarily carbon dioxide (CO_2) and water vapour (H_2O). A larger ratio signifies under-ventilated conditions, causing the flame to fan-out towards the oxidiser stream, producing a tulip shape that enables unburnt gases to escape through its centre [132]. Figure 6.1 summarises these scenarios, displaying the two extreme flame geometries predicted by the Burke-Schumann framework [133].

Despite the progress made by Burke and Schumann, the assumption that the flame will always be present under a stoichiometric fuel:oxidiser ratio does not always hold true. Work involving counterflow burners has demonstrated that variables including scalar dissipation have a significant role on determining the characteristics and location of the flame [134]. Since the original advances, it is evident that simplified configurations for solely gas-phased fuels, such as those found in co-flow burners, no longer enable interrogation of all the relevant variables.

6.2.2 Condensed-phase Fuels

As most fire scenarios involve fuels in the condensed phase, the gaseous flow rate of fuel is dictated by pyrolysis-dominated processes. The MLR encompasses all the fuel mass transitioning from the condensed phase into the gaseous state, regardless of whether the gaseous molecules get oxidised by a flame. It therefore follows that the MLR describes the flow rate of gaseous fuel molecules arising from a condensed-phase fuel.

Under conditions favouring complete combustion, a) in Figure 6.1, this value may be close to the burning rate. However, as a flame transitions into a fuel dominated regime, the flame tip begins to fan-out forming a tulip structure. Under these conditions, species may pass into the effluent without being completely oxidised as they do not directly interact

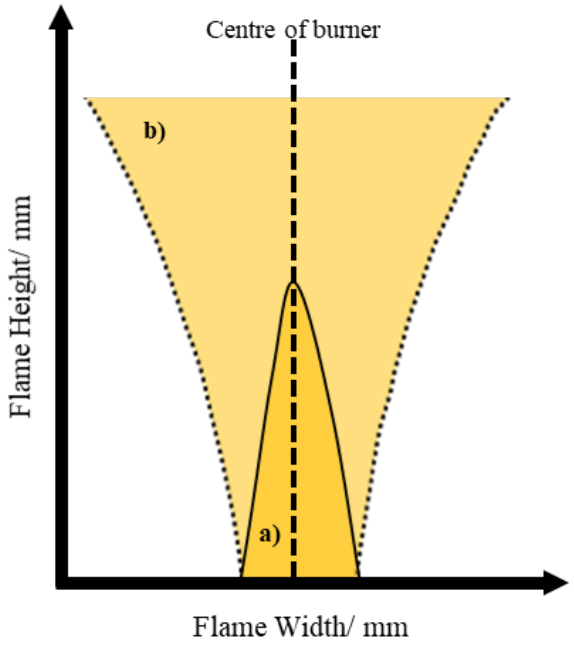

Figure 6.1: A schematic representation of the Burke-Schumann flame structure. The region marked a) shows a closed flame tip in the centre of a burner, correlating with over-ventilated conditions, while the region marked b) shows the umbrella-shaped flame, formed when the flame fans out from the burner during under-ventilated conditions.

with the flame. During these scenarios the MLR differs significantly from the burning rate. Thus, it follows that the MLR can be used to describe the gaseous fuel injection rate for condensed-phase fuels, however the MLR does not necessarily represent the burning rate.

The MLR is coupled to the combustion environment, varying with the external heat flux and the oxidative conditions. It therefore follows that the impact of oxidiser availability on flame geometry can only be assessed under a fixed MLR over a range of different oxidative environments. During combustion the MLR will vary based upon the net heat flux received at the surface, as illustrated by Equation 6.1. This overall heat flux includes contributions from the external heating ($\dot{Q}''_E$), the flame ($\dot{Q}''_F$), heat losses from the surface ($\dot{Q}''_L$) and the heat of vaporisation (the energy required to sustain pyrolysis) (L_v) of the solid [2, 3].

$$\text{MLR} = \frac{\dot{Q}''_E + \dot{Q}''_F - \dot{Q}''_L}{L_v} \tag{6.1}$$

Most of the bench-scale fire tests discussed in Chapter 2 select and maintain a constant $\dot{Q}''_E$, resulting in the values of $\dot{Q}''_F$ and $\dot{Q}''_L$ changing based upon a combination of the fire dynamics and the material properties.

6.3 Controlling Flaming Combustion

As first introduced in Chapter 4, the modified means of controlling the FPA can be used to control the MLR of bench-scale samples. Once the MLR becomes a fixed variable, the supply of gaseous fuel can be independently controlled, breaking the coupling to the oxidiser flow. Such control allows the flame geometry and effluent composition to be explored as a function of the combustion environment.

The use of a proportional integral derivative (PID) controller enables the energy supplied by the FPA lamps, $\dot{Q}''_E$, to be adjusted. Changing $\dot{Q}''_E$ with time can be used to obtain a controlled MLR if the values of $\dot{Q}''_F$ and $\dot{Q}''_L$ provide a constant net heat flux to the surface. Once an appropriate MLR has been selected, one that enables a flame to be sustained, then the analysis of the changing magnitude of $\dot{Q}''_F$ will enable the effect of different oxidative environments on flame geometry to be probed.

6.3.1 Sustaining a Flame

The modified means of controlling the FPA was used as discussed during Chapter 4, where the constants for the PID controller were set to 2, 0.01 and 8 for K_p, K_i and K_d respectively. This section contains any deviations from the materials and the methodology presented thus far.

Two synthetic straight-chain polymers were commercially sourced: opaque, black circular discs (70 mm diameter) of polyoxymethylene (POM) type h (homopolymer) and polymethylmethacrylate (PMMA). Consulting literature, PMMA has a higher ideal burning rate in comparison to POM when assessing these thermoplastics burning in the FPA [12,13]. To enable a flame to be sustained for similar durations, thicker samples (21 mm) of PMMA were used in comparison to the POM (12 mm). These differing thicknesses resulted in the samples weighing 100 g and 75 g for the PMMA and POM respectively. Each sample had its rear face wrapped in foil, preventing molten material falling from the sample holder.

The circular samples were placed onto the pedestal connected to the load cell within the combustion chamber of the FPA, where the presence of a pilot flame (60 % air, 40 % ethylene) was used to facilitate ignition. A quartz tube (435 mm high, outer diameter 174 mm, inner diameter 164 mm) was placed over the sample. The modified means of controlling the FPA was used to sustain the MLR of 5 $\pm$ 2.03 g s^{-1} m^{-2} for the POM and 13 $\pm$ 2.70 g s^{-1} m^{-2} for the PMMA, values great enough to sustain flaming combustion under ambient conditions during preliminary experiments. After an initial ramp (0.02 kW m^{-2} s^{-1}, 60 s) the PID controller was initiated, controlling the voltage supplied to the lamps and therefore the heat flux supplied to the specimen over the 1400 second experimental period.

An oxidiser stream, 177 L min^{-1}, was flowed around the circular samples to enable a uniform flow, minimising any disruption to the flame geometry as shown in Table 6.1. The composition of this flow ranged from 0 to 20.9 % oxygen with the balance being nitrogen.

Samples were allowed to stabilise under ambient oxidative conditions for 200 seconds once ignition had been achieved. From this point, the desired oxidative conditions were gradually introduced over 500 seconds to minimise disruption to the established flame. Once the flame had stabilised under the intended oxidative environment, $t = 900$ seconds, FT-IR emission sampling occurred for 500 seconds as per Chapter 4. The precise oxidative atmospheres used for each thermoplastic varied to ensure oxidative conditions covered the region in which flaming combustion was quenched and the sample behaviour transitioned to pyrolysis only, ∼9.25 % and ∼12.75 % oxygen for the POM and PMMA, respectively.

By focusing on assessing changes in asphyxiant yields, FT-IR sampling was deemed to adequately monitor species with low boiling points like CO. As such, GC-MS sampling did not occur during these experiments when assessing POM and PMMA. Such data would be beneficial to obtain, providing an opportunity for future research to occur.

6.3.2 Controlled Mass Loss Rate

In order to sustain a flame, each thermoplastic was required to burn for the entire sampling duration, 1400 seconds, ensuring that a stabilised flame was generated for effluent sampling. During preliminary trials, the high volumetric flow rate, 177 L min^{-1}, required elevated sample MLRs to ensure combustion species and pyrolysis gases were being generated above the limits of detection. Table 6.1 summarises the MLRs used across each of these experiments.

Table 6.1: The mean average and standard deviation (SD) of the smoothed mass loss rates (MLRs) obtained during the flaming combustion/ pyrolysis of POM and PMMA under several differing environmental conditions.

POM			**PMMA**		
O_2 / %	MLR / g s^{-1} m^{-2}	SD /	O_2 / %	MLR / g s^{-1} m^{-2}	SD /
0	5.02	0.08	0	12.60	0.38
5	5.05	0.16	5	13.04	0.16
7	5.07	0.41	10	12.00	1.03
8.5	5.02	0.09	12.5	12.48	0.44
9	4.94	0.12	12.75	13.09	0.12
9.25	5.07	0.08	13	12.99	0.33
9.5	5.21	0.25	13.5	13.04	0.24
10	5.25	0.21	14	13.16	0.30
15	5.23	0.27	15	13.01	0.12
18	5.68	0.18	18	12.90	0.18
20.9	6.74	0.21	20.9	13.77	0.60

The MLRs for each experiment in Table 6.1 are plotted in Figure 6.2. A controlled MLR was obtained for both thermoset polymers across each of the investigated oxidative environments. Ambient atmospheres, 20.9 % oxygen, resulted in slightly higher MLRs, yet overall, the values were consistently maintained. These slightly higher MLR suggested that the ambient oxidative environments resulted in a reduced degree of control over the MLR, a potential limitation of the technique.

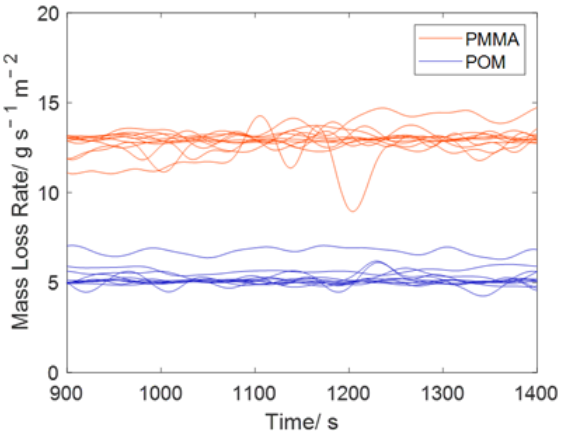

Figure 6.2: The smoothed (Gaussian filter, 60 periods) mass loss rates (MLRs) obtained for the PMMA and POM experiments over the range of oxidative conditions presented in Table 6.1.

Figure 6.2 shows that the PID controller could successfully be used to control the MLR during both flaming combustion and pyrolysis. Flames were quenched when the oxygen percentages fell below 12.75 % (PMMA) and 9.25 % (POM). The absence of a flame during the experiments under lower oxidative conditions did not alter the set MLR, demonstrating that the impact of the oxidiser had been decoupled from any effects arising from the flame, enabling the impact of oxygen on the flame to be independently assessed.

6.4 Differing Flame Types

Due to their lack of complexity, simple synthetic polymers are often used to assess combustion phenomena. PMMA and POM are examples of such simple straight-chain polymers, each constructed from the repetition of a single monomer unit. Figure 6.3 shows the structures of these polymers and their principal monomers.

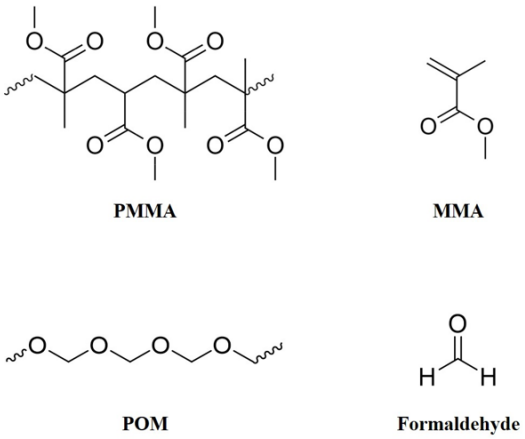

Figure 6.3: The structures of the polymers PMMA and POM are shown to the left, with their monomers (methyl methacrylate (MMA) and formaldehyde) displayed to the right.

Both POM and PMMA contain oxygen within their structures, acting as a source of oxidiser during combustion. POM has a higher percentage of oxygen by mass and as a result it burns with an essentially soot-free blue flame [135]. Although PMMA also contains oxygen, the ratio to carbon and hydrogen is reduced, resulting in PMMA burning with a more sooty, luminous flame. These differences are shown in the images presented in Figure 6.4.

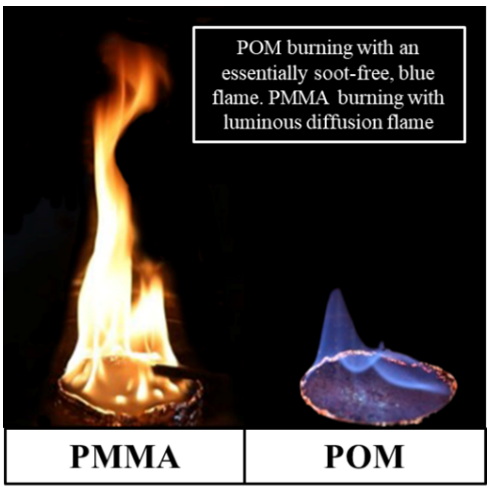

Figure 6.4: The combustion of PMMA and POM. The PMMA to the left burns with a luminous diffusion flame while the additional oxygen within the POM results in an essentially soot-free blue flame on the right.

The flames depicted in Figure 6.4 are fuelled by a gaseous stream of pyrolysis products. During pyrolysis, both the POM and PMMA primarily generate their respective monomers, Figure 6.3, where yields ≥90 % have been recorded in literature [15–18]. Therefore, the detection of methyl methacrylate (MMA) or formaldehyde alongside the observation of a flame would indicate that unoxidised pyrolysis products were entering the effluent, bypassing the flame.

If the generated pyrolysis products pass through the flame envelope, they are oxidised producing a variety of combustion products including carbon monoxide (CO), CO_2 and H_2O. Equations 6.2 and 6.3 depict the complete oxidation of the investigated monomers, formaldehyde (CH_2O) and MMA ($C_5H_8O_2$), under a fully oxygenated environment.

$$CH_2O_{\,(g)} + O_{2\,(g)} \rightarrow CO_{2\,(g)} + H_2O_{\,(g)} \tag{6.2}$$

$$2\ C_5H_8O_{2\,(g)} + 6\ O_{2\,(g)} \rightarrow 5\ CO_{2\,(g)} + 4\ H_2O_{\,(g)} \tag{6.3}$$

Stoichiometrically, a single mole of oxygen is required to facilitate the complete combustion of formaldehyde. This ratio is six times smaller than the oxygen requirement per mole of MMA, explaining the relative ease of POM combustion under oxidative conditions and hence the blue flame in Figure 6.4. If the flame moves into an under-ventilated regime, incomplete oxidation of the pyrolysis products will occur. Under these conditions formaldehyde has been shown to generate CO, as outlined by Equation 6.4 [136]. Such behaviour indicates that CO may be produced by POM under completely inert atmospheres.

$$CH_2O_{\,(g)} \rightarrow CO_{\,(g)} + H_{2\,(g)} \tag{6.4}$$

6.4.1 Qualitative Flame Geometry

Visual differences between the flames established under each of the assessed oxidative environments were noted. Images comparing the qualitative differences between the stabilised flames are presented in Figures 6.5 and 6.6. Under periods of heightened heat flux, the intensity of the FPA lamps obscured the flame, particularly true for the lower luminosity POM experiments. To negate these effects, images were selected during periods of low incident heat flux, enabling visualisation of the flame envelope.

Despite being qualitative, the images in Figures 6.5 and 6.6 show the impact of changing the oxidative environment on the flame geometry. In comparison to the PMMA, changes in the POM flame geometry were much harder to observe, however an increase in the luminosity and a decrease in the flame width was noted as the oxidative conditions were increased.

Focussing on the PMMA flames presented in Figure 6.6, the greater luminosity enabled more detailed qualitative observations to be made. The flame envelope appeared to be

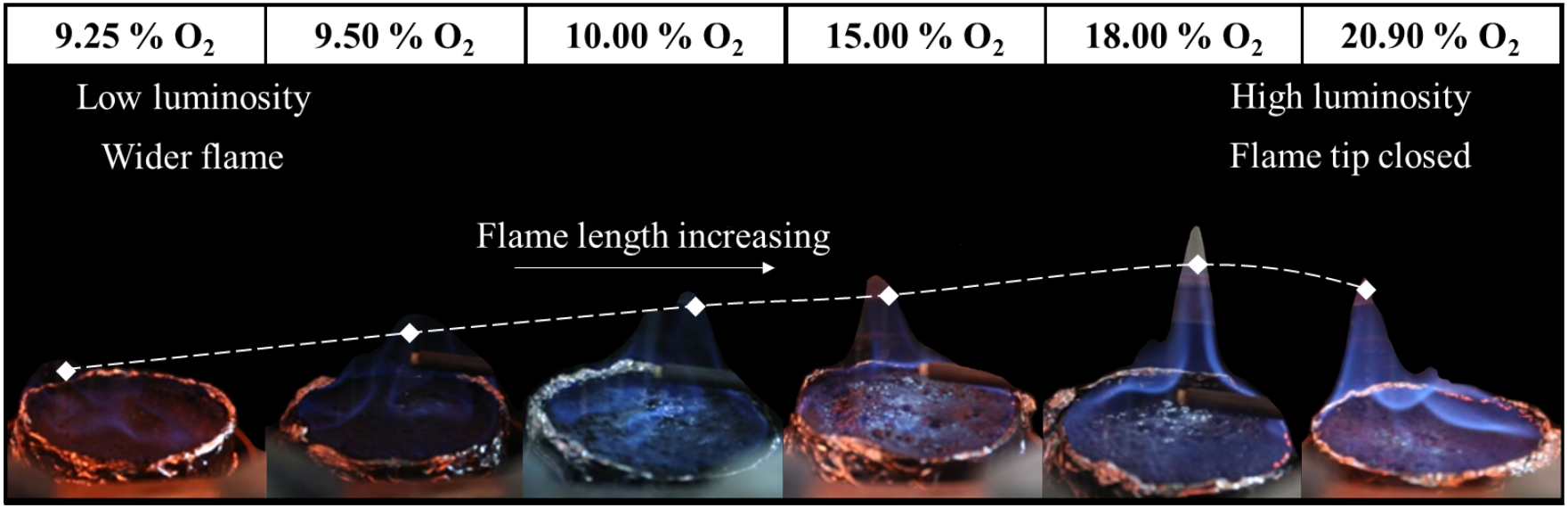

Figure 6.5: The turbulent POM flames observed when the environmental conditions varied between 9.25 % and 20.90 % oxygen. Still images were edited to remove the background glare from the quartz tube. Time averaged images could not be generated as the light generated by the FPA lamps prevented visualisation of the flame.

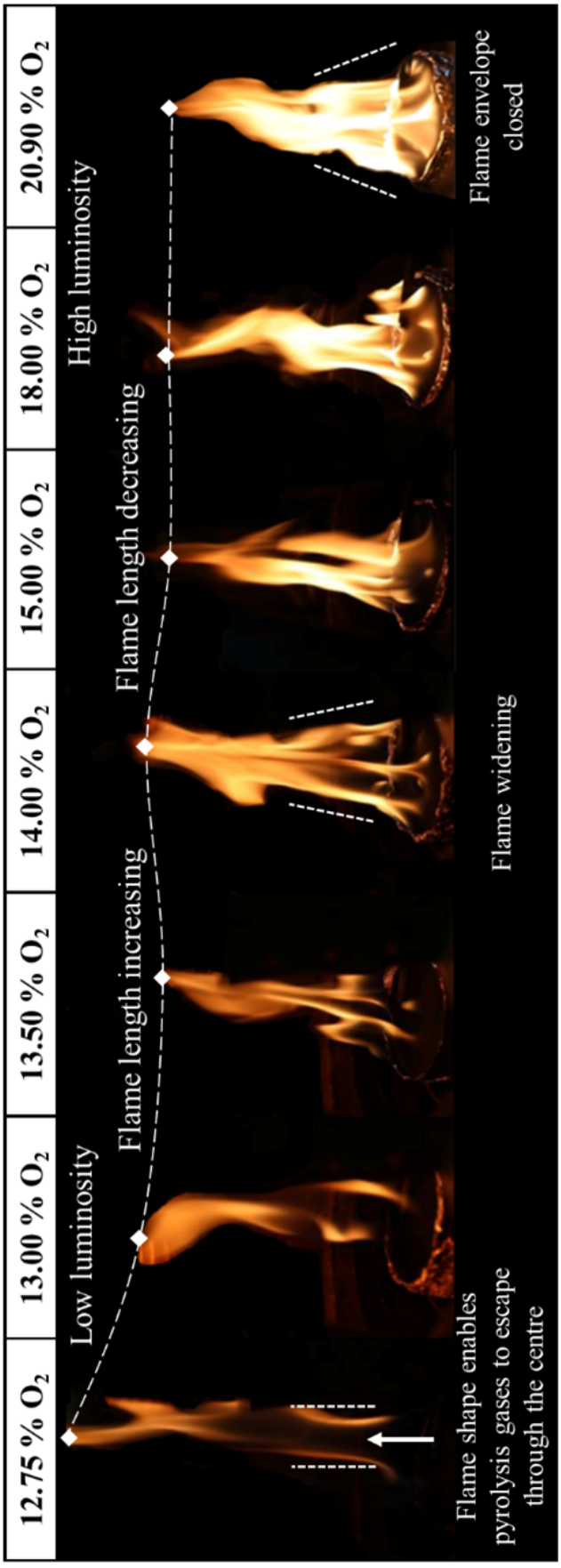

Figure 6.6: The turbulent PMMA flames observed when the environmental conditions varied between 12.75 % and 20.90 % oxygen. Still images were edited to remove the background glare from the quartz tube. Time averaged images could not be generated as the light generated by the FPA lamps prevented visualisation of the flame.

completely closed under the 18.0 % and 20.9 % oxygen environments, suggesting a well-ventilated burning regime dominated by complete combustion. These flames were also the most luminous, correlating with an increase in combustion efficiency. It appeared that the closed flame structure largely prevented the emission of unoxidised species.

Flame heights were also shown to vary with the oxidative environment, aligning with the predictions made by the Burke-Schumann development. Under the lowest oxidative conditions that sustained a flame, 12.75 % and 13.0 % oxygen, a reduction in the concentration gradient lessened the rate of oxygen diffusion towards the flame. Having a restricted oxygen supply resulted in a decreased rate of reaction, reducing the flame temperature hence causing a decrease in combustion efficiency. The lower flame temperatures subsequently reduced the rate of oxygen diffusion to the flame front, resulting in an increase in the average flame height for the PMMA [137]. The POM flame heights appeared to decrease under the lower oxidative environments, however, the reduced luminosity decreased the visibility of the flame tip, thus full conclusions regarding the flame location under incidences of high heat flux and low oxidative conditions could not be made.

The PMMA flame tips observed under the lowest two oxidative conditions in Figure 6 appeared to have widened, creating a central passage through the flame. It is plausible that pyrolysis products could pass through this passage and into the effluent without interacting with the flame envelope. This phenomenon was most evident at 12.75 % oxygen, where the flame appeared to mimic the characteristics of the Burke-Schumann flame structure albeit within the confines of an environment with comparatively less control than a co-flow burner. These qualitative observations were used to inform the quantitative work conducted in the next section.

6.4.2 Quantitative Flame Geometry

To facilitate quantitative flame analysis, the video files recorded during the PMMA experiments were analysed by isolating the red colour channel. When the FPA lamps reached their upper limits, the intensity of the lamps masked the flame, thus saturated video frames were discarded from the analysis. Figure 6.7 shows the average flame location recorded over a 500 second period during the steady state combustion of PMMA. A second version of this plot with an alternative colour scheme is presented in Figure D.1 and can be found in Appendix D.

A similar plot could not be obtained for the POM flames due to a combination of the decreased flame luminosity and reduced flame height. As per Figure 6.5, the POM flames under the lower oxidative conditions were barely visible due to the increased FPA lamp intensity combined with the reduced luminosity of the blue flames. As such, image distortion from the light emitted by the FPA lamps prevented image quantification for the POM flames.

The slight offset of the camera alongside cropping the video frames to block out the FPA lamps explains the slightly asymmetric nature of the flame observed at 12.75 % oxygen. The other discrepancy in Figure 6.7 occurred for the flames at 18 % and 21 % oxygen where the flame appeared to consist of two parts. The apparent upper part of the flame

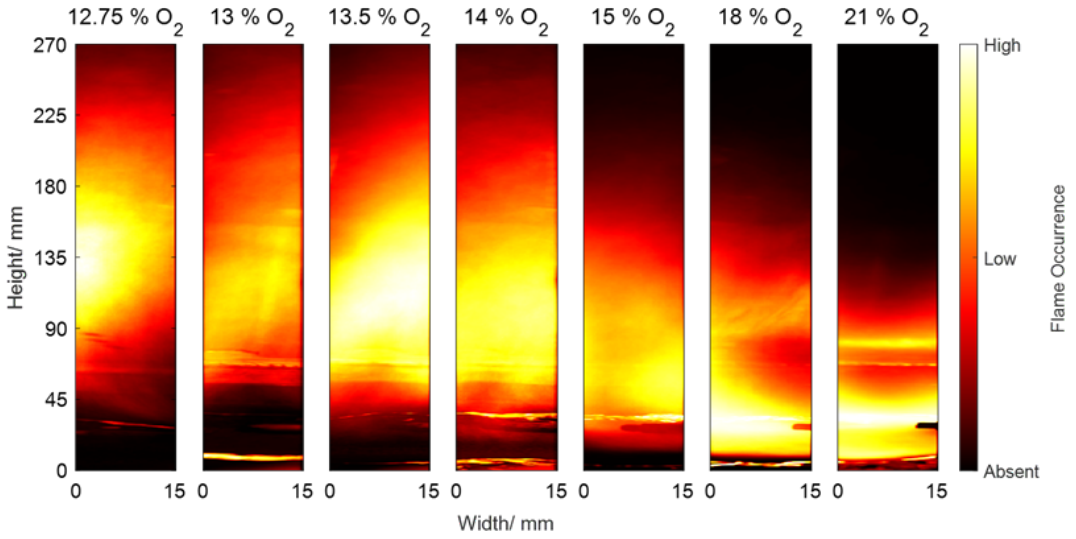

Figure 6.7: The average flame occurrence obtained during the steady state combustion of PMMA under a range of oxidative conditions. Yellow areas indicate high flame occurrence, while black regions denote the absence of a flame.

is a reflection of the flame in the FPA quartz tube. A combination of the reduced flame heights and greater luminosities under these oxidative conditions enhanced this reflective effect. These reflections could not be easily removed during the image analysis and were only notable for short, luminous flames.

For the PMMA flames, the lower oxidative environments, 12.75 % oxygen, resulted in the average flame location being ∼90 mm further from the surface of the polymer compared to the ambient conditions. The increased flame anchoring under ambient oxidative environments caused a ∼180 mm reduction in the average flame height from ∼225 mm to ∼45 mm. The low occurrences of flaming, shown in red, increased in abundance under the lower oxidative environments, highlighting the greater variability in flame structure associated with under-ventilated combustion.

To further quantify these flames, the heat flux supplied by the FPA to control the MLR was assessed. As shown by Figure 6.8, an increased heat flux was required to sustain the steady state MLR under reduced oxidative environments. Once the percentage of available oxygen dropped below 18 %, both polymers displayed this oxygen dependency. Such results indicated that a reduced heat flux was being returned to the surface of the polymers under lower oxidative environments, correlating with a decrease in combustion efficiency.

Once the flames had been quenched, $\leq$ 12.75 % and $\leq$ 9.25 % oxygen for the PMMA and POM, the heat flux required to maintain pyrolysis could be assessed. The PMMA showed little variation in the supplied heat flux whilst maintaining the target MLR, aligning with the conclusions drawn in Chapter 4. However, it was noted that an increased heat flux was required to maintain the MLR of the POM under inert environments, indicating that the POM had a greater oxygen dependency than the PMMA in the absence of a flame. Further investigation into the impacts of oxygen on POM pyrolysis pathways would be required before firm conclusions can be drawn.

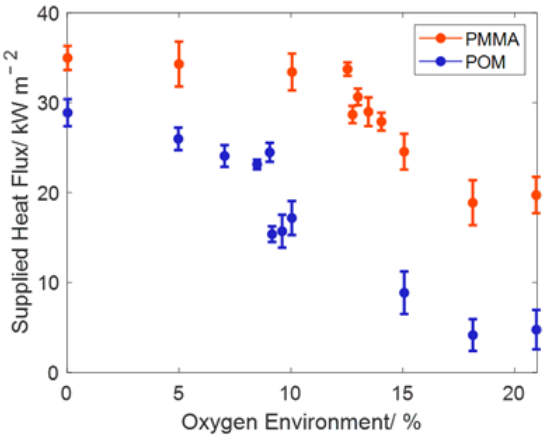

Figure 6.8: The average heat fluxes supplied by the FPA to maintain the controlled MLR of 13 g s^{-1} m^{-2} and 5 g s^{-1} m^{-2} for PMMA and POM respectively, across a range of differing oxidative environments.

Rearranging Equation 1, assuming L_v values of 1.62 and 2.43 kJ g^{-1} for PMMA and POM respectively whilst also assuming that the energy losses, $\dot{Q}''_L$, were constant for each material, enabled the heat flux supplied by the flame to the sample's surface, $\dot{Q}''_F$, to be calculated [2, 138]. Using this calculation, the average heat feedback supplied by the flame was obtained and is plotted in Figure 6.9 for both PMMA and POM across the differing oxidative environments during which flaming combustion was sustained.

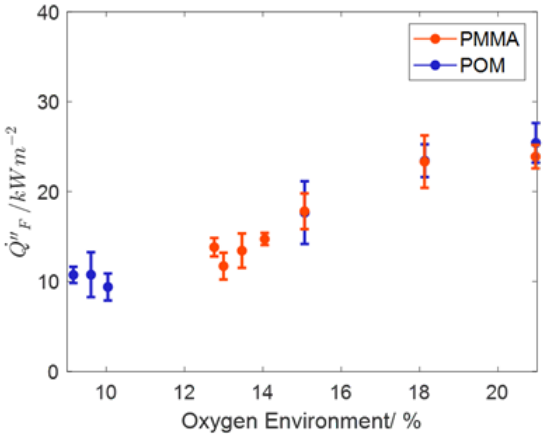

Figure 6.9: The average heat flux supplied by a flame to the surface of a sample, $\dot{Q}''_F$, for PMMA and POM across a range of differing oxidative environments during which flaming combustion was sustained. These values have been calculated using latent heat of vaporization (L_v) and $\dot{Q}''_L$, values from literature [2, 138].

Figure 6.9 only includes the oxidative environments during which flaming combustion was sustained. Overall, decreasing the oxidative environment decreased the heat flux supplied by the flame for both the PMMA and the POM. For both polymers, the lowest oxidative conditions that sustained a flame resulted in a slightly larger value of $\dot{Q}''_F$, when

compared to the neighbouring values. It was proposed that the flame structure during these experiments was unstable, as evidenced by the central passage opening up in Figure 6.6, with the onset of flame quenching potentially distorting the obtained values.

Under a given oxygen environment, the $\dot{Q}''_F$ values obtained for POM and PMMA appeared to align, despite the significant differences in flame height and flame luminosity between the plastics. Two contributors to $\dot{Q}''_F$, the flame temperature and the soot volume fraction, could not be individually distinguished. It is likely that the combination of the differing magnitudes of these values (a higher flame temperature but lower soot volume fraction for POM versus a lower flame temperature but higher soot volume fraction for PMMA) resulted in POM and PMMA having similar $\dot{Q}''_F$ values.

These results agreed with literature where linear fuels containing oxygen, like POM and PMMA, are known to have a similar $\dot{Q}''_F$, reported as 38.5 kW m^{-2} [138]. The values obtained during the experiments presented here, 25.4 $\pm$ 2.2 kW m^{-2}, are likely to differ in magnitude in part due to the differing methodologies used to obtain the data. Despite these differences, the alignment between the polymers within each study is significant, highlighting the usefulness of the modified means of controlling the FPA for assessing flaming combustion.

The values of $\dot{Q}''_F$ clustered together, around 11 kW m^{-2}, for the POM experiments conducted between 9.25 % and 10.0 % oxygen. These oxidative environments each sustained a relatively weak flame as evidenced by Figure 6.5. The slight rise in the magnitude of the $\dot{Q}''_F$ values obtained around the flame quenching point mirrored the behaviour exhibited by the PMMA, once again suggesting that instabilities in the flame envelope impacted the calculated value of $\dot{Q}''_F$. It appeared that POM and PMMA exhibited similar flame behaviour under low oxidative environments, however additional data investigating more intermediate oxidative values would be required to confirm the apparent trends.

6.5 Effluent Composition

Given the discussed differences in flame geometry noted across the experiments, mirroring the Burke-Schumann framework, changes in effluent composition were expected. For each thermoplastic, three chemical species were monitored in the effluent: the monomer (MMA or formaldehyde), CO and CO_2. To account for the minor discrepancies in the MLR and therefore slight variations in the gaseous fuel flow rate, species yields rather than concentrations were plotted.

Once stabilised, the effluent was sampled every three seconds over a 500 second period, yielding 165 data points for each investigated oxidative environment. To account for the large volume of data, average yields are plotted in Figures 6.10 and 6.11 with error bars summarising the error in the FT-IR measurements alongside variance caused by the occasional intermittent generation of pyrolysis gases when the PID controller adjusted the MLR of the sample.

When the oxidative conditions dropped below 12.75 % and 9.25 % for the PMMA and POM respectively, the flames were quenched, causing the monomer yields to rise and the CO_2 yields to fall. Comparing Figures 6.10 and 6.11, the main difference surrounded the oxidative conditions that promoted CO formation, with the POM preferentially generating CO under lower oxidative environments while the PMMA required a flame alongside higher oxidative conditions to generate detectable yields of CO.

As per Equation 6.4, the POM generated CO alongside formaldehyde in the absence of a flame [18]. Once flaming combustion became established, the CO yield reduced before becoming negligible when the oxidative environment rose above 10 %. Under these higher oxidative environments, the generated CO could be completely oxidised to CO_2, causing the yield to rise to approximately 1.15 g g^{-1}. Despite this plausible explanation, the FT-IR band responses for CO_2 and formaldehyde overlap, potentially resulting in a degree of misallocation. As the CO_2 yield stabilised for environments $\geq$15 %, it is likely that the high flow rates enabled a stoichiometric mixture, resulting in effectively complete combustion. The relationship between the CO and CO_2 generation for POM is worth investigating further via analysis of additional intermediate oxidative condition under differing flow rates.

Returning to the composition of the PMMA effluent in Figure 6.10, unoxidised MMA monomers comprised the majority of the effluent in the absence of a flame, i.e, oxidative environments below 12.75 % oxygen. During pyrolysis, there appeared to be some evidence to support a slight decline in MMA yield as the oxygen levels increased, suggesting that some oxygen dependent pyrolysis pathways were being utilised. At 12.75 % oxygen, the presence of a flame enabled oxidation of the pyrolysis products resulting in an increased CO and CO_2 yield. The decreased oxygen percentage by mass within the chemical composition of the PMMA compared to the POM resulted in a decreased combustion efficiency for the PMMA, thus explaining the increased CO yield under oxidative environments that facilitated flaming combustion.

At 12.75 % oxygen, the MMA yield was greatly reduced, 0.02 g g^{-1}, however, the detection

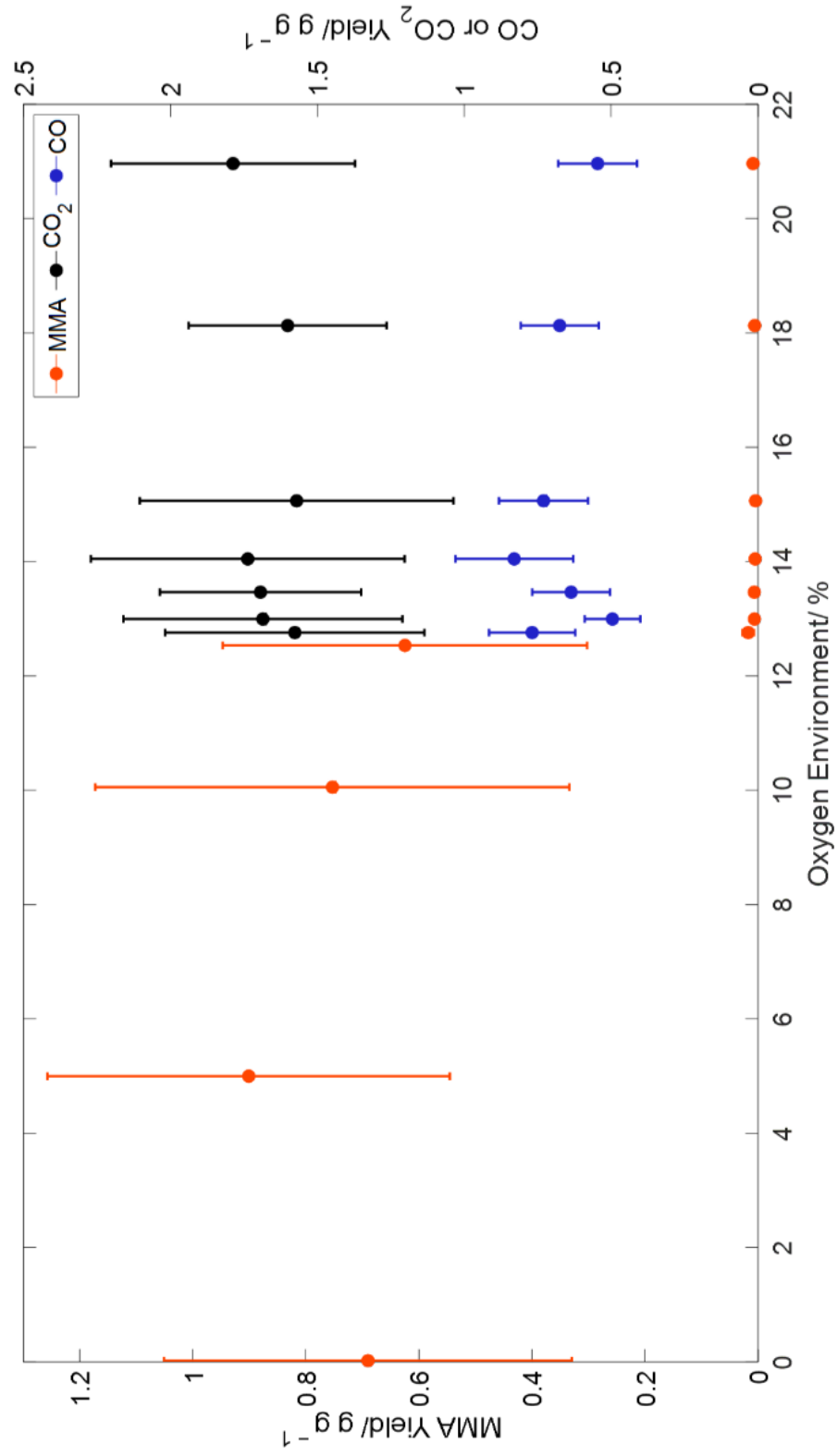

Figure 6.10: The average yields of MMA, CO and CO_2 obtained during the combustion and pyrolysis of PMMA under a fixed MLR over a range of oxidative environments.

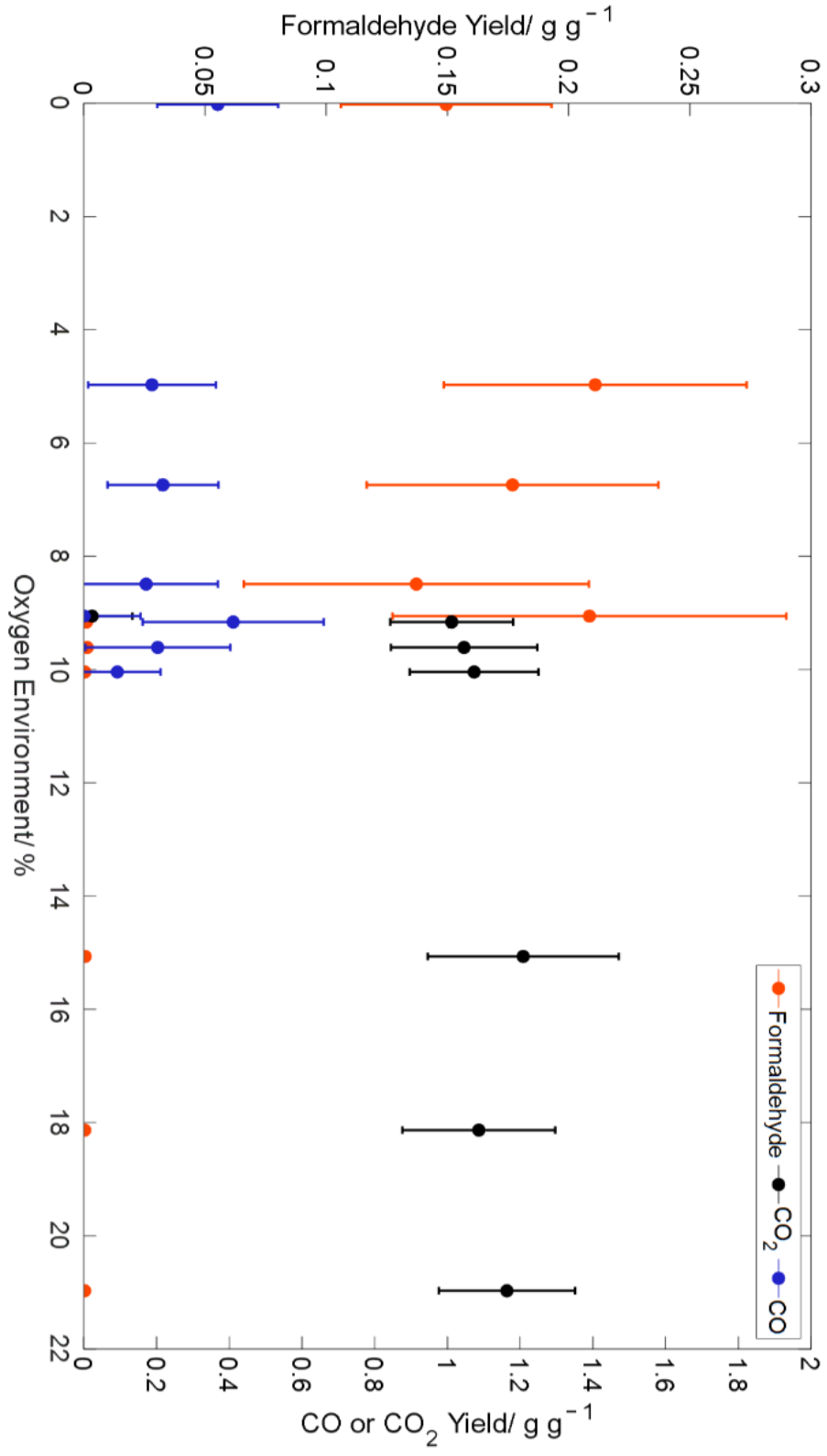

Figure 6.11: The average yields of formaldehyde, CO and CO_2 obtained during the combustion and pyrolysis of POM under a fixed MLR over a range of oxidative environments.

of MMA confirmed that pyrolysis products were entering the effluent in the presence of a flame. Such results support the response of the open flame structure described in the Burke-Schumann framework, Figure 6.1, in which the flame envelope fans-out under low oxidative environments, enabling pyrolysis gases to escape through the centre.

6.5.1 Monomer Emissions

Due to the flame shapes outlined in Figure 6.6, the prevalence of the monomer MMA was expected to vary with the oxidative conditions. By focusing on the emission of the monomer MMA, the dominant pyrolysis product from PMMA, assessment of the extent of oxidation arising from flaming combustion could be made. Figure 6.12 shows how the MMA yield varied during the investigated oxidative conditions that sustained a flame close to the flame quenching point. A similar plot for POM and formaldehyde, Figure D.2, is included in Appendix D.

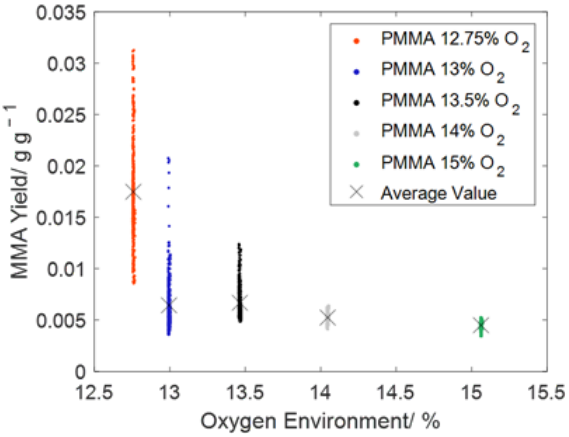

Figure 6.12: The MMA yields obtained during the combustion of PMMA under a fixed MLR across a range of oxidative environments.

Figure 6.12 showed that the emission of MMA varied with oxygen composition, with the range of the MMA yield decreasing as the oxidative environment increased. The largest range for the MMA yield occurred when flaming combustion was established at 12.75 % oxygen. Here the turbulence decreased the flame stability, disrupting the central passage in the flame and therefore impacting the extent of unoxidised species entering the effluent. Comparing the variation between the 14 % and 15 % oxygen cases to the 12.75 %, 13 % and 13.5 % oxygen experiments showed that it was preferable for unoxidised species to enter the effluent close to the flame quenching point, reinforcing the conclusions made during the analysis of the flame geometry. The Burke-Schumann effect was enabling monomer species to pass into the effluent unoxidised.

6.5.2 Changing the Combustion Environment

Further experimental work was undertaken to determine whether intermediate yields of each monomer and the combustion product CO_2 could be detected when changing the composition of the oxidiser flow during an experiment. For these experiments, once the flame had stabilised under ambient conditions, the oxidative environment was gradually reduced from 20.9 % to 0 % oxygen pausing at each oxygen concentration listed in Table 6.1 at regular 150 second intervals.

As the monomer yields were shown to rise and the CO_2 yields were shown to decrease when approaching the flame quenching point, sweeping the oxidative conditions over this range was expected to generate intermediate species yields. However, changing the oxidative environment still resulted in a sudden yield transition, as evidenced by Figure 6.13 in the prose and Figure D.3 in Appendix D.

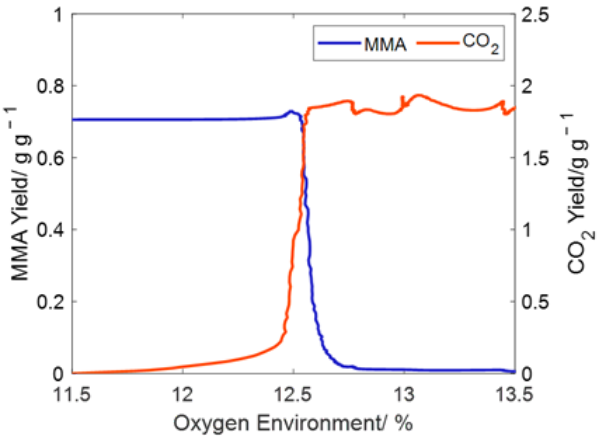

Figure 6.13: The yields of MMA and CO_2 obtained during the combustion of PMMA when sweeping the oxidative conditions between 11.5 % and 13.5 % oxygen.

Altering the percentage of oxidiser available during an experiment resulted in an abrupt change in the effluent composition over the quenching region. Between 12.41 % and 12.57 % oxygen, slightly lower than the environments found to sustain a flame during the controlled MLR experiments, the effluent composition flipped from a combustion dominated processes to a pyrolysis dominated regime. During this interval, once the flame began to fan-out, causing a rise in monomer yields, the flame was rapidly quenched, which caused the MLR to be completely sustained by pyrolysis.

The POM flame was also found to sustain itself under much lower oxidative environments, 7.5 % oxygen, during these sweeping trials. These results suggested that the POM flame had not fully stabilised under the changing environments, thus more work with reduced flow rates and greater intermediate oxidative conditions is required to further investigate quenching phenomena. The modified means of controlling the FPA has enabled a new means of assessing the impact of oxidiser on effluent composition, opening up the potential for the technique to be used to study flame quenching in greater detail.

6.6 Methodology Overview

Using the developed methodology, the flame geometry for two condensed-phase fuels, POM and PMMA, was systematically varied via the independent control over the MLR across a range of oxidative conditions. A controlled gaseous fuel injection rate (MLR), facilitated by the modified means of controlling the FPA, enabled the impact of ventilation on the generated diffusion flames to be decoupled from the burning rate. Such a decoupling prevented positive feedback cycles associated with the surface energy balance increasing the fuel injection rate and/or the energy released by the flame.

Under a 15 % oxygen environment, $\dot{Q}''_F$ values of 25.4 $\pm$ 2.2 kW m^{-2} were obtained for both POM and PMMA. Despite having visually different flames, the alignment of these values for these thermoplastics agreed with existing literature. In comparison to PMMA, it is believed that the higher flame temperature associated with POM was offset by the low soot volume fraction, leading to a similar $\dot{Q}''_F$. Further work assessing other thermoplastics, particularly those with a low oxygen composition, should aim to evaluate the robustness of the presented methodology. It is evident that the modified means of controlling the FPA provides a useful means of quantifying flaming combustion.

The successful decoupling of the fuel and oxidiser enabled insights between the flame geometry and effluent composition to be drawn. CO_2 yields, calculation of the flame heat feedback, visual observations and monomer generation all indicated behaviour in agreement with the Burke-Schumann framework. Under low oxidative environments the diffusion flames were observed to open up, creating a central passage that enabled unoxidised pyrolysis products to be emitted into the effluent. As the oxidative conditions increased, flames increased in luminosity, reduced in height and the flame tips narrowed before eventually closing. $\dot{Q}''_F$ values rose from 9.4 kW m^{-2} to 25.4 kW m^{-2} for the POM and from 13.0 kW m^{-2} to 23.8 kW m^{-2} for the PMMA, while respective monomer yields fell, reflecting the increased combustion efficiency of the flames under ambient atmospheres.

Such insights could only be provided by decoupling the link between MLR and oxidiser flow, enabled by the modified means of controlling the FPA. As such, it was verified that the FPA could be used to control the burning rate of simple polymeric materials, allowing effluent composition to be probed whilst enabling investigation into the reasons for these changes (i.e., observations of the flame geometry).

This chapter has demonstrated that the fire science field can begin to move away from simplifying flames as point sources from which chemical species may enter the effluent. The use of the modified means of controlling the FPA has shown that these flames behave as diffusion flames with their geometry varying as a function of the oxidative environment. Accounting for this behaviour, the impacts of flame geometry on effluent composition should be further investigated utilising the technique, enhancing our understanding of fire effluent across a range of scenarios. It is hoped that future work will focus on assessing the impacts of controlled flaming combustion on the generation of irritant species that may be tracked through other analytical means (GC-MS).

This page has been intentionally left blank.

Chapter 7

Conclusions

"Though the embers of ambition burn."

– Maxïmo Park
All of Me (Nature Always Wins, 2021)

This page has been intentionally left blank.

7.1 Overview

Through the assessment of various materials, this thesis has demonstrated that controlled bench-scale conditions can enable differing asphyxiants and combustion processes to be quantified in a novel manner. The generation of hydrogen cyanide (HCN) during the char oxidation of polyisocyanurate (PIR) foam was shown to favour oxygenated conditions, overturning previously accepted literature. Furthermore, independent control over the oxidative environment demonstrated that carbon monoxide (CO) was not a major pyrolysis product generated by PIR or phenolic foam. Instead, it was determined that CO is primarily a product indicative of char oxidation for these foams. By increasing our understanding of the means by which asphyxiants are generated, fire safety models and material designs can aim to restrict specific combustion pathways.

Advancements in the assessment of flame structures have enabled insights into the origin of pyrolysis products for condensed-phase fuels, previously unseen for real-world materials. Flame structures were shown to mirror the Burke-Schumann development, explaining the presence of unoxidised monomer species in fire effluent close to the flame quenching point. Such insights into the origins of these species in fire effluent will enable existing materials to be screened, advancing our understanding of effluent generating pathways in relation to flame geometry. These advancements will enable future thermoplastics to be designed with more predictable combustion behaviours.

A new methodology has been presented, enabling the effects of oxidiser composition on heat and mass transfer processes to be assessed for diffusion flames and pyrolysis processes. This work decoupled the link between the gaseous fuel flow rate and the oxidiser composition, through external control over the mass loss rate (MLR) of a sample. Independent control over the MLR prevented unrepresentative pyrolysis process arising from the increased flame temperatures associated with high oxygen environments. Such control enabled the oxidiser composition to be varied as an independent variable, generating a representative effluent stream for sampling. To date a methodology has not been able to decouple these variables for condensed-phase fuels.

This control over the MLR was achieved by modifying the means of controlling the Fire Propagation Apparatus (FPA), to enable the heat flux being supplied to a sample to be altered in real time. The controlled MLR was found to generate a constant stream of effluent, enabling analytical sampling to reflect the conditions at the surface of the sample. Species in the effluent were positively identified through a combination of Fourier transformed - infrared spectroscopy (FT-IR) and gas chromatography - mass spectrometry (GC-MS), increasing the confidence in the species identified in the effluent. The combination of analytical techniques led to an increased understanding of effluent composition whilst improving the means of quantifying species of interest. Key results obtained utilising the novel technique over the course of this thesis included:

- **Identified changes in the geometry of diffusion flames across differing oxidative environments.** The controlled combustion of polymethylmethacrylate (PMMA) and polyoxymethylene (POM) generated flames that exhibited behaviours consistent with the Burke-Schumann development. Flames were observed to open-up

and pyrolysis products were found to enter the effluent unoxidised, observations previously unreported for condensed-phase fuels. Such insights advance existing understandings of the relationships between flame geometry and combustion chemistry for real-world materials. These insights are critical for improving fire safety models and designing materials with predictable combustion behaviours.

- **Successfully decoupling the gaseous fuel flow rate from the oxidiser flow for condensed-phase fuels.** External control over the MLR was shown to disrupt heat feedback loops known to alter the rate of pyrolysis. Through control over the MLR for PMMA and POM, these positive feedback cycles were effectively cut. The decoupling of these parameters, afforded by the methodology, enabled the effects of oxygen on flame dynamics to be investigated in a controlled manner. This novel methodology enables more precise fire testing conditions to be established, reducing confounding variables in combustion research. These methodology advancements are also predicted to improve the reliability of generated effluent data.

- **The generation of a representative stream of emissions for effluent analysis.** The control over the MLR of PMMA sample during pyrolysis was found to generate and maintain a stream of emissions with a consistent composition. Such consistency enabled links between effluent composition and oxidative conditions at the surface of the sample to be made. Stable and representative effluent streams are essential for the accurate assessment of fire effluent, ultimately supporting the introduction of improved hazard evaluations and eventually regulatory recommendations.

- **Quantifying the heat release contribution from char oxidation.** The control over the MLR enabled differences in the supplied heat flux to be linked to burning behaviours. The developed methodology enabled changes in the heat flux supplied to maintain the controlled MLR to be tracked. Such data alongside effluent analysis was used to determine the contribution to char oxidation from PIR and phenolic insulation foams. An improved understanding of the heat release rate associated with char oxidation will improve fire growth predictions when modelling buildings lined with insulation materials. Refinement of these models based on data obtained using the methods outlined in this thesis will inform safer building designs and future material selection.

7.2 Detailed Conclusions

Following on from the key bullet points mentioned in the previous section, the subsections here detail the conclusions discussed throughout the individual chapters that comprise this thesis.

7.2.1 Gaps in the Literature

A detailed literature review focused on three key areas associated with the assessment of fire effluent: the generation, the sampling and the chemical analysis of the effluent. The review concluded that the existing range of analytical techniques was sufficient to successfully analyse fire effluent, provided that the generated data was interpreted correctly. Confidence in any chemical speciation could often be improved by obtaining results from a secondary analytical technique, although the methods were in part limited based upon a priori knowledge of potential species of interest. Fire scientists needed to know the structure of the chemical species that they were likely to detect before being able to finetune the analysis. A similar conclusion was reached when reviewing the sampling strategies. The most favourable sampling strategy depended on the selected analytical method, which often dictated the physical state that the sample had to be acquired in. Despite recorded successes utilising various trapping strategies, overall inline gaseous sampling was preferable whenever it was possible to be successfully implemented.

The biggest gap unearthed during the literature review surrounded the means of generating fire effluent in a representative, yet meaningful, manner. The intricacies of genuine fires were found to be best replicated under larger scales. Room-scale testing methods such as the international organisation for standardisation (ISO) 9705 room provided large enough compartments to experimentally determine how a fire interacts and spreads over a large enclosure. Bench-scale approaches that attempted to replicate these phenomena failed to mirror genuine fire behaviours. These findings resulted in this thesis aiming to develop a methodology that was representative whilst also attempting to decouple the link between the surface energy balance (the oxidiser and the MLR), as existing methodologies simply cannot do this.

7.2.2 Representative Effluent Generation

ISO 9705 room-scale experiments were conducted, screening fuels individually over a range of differing ventilation factors. Changing the ventilation factor enabled differing oxidative environments to become established; however, these changes also caused the flow rate into, and out of, the compartment to vary. The combination of the differing flows and oxidative conditions resulted in compartment temperatures fluctuating, impacting flame spread and effluent mixing timescales. The combined effect of these uncontrolled variables, alongside the differing material properties, caused changes in the MLR, which impacted the burn duration for each material.

The heat release rates (HRRs) determined the energy available to drive the smoke and air flows within the compartment. The unintentional changing of multiple variables between experiments prevented conclusions regarding the impact of the oxidiser from being drawn. It became apparent that changes in the effluent composition needed to be linked to a single changeable variable, thus, bench-scale techniques were developed.

7.2.3 Method Development

The means of controlling the FPA was modified to include a proportional, integral, derivative (PID) controller that could adjust the voltage sent to the lamps based upon the MLR of a sample. The automatic adjustment of the heat flux being sent to the sample enabled the MLR to be controlled and established at a set value. Additionally, an unobstructed view of the sample enabled observations to be linked to the effluent composition. The methodology was successfully used to investigate the pyrolysis of PMMA, polystyrene and timber. Sampling of the effluent occurred via GC-MS and FT-IR, enhancing the confidence in the chemical speciation and the quantification of the effluent.

This new methodology enabled the MLR to become a fixed control variable, decoupling it from the oxidiser composition, thus enabling the composition of effluent to be linked to a single changeable variable. The unique decoupling has yet to be seen for condensed-phase fuels allowing the technique to investigate the effects of oxidiser composition on pyrolysis and combustion processes in a novel manner.

7.2.4 Oxidative Processes

Alongside enabling an unobstructed view of the sample throughout an experiment, the developed methodology was able to record the heat flux required to maintain the set MLR. When assessing PIR and phenolic insulation foams using the methodology, the surfaces of the foams were observed to form a char layer which, under oxidative conditions, correlated with an increased CO yield in the effluent. The methodology not only enabled this change to be observed, but through comparison to the inert experiments (conducted under nitrogen to prevent the char being oxidised), the effect of char oxidation could be quantified.

These results highlight the complex behaviours exhibited by different materials, showing the value of observing a sample throughout an experiment. By maintaining the MLR at a set value, the differences in the supplied heat flux provided a key insight into heat transfer processes. Previous methodologies had to contend with alterations in the MLR when assessing char oxidation, preventing the quantification of the char oxidation that this new methodology enabled.

7.2.5 Flaming Combustion

The modified means of controlling the FPA was demonstrated to control the flaming combustion of two thermoplastics: polyoxymethylene (POM) and PMMA. Flames could be produced and sustained if the MLR was set above the burning rate required to maintain the flame, indicating that the methodology had complete control over flaming combustion. The decoupling between the MLR and the oxidiser enabled the effect of oxygen composition on flame geometry and the resultant emissions to be analysed.

The diffusion flame geometry for these two condensed-phase fuels was shown to follow the Burke-Schumann development, where the flame widened under lower oxidative conditions, enabling the emission of unoxidised pyrolysis products. The monomer methyl methacrylate (MMA) was detected in the effluent generated by flames sustained by PMMA under oxidative conditions close to the quenching point, aligning with the observed changes in flame geometry and luminosity. Early characterisation work has begun to characterise the flame through the investigation of simple polymers in terms of the Burke-Schumann effect. The developed methodology has enabled the gas-phase combustion problem to be independently studied for condensed-phase fuels.

7.3 Research Applications

The use of the modified means of controlling the FPA to assess flame behaviour enables the effects of the oxidiser to be studied independently from other variables, most notably the MLR. This approach has been shown to enable insights into the char oxidation of both timber and insulation foams, where further investigation into differing oxidiser compositions will aid our understanding of the char oxidation phenomena. The quantification of the rate of char oxidation under differing environments will provide information on structural retention times for timber beams and enhance evacuation models focused on CO generation during the char oxidation of insulation foam linings.

Most notably, the approach enables thermal and oxidative environments to be used to evaluate flame geometry. The fixed MLR has enabled diffusion flames to be screened across a range of oxidative conditions, detailing changes in flame geometry and effluent composition. Such insights confirming that the flame geometry had changed during combustion could only be provided by decoupling the link between MLR and oxidiser flow, enabled by the developed methodology. By increasing our understanding of the oxidiser and the thermal environment, the impact of the changes in flame geometry on effluent composition can be assessed. These findings will increase our understanding of the conditions that enable products of concern, like HCN and CO to be formed.

Existing fire models understandably fail to account for the complex relationship between flame structure, combustion chemistry and effluent composition, resorting to simplify it. Now that the coupling between the MLR and the oxidiser has been shown to be separated, the fire science field can begin to treat simple flames as diffusion flames rather than simplifying flames as point sources from which chemical species may enter the effluent. Fire models and evacuation simulations will be able to enhance the accuracy of the smoke composition by adjusting their models to account for the diffusion flame behaviours that vary with oxygen composition as outlined in this thesis. Such improvements will help inform building design policies, material development and building regulations.

7.3.1 Future Recommendations

Further work linking the effluent composition to flame geometry is expected to enhance the findings presented in this thesis. As the FPA enables control over the air flowing over a sample, it is hoped that effect of differing flow rates on flame geometry will now be assessed. The flow rates can be modified to the precise stoichiometric conditions required to sustain a flame, enabling investigation into flame quenching processes as a function of flow rate. The effects of higher flow rates on flame geometry, particularly flame length, and the resultant impact on effluent composition are hoped to enhance the discussed links between combustion chemistry and flame geometry.

Future work may utilise the methodology to assess the flame geometries of hydrocarbon thermoplastics. The investigation of polystyrene or polypropylene flames, with their higher soot fractions, is expected to increase the magnitude of the $\dot{Q}''_F$ values reported for POM and PMMA in this thesis. Comparing the results of such work to literature would increase

the robustness of the developed methodology. It is hoped that further work adjusting the target MLRs, materials and oxidiser flows will continue to enable the developed methodology to offer insights into the heat and mass transfer processes that impact the effluent generated by flames.

This thesis focussed on quantifying asphyxiants associated with fire effluent. Species including HCN and CO could be readily tracked through FT-IR analysis. Future work should aim to investigate the links between combustion chemistry and flame geometry on irritant species. Some of these species could be tracked using the GC-MS setup discussed during this thesis; however, collecting soot deposits and applying multidimensional chromatography may provide additional insights. Assessing the impacts of a controlled MLR on the variety of species being generated will increase our understanding of mass transfer processes, bringing us one step closer to closing the combustion mass balance.

This page has been intentionally left blank.

References

(1) Y. Chen, J. Fang, X. Zhang, Y. Miao, Y. Lin, R. Tu and L. Hu, *Progress in Energy and Combustion Science*, 2023, **95**, 101070.

(2) D. Drysdale, *An Introduction to Fire Dynamics*, Wiley, 2011, pp. 1–551.

(3) I. Glassman, *Combustion and Flame*, 1977, **29**, 103–105.

(4) I. Marková, J. Lauko, L. Makovická Osvaldová, V. Mózer, J. Svetlík, M. Monoši and M. Orinčák, *International Journal of Environmental Research and Public Health*, 2020, **17**, 411.

(5) S. Dutta, N. K. Kim, R. Das and D. Bhattacharyya, *Composites Part B: Engineering*, 2019, **157**, 195–206.

(6) E. Rezvani Ghomi, F. Khosravi, Z. Mossayebi, A. Saedi Ardahaei, F. Morshedi Dehaghi, M. Khorasani, R. E. Neisiany, O. Das, A. Marani, R. A. Mensah, L. Jiang, Q. Xu, M. Försth, F. Berto and S. Ramakrishna, *Molecules*, 2020, **25**, 5157.

(7) Chuanmei Jiao, Xilei Chen and Jun Zhang, *Journal of Thermoplastic Composite Materials*, 2010, **23**, 501–512.

(8) F. Richter and G. Rein, *Combustion and Flame*, 2020, **216**, 316–325.

(9) C. Di Blasi, C. Branca, F. E. Sarnataro and A. Gallo, *Energy & Fuels*, 2014, **28**, 2684–2696.

(10) J. G. Quintiere, *Fundamentals of Fire Phenomena*, Wiley, 2006.

(11) M. Sibulkin, *Progress in Energy and Combustion Science*, 1988, **14**, 195–212.

(12) G. E. Hartzell, S. C. Packham, A. F. Grand and W. G. Switzer, *Journal of Fire Sciences*, 1985, **3**, 195–207.

(13) M. Panda and N. C. Robinson, *Biochemistry*, 1995, **34**, 10009–10018.

(14) T. Stuttmann, A. Scheerer, T. S. Prince and L. A. Goldstein, *The Journal of the American Board of Family Practice*, 1998, **11**, 481–484.

(15) D. Purser and J. Purser, *Fire Safety Science*, 2008, **9**, 1117–1128.

(16) A. A. Stec and T. R. Hull, *Energy and Buildings*, 2011, **43**, 498–506.

(17) S. T. McKenna, N. Jones, G. Peck, K. Dickens, W. Pawelec, S. Oradei, S. Harris, A. A. Stec and T. R. Hull, *Journal of Hazardous Materials*, 2019, **368**, 115–123.

(18) A. Witkowski, A. A. Stec and T. R. Hull, *SFPE Handbook of Fire Protection Engineering, Fifth Edition*, 2016, 167–254.

(19) T. Bhaskar, R. Negoro, A. Muto and Y. Sakata, *Green Chemistry*, 2006, **8**, 697–700.

(20) W. Kaminsky and C. Eger, *Journal of Analytical and Applied Pyrolysis*, 2001, **58-59**, 781–787.

(21) H. Arisawa and T. B. Brill, *Combustion and Flame*, 1997, **109**, 415–426.

(22) F. Knez, M. Uršič, N. Knez, K. Peeters, M. Franko and P. Zidar, *Fire and Materials*, 2021, DOI: 10.1002/FAM.3042.

(23) T. Ohlemiller, *Progress in Energy and Combustion Science*, 1985, **11**, 277–310.

(24) S. Bhoite, B. Windom, J. Singh, D. Montgomery and A. J. Marchese, *Proceedings of the Combustion Institute*, 2023, **39**, 2533–2542.

(25) S. P. Burke and T. E. W. Schumann, *Industrial & Engineering Chemistry*, 1928, **20**, 998–1004.

(26) I. Glassman and R. A. Yetter, *Combustion*, Elsevier Inc., 4th edn., 2008, vol. 4, pp. 311–331.

(27) S. Fukutani, N. Kunioshi and H. Jinno, *Symposium (International) on Combustion*, 1991, **23**, 567–573.

(28) E. Mastorakos, *Progress in Energy and Combustion Science*, 2009, **35**, 57–97.

(29) B. Andersson, G. Holmstedt and A. Dagneryd, *Fire Safety Science*, 2003, **7**, 295–308.

(30) A. L. Lavoisier, *Traité élémentaire de chimie t.1*, Chez Cuchet, 1789.

(31) S. Kropotova, G. Kuznetsov and P. Strizhak, *Fire Safety Journal*, 2022, **132**, 103643.

(32) B. Prime, H. Bair, S. Vyazovkin, P. Gallagher and A. Riga, *Thermal Analysis of Polymers: Fundamentals and Applications*, ed. J. Menczei and B. Prime, John Wiley & Sons, New Jersey, 2009, pp. 241–253.

(33) N. Saadatkhah, A. Carillo Garcia, S. Ackermann, P. Leclerc, M. Latifi, S. Samih, G. S. Patience and J. Chaouki, *The Canadian Journal of Chemical Engineering*, 2020, **98**, 34–43.

(34) J. Cervantes-Uc, J. Cauich-Rodríguez, H. Vázquez-Torres and A. Licea-Claveríe, *Polymer Degradation and Stability*, 2006, **91**, 3312–3321.

(35) J. Yang, H. Chen, W. Zhao and J. Zhou, *Journal of Thermal Analysis and Calorimetry*, 2015, **124**, DOI: 10.1007/s10973-015-5168-x.

(36) D. Morrisset, J. Burnford, A. O. Ojo, B. Peterson, A. Law and R. M. Hadden, *Proceedings of the Combustion Institute*, 2024, **40**, 105355.

(37) D. Gross, J. J. Loftus and A. F. Robertson, *Symposium on Fire Test Methods—Restraint & Smoke*, 1966, 166–166.

(38) The International Organization for Standardization, *ISO 5659-2:2017 - Plastics - Smoke generation - Part 2: Determination of optical density by a single-chamber test*, 2017.

(39) N. Wolter, V. C. Beber, A. Sandinge, P. Blomqvist, F. Goethals, M. Van Hove, E. Jubete, B. Mayer and K. Koschek, *Polymers 2020, Vol. 12, Page 2379*, 2020, **12**, 2379.

(40) D. M. Marquis, F. Hermouet and É. Guillaume, *Fire and Materials*, 2017, **41**, 245–274.

(41) N. D. Marsh, R. Gann, R. G. Gann, J. D. Averill and M. R. Nyden, *Proceedings of the 9th International Symposium on Fire Safety Science*, 2008, 687–698.

(42) R. G. Gann and N. D. Marsh, *Fire and Materials*, 2021, **45**, 225–249.

(43) B. Schartel, M. Bartholmai and U. Knoll, *Polymer Degradation and Stability*, 2005, **88**, 540–547.

(44) M. L. Janssens, *Fire Technology 1991 27:3*, 1991, **27**, 234–249.

(45) J. Barton, O. Rios, M. Runefors and P. van Hees, *Fire and Materials*, 2021, DOI: 10.1002/FAM.3006.

(46) The International Organisation for Standardization, *ISO 5660-5 Reaction-to-fire tests — Heat release, smoke production and mass loss rate*, 2020.

(47) D. Marquis, E. Guillaume and D. Lesenechal, *Procedia Engineering*, 2013, **62**, 103–119.

(48) D. Marquis and E. Guillaume, Fire and Materials 2013 - Conference Proceedings of the 13th International Conference and Exhibition, San Francisco, 2013.

(49) A. Tewarson, F. Jiang and T. Morikawa, *Combustion and Flame*, 1993, **95**, 151–169.

(50) A. Tewarson, *Fire Hardening Assessment (FHA) Technology for Composite Systems*, tech. rep., Factory Mutual Research Corporation, Norwood, MA, 1994.

(51) R. Chaffer, Ph.D. Thesis, University of Maryland, College Park, Md., 2021, pp. 1–21.

(52) P. Girods, H. Bal, H. Biteau, G. Rein and J. Torero, *Fire Safety Science*, 2011, **10**, 889–901.

(53) N. Bal and G. Rein, *Combustion and Flame*, 2011, **158**, 1109–1116.

(54) The International Organization for Standardization, *ISO/TS 19700:2016 - Controlled equivalence ratio method for the determination of hazardous components of fire effluents steady-state tube furnace*, 2016.

(55) A. A. Stec, T. R. Hull, J. A. Purser, P. Blomqvist and K. Lebek, *Fire Safety Science*, 2009, 653–664.

(56) A. A. Stec, T. R. Hull and K. Lebek, *Polymer Degradation and Stability*, 2008, **93**, 2058–2065.

(57) International Electrotechnics Commission, *IEC TS 60695-7-50 Part 7-51: Toxicity of fire effluent - Estimation of toxic potency: Calculation and interpretation of test results*, 2002.

(58) K. Lebek, T. R. Hull and D. Price, in 2005, pp. 334–347.

(59) British Standards Institute (BSI), *BS EN 13823:2020 Reaction to fire tests for building products — Building products excluding floorings exposed to the thermal attack by a single burning item*, 2020.

(60) R. Van Mierlo and B. Sette, *HERON*, 2005, **50**, 191–207.

(61) B. Messerschmidt, *Fire and Building Safety in the Single European Market*, 2008, 70–81.

(62) The International Organisation for Standardization (ISO), *ISO 9705-1 Reaction to fire tests — Room corner test for wall and ceiling lining products —*, 2016.

(63) X. Qiang, G. Griffin, G. Bradbury and V. Dowling, ed. J. J. Miles, G. R. Peacock and K. M. Knettel, 2006, p. 62051M.

(64) J. C. Posner and W. J. Woodfin, *Applied Industrial Hygiene*, 1986, **1**, 163–168.

(65) J. Z. Dong and S. M. Debusk, *Chromatographia*, 2010, **71**, 259–265.

(66) J. H. Hodgkin, M. N. Galbraith and Y. K. Chong, *Journal of Macromolecular Science: Part A - Chemistry*, 1982, **17**, DOI: 10.1080/00222338208056463.

(67) L. Bengtström, M. Salden and A. A. Stec, *Annals of Work Exposures and Health*, 2018, **62**, 1171–1175.

(68) Z. Jiang, W. K. Chow, J. Tang and S. F. Li, *Polymer Degradation and Stability*, 2004, **86**, 293–300.

(69) A. M. Dhabbah, A. Y. Badjah-Hadj-Ahmed, A. A. Stec and T. R. Hull, *American Journal of Analytical Chemistry*, 2019, **10**, 23–37.

(70) V. Agotici and L. Ciucanu, *Annuals of West University of Timisoara*, 2008, **17**, 73–82.

(71) *Infrared Spectroscopy Absorption Table - Chemistry LibreTexts*.

(72) J. Hietaniemi, R. Kallonen and E. Mikkola, *Fire and Materials*, 1999, **23**, 171–185.

(73) D. Shaw, *Fourier transform N.M.R. spectroscopy*, Elsevier, 1984, p. 344.

(74) A. Santamaría, F. Mondragón, A. Molina, N. D. Marsh, E. G. Eddings and A. F. Sarofim, *Combustion and Flame*, 2006, **146**, 52–62.

(75) M. Duer, *Solid State NMR Spectroscopy: Principles and Applications*, ed. M. Duer, Blackwell Science, Paris, 1st edn., 2002, pp. 3–14.

(76) *University of Ottawa NMR Facility Blog: Magic Angle Spinning*, 2007.

(77) J. W. Gilman, S. M. Lomakin, T. Kashiwagi, D. L. Vanderhart and V. Y. Nagy, *Fire and Materials*, 1998, **22**, 61–67.

(78) J. H. Gross Springer-Verlag Heidelberg and O. David Sparkman, *American Society for Mass Spectrometry*, 2005, **16**, 793–795.

(79) W. R. Zeng, S. F. Li and W. K. Chow, *JOURNAL OF FIRE SCIENCES*, 2002, **20**, DOI: 10.1106/073490402027989.

(80) C. Branca, P. Giudicianni and C. Di Blasi, *Industrial & Engineering Chemistry Research*, 2003, **42**, 3190–3202.

(81) Z. An, H. Ren, M. Xue, X. Guan and J. Jiang, *Journal of Chromatography A*, 2020, **1625**, 461336.

(82) A. I. Balabanovich, M. P. Luda and L. Operti, *JOURNAL OF FIRE SCIENCES*, 2005, **23**, DOI: 10.1177/0734904105047006.

(83) J. Mitera and J. Michal, *Fire and Materials*, 1985, **9**, DOI: 10.1002/fam.810090302.

(84) L. M. McKenzie, W. M. Hao, G. N. Richards and D. E. Ward, *Atmospheric Environment*, 1994, **28**, 3285–3292.

(85) R. Jian, P. Wang, W. Duan, J. Wang, X. Zheng and J. Weng, *Industrial and Engineering Chemistry Research*, 2016, **55**, 11520–11527.

(86) S. M. Dakka, G. S. Jackson and J. L. Torero, *Proceedings of the Combustion Institute*, 2002, **29**, 281–287.

(87) S. Maher, F. P. Jjunju and S. Taylor, *Reviews of Modern Physics*, 2015, **87**, DOI: 10.1103/RevModPhys.87.113.

(88) A. Eschenbacher, R. J. Varghese, J. Weng and K. M. Van Geem, *Journal of Analytical and Applied Pyrolysis*, 2021, **160**, 105374.

(89) A. Mostafa, M. Edwards and T. Górecki, *Journal of Chromatography A*, 2012, **1255**, 38–55.

(90) K. Dreisewerd, *Chemical Reviews*, 2003, **103**, 395–425.

(91) F. Hillenkamp and P. O'Connor, *Maldi MS: A Practical Guide to Instrumentation, Methods and Applications*, ed. F. Hillenkamp and J. Peter-Katalinic, Wiley-VHC, Munster, 1st edn., 2007, pp. 29–39.

(92) M. Nyden, W. Wallace and W. H. Awad, *Journal of The American Chemical Society*, 2003, **88**, 178–179.

(93) J. Åström, M. McNamee, B. Truchot, G. Marlair and P. van Hees, *Fire Technology*, 2023, DOI: 10.1007/S10694-023-01440-5.

(94) D. MacKenzie, *How Do We Know the Properties of Artifacts? Applying the Sociology of Knowledge to Technology*, ed. R. Fox, Routledge, London, 1st edn., 1996, pp. 247–263.

(95) J. Downer, *Social Studies of Science*, 2007, **37**, 7–26.

(96) R. Friedman, *Fire Safety Science*, 1986, **1**, 349–359.

(97) P. Blomqvist and A. Lonnermark, *Fire and Materials*, 2001, **25**, 71–81.

(98) A. M. Borrero-López, V. Nicolas, Z. Marie, A. Celzard and V. Fierro, *Polymers*, 2022, **14**, 3974.

(99) C. Mougel, T. Garnier, P. Cassagnau and N. Sintes-Zydowicz, *Polymer*, 2019, **164**, 86–117.

(100) X. Sui and Z. Wang, *Polymers for Advanced Technologies*, 2013, **24**, 593–599.

(101) P. K. Johnston, E. Doyle and R. A. Orzel, *International Journal of Toxicology*, 1988, **7**, 201–220.

(102) S. T. McKenna and T. R. Hull, *Fire Science Reviews 2016 5:1*, 2016, **5**, 1–27.

(103) Z. Campbell-Lochrie, R. M. Hadden, E. V. Mueller, C. Walker-Ravena, M. R. Gallagher, K. L. Clark, J. L. Hom, R. L. Kremens, J. A. Cole, M. M. Patterson, A. I. Everland and N. S. Skowronski, *Multi-scale analyses of wildland fire combustion processes: Small-scale field experiments – Transportable Analyzer for Calorimetry Outside (TACO)*, 2022.

(104) D. A. Purser, *Polymers*, 2016, **8**, DOI: 10.3390/POLYM8090330.

(105) J. P. Hidalgo, J. L. Torero and S. Welch, *Fire and Materials*, 2018, **42**, 358–373.

(106) M. Günther, A. Lorenzetti and B. Schartel, *Polymers*, 2018, **10**, 1166.

(107) A. Stec, *Grenfelll Tower Inquiry*, 2022, 1–5.

(108) O. G. Buzykin, S. V. Ivanov, A. A. Ionin, A. A. Kotkov and A. Y. Kozlov, *Journal of Russian Laser Research*, 2005, **26**, 402–426.

(109) X. Zhao, H. Yoshioka, T. Noguchi, S. Fujimoto, Y. Tanaike, T. Hayakawa, Y. Hase and T. Naruse, *Fire Science and Technology*, 2017, **36**, 11–24.

(110) J. Gong and L. Yang, *Fire Technology*, 2022, DOI: 10.1007/s10694-022-01339-7.

(111) American Society for Testing and Materials, *ASTM E2058 - 19 Standard Test Methods for Measurement of Material Flammability Using a Fire Propagation Apparatus (FPA)*, 2019.

(112) J. D. Peterson, S. Vyazovkin and C. A. Wight, *Journal of Physical Chemistry B*, 1999, **103**, 8087–8092.

(113) J. D. Peterson, S. Vyazovkin and C. A. Wight, *Macromol. Chem. Phys*, 2001, **202**, 775–784.

(114) S. Santamaria Garcia, Ph.D. Thesis, 2021.

(115) O. Yllmaz, Ç. K. Özkan, C. N. Yllmaz, A. Yorgancloğlu, H. Özgünay and H. A. Karavana, *AIP Conference Proceedings*, 2017, **1918**, 20006.

(116) Y. Ding, W. Zhang, X. Zhang, D. Han, W. Liu and J. Jia, *Fuel*, 2022, **319**, 123717.

(117) M. Stickler and G. Meyerhoff, *Die Makromolekulare Chemie*, 1980, **181**, 131–147.

(118) P. J. Linstrom and W. G. Mallard, in *NIST Standard Reference Database Number 69, National Institute of Standards and Technology*, Gaithersburg MD, 20899, 2023.

(119) R. Chen and M. Xu, *Waste Management*, 2020, **113**, 51–61.

(120) N. Boonmee and J. G. Quintiere, *Proceedings of the Combustion Institute*, 2002, **29**, 289–296.

(121) M. J. Spearpoint and J. G. Quintiere, *Combustion and Flame*, 2000, **123**, 308–325.

(122) D. Morrisset, R. M. Hadden, A. I. Bartlett, A. Law and R. Emberley, *Fire Safety Journal*, 2021, **120**, 103058.

(123) C. E. Macleod, A. Law and R. M. Hadden, *Fire Safety Journal*, 2023, **138**, 103793.

(124) S. Lin, Y. Qin, X. Huang and M. Gollner, *Fire Safety Journal*, 2023, **136**, 103745.

(125) F. Shafizadeh and Y. Sekiguchi, *Combustion and Flame*, 1984, **55**, 171–179.

(126) F. Hermouet, E. Guillaume, T. Rogaume, F. Richard and X. Ponticq, 3rd International conference on Fire in Vehicles (FIVE), Berlin, 2014, pp. 99–110.

(127) C. Dick, E. Dominguez-Rosado, B. Eling, J. Liggat, C. Lindsay, S. Martin, M. Mohammed, G. Seeley and C. Snape, *Polymer*, 2001, **42**, 913–923.

(128) J. P. Hidalgo, N. Gerasimov, R. M. Hadden, J. L. Torero and S. Welch, *Journal of Building Engineering*, 2016, **8**, 249–259.

(129) K. Homann, *Combustion and Flame*, 1967, **11**, 265–287.

(130) A. Liñán, *Acta Astronautica*, 1974, **1**, 1007–1039.

(131) F. A. Williams, *Combustion Theory*, CRC Press, 2nd edn., 2018.

(132) C. Clanet and G. Searby, *Combustion and Flame*, 1996, **105**, 225–238.

(133) S. H. Chung and C. K. Law, *Combustion Science and Technology*, 1984, **37**, 21–46.

(134) I. Puri and K. Seshadri, *Combustion and Flame*, 1986, **65**, 137–150.

(135) I. T. Leventon, K. T. Korver and S. I. Stoliarov, *Combustion and Flame*, 2017, **179**, 338–353.

(136) G. Berkowicz, T. M. Majka and W. Żukowski, *Energy Conversion and Management*, 2020, **214**, 112888.

(137) I. Glassman and P. Yaccarino, *Combustion Science and Technology*, 1980, **24**, 107–114.

(138) A. Tewarson and R. Pion, *Combustion and Flame*, 1976, **26**, 85–103.

List of Figures

This page has been intentionally left blank.

List of Tables

This page has been intentionally left blank.

Appendix A

Chapter 3: Supplementary Information

"... but my hands are on fire."

– The Pigeon Detectives
Through the Door (Up, Guards and at 'Em!, 2011)

This page has been intentionally left blank.

A.1 Appendix A

This appendix details the additional information relevant to the content discussed in Chapter 3.

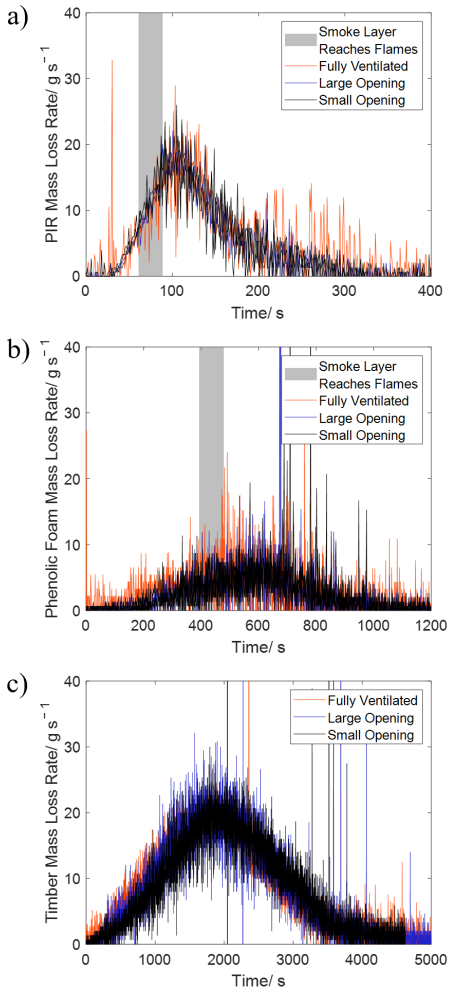

Figure A.1: The unsmoothed calculated heat release rates (HRRs) for each of the materials investigated in this study: a) PIR, b) Phenolic foam and c) Timber. Note that the highlighted smoke layer region does not apply to the fully-ventilated experiments.

Figure A.2: An annotated photograph of the ISO room sampling setup: 1) Smoke escaping the upper opening, 2) Sampling points, 3) Heated sampling line, 4) ISO room and 5) Condenser.

Figure A.3: A photograph of the PIR crib burning in an ISO room with the larger opening. Photograph taken after approximately 100 seconds.

Figure A.4: A photograph of the phenolic foam crib burning in an ISO room with the larger opening. Photograph taken after approximately 700 seconds.

Figure A.5: A photograph of the timber crib burning in an ISO room with the larger opening. Photograph taken after approximately 1900 seconds.

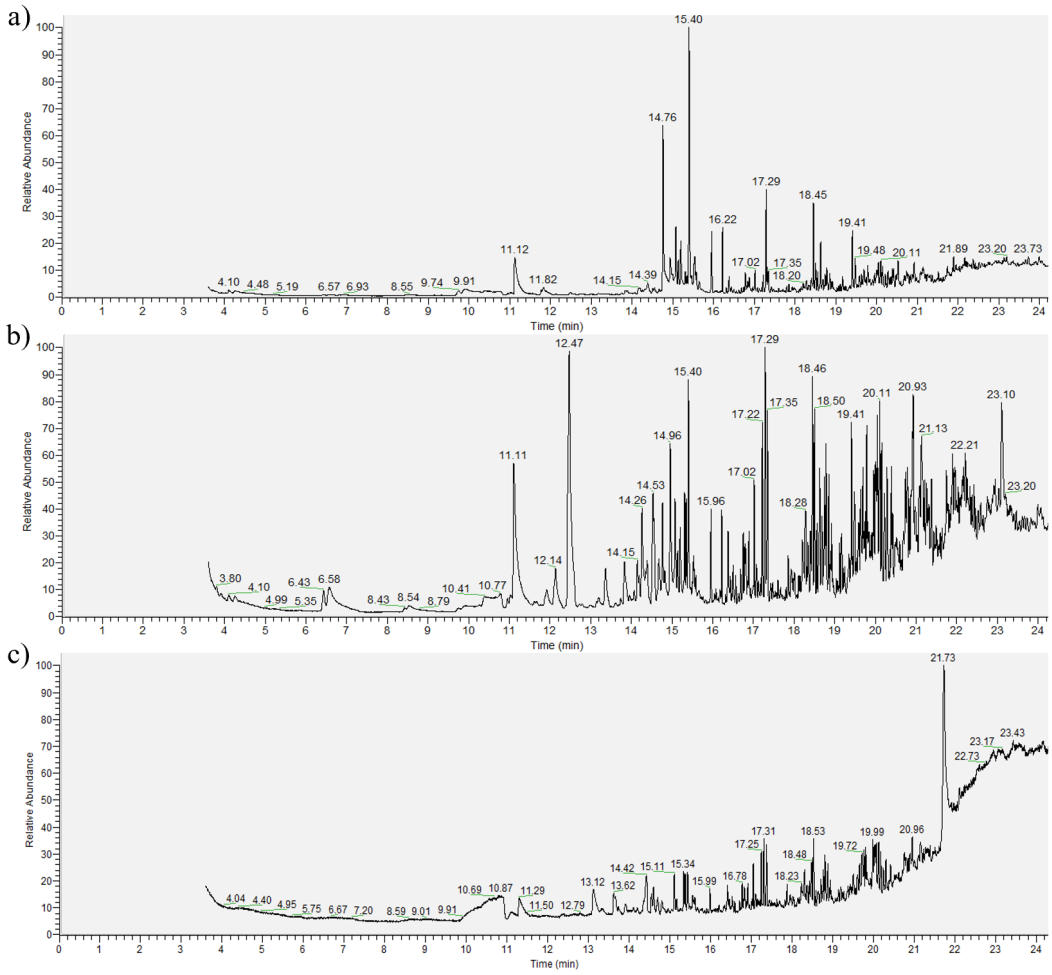

Figure A.6: Total ion chromatograms for the condensed effluent obtained during the combustion of timber cribs under differing ventilation conditions.a) is the small opening ISO room experiment, b) is the large opening ISO room experiment and c) is the fully-ventilated experiment.

Table A.1: The most prominent species identified via GC-MS in phenolic foam effluent collected under three differing ventilation conditions.

Opening	Small 1	Small 2	Small 3	Large	Fully-ventilated
Species detected in descending order of abundance	Methylbenzene	2,4-bis(1,1-dimethylethyl)-phenol	Methylbenzene	Methylbenzene	Methyl phenyl ether
	1,3-Dimethylbenzene	1,3-Dimethylbenzene	1,4-Dimethylbenzene	1,3-Dimethylbenzene	2-Methylphenol
	1,4-Dimethylbenzene	Methylbenzene	2,4-bis(1,1-dimethylethyl)-phenol	2-Phenethyl-β-phenylpropionate	Phenol
	2,4-bis(1,1-dimethylethyl)-phenol	2-Phenyl-2-propanol	α,α-Dimethyl-benzenemethanol	α,α-Dimethyl-benzenemethanol	1,4-Dimethylbenzene
	2-Phenethyl-β-phenylpropionate	Heptane,2,2,4,6,6-pentamethyl-	Heptane,2,2,4,6,6-pentamethyl-	Phenylethyne	1,3-Dimethylbenzene
	Phenylethyne	Phenylethyne	1,4-Dimethyl-7-(1-methylethyl)-azulene	Ethylbenzene	-
	1,2,4-Trimethylbenzene	1,2,4-Trimethylbenzene	Ethylbenzene	-	-

Table A.2: The most prominent species identified via GC-MS in timber effluent collected under three differing ventilation conditions.

Opening	Small	Large	Fully-ventilated
Species detected in descending order of abundance	α, α-Dimethyl-benzenemethanol	2-Isopropzyl-5-methyl-1-heptanol	4-Methyldocosane
	2-Ethyl-1-hexanol	3-Ethyl-5-(2-ethylbutyl)-octadecane	8-Methylenepentadacane
	2-Methyl-1-hexadecanol	α, α-Dimethyl-benzenemethanol	1-(2,2-dimethylcyclopentyl)-Ethanone
	2,6-Bis(1,1-dimethyethyl)-4-(1-oxopropyl)phenol	2-Methyl-1-hexadecanol	Methyl-6-oxoheptanoate
	2,4-Dimethyl-heptane	2,2,4,6,6-Pentamethyl-heptane	3-Ethyl-5-(2-ethylbutyl)-octadecane
	4-Methyloctane	-	-

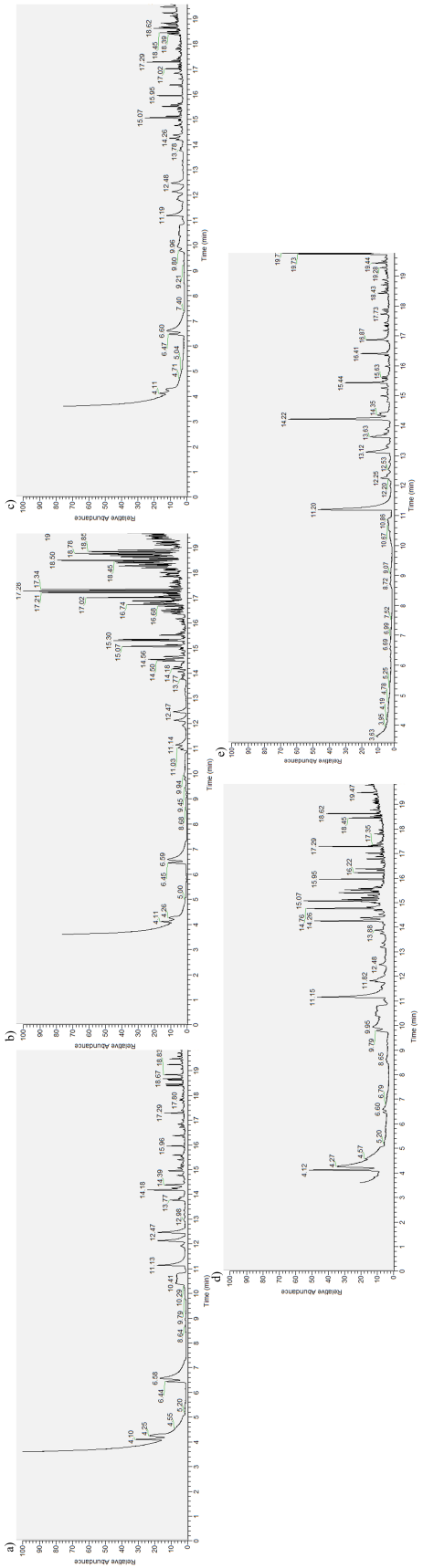

Figure A.7: Total ion chromatograms for the condensed effluent obtained during the combustion of PIR cribs under differing ventilation conditions.a), b) and c) are the small opening ISO room experiments, d) is the large opening ISO room experiment and e) is the fully-ventilated experiment.

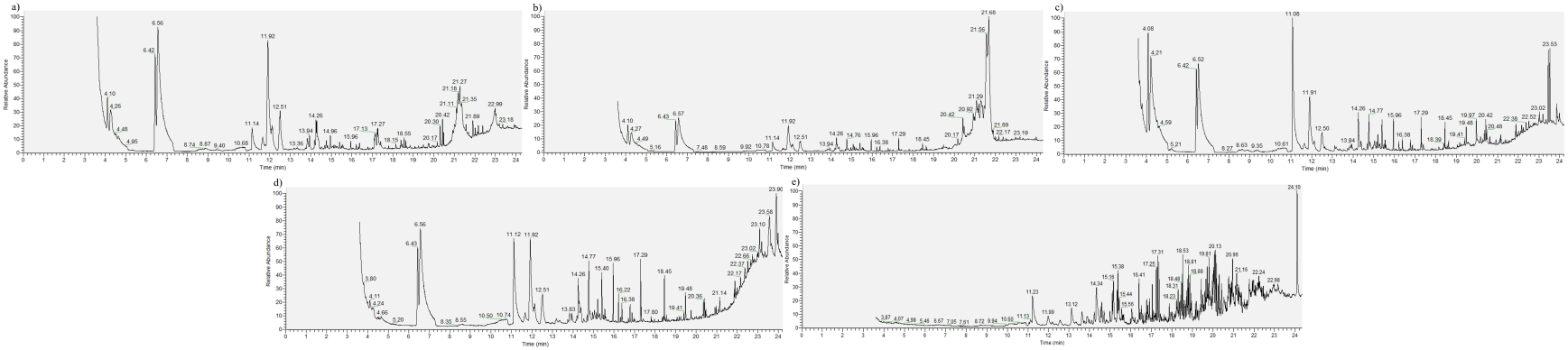

Figure A.8: Total ion chromatograms for the condensed effluent obtained during the combustion of phenolic foam cribs under differing ventilation conditions.a), b) and c) are the small opening ISO room experiments, d) is the large opening ISO room experiment and e) is the fully-ventilated experiment.

Appendix B

Chapter 4: Supplementary Information

"There is a poison in the air, a mix of chemicals and fear."

– Maxïmo Park
Our Velocity (Our Earthly Pleasures, 2007)

This page has been intentionally left blank.

B.1 Appendix B

This appendix details the additional information relevant to the content discussed in Chapter 4.

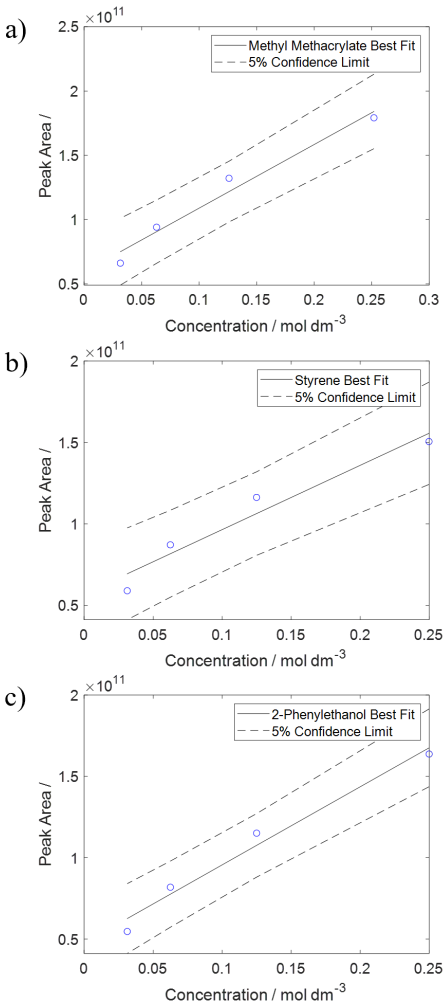

Figure B.1: The GC-MS calibration standards used to convert obtained peak areas into concentrations for a) MMA, b) styrene and c) 2-methoxyphenol.

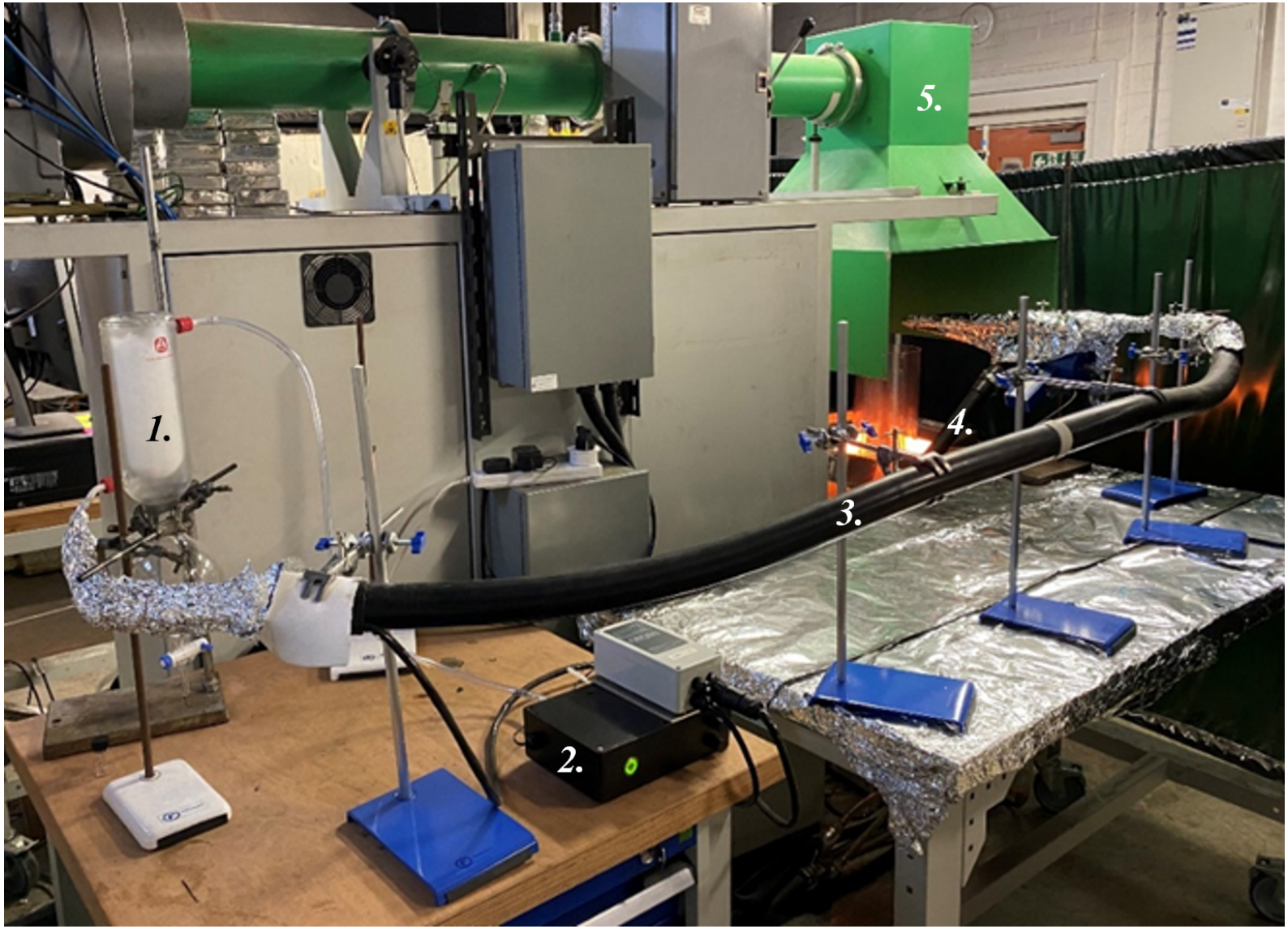

Figure B.2: An annotated photograph of the FPA sampling setup: 1) The condenser, 2) Pump, 3) Heated sampling line, 4) FT-IR sampling line and 5) FPA extraction hood.

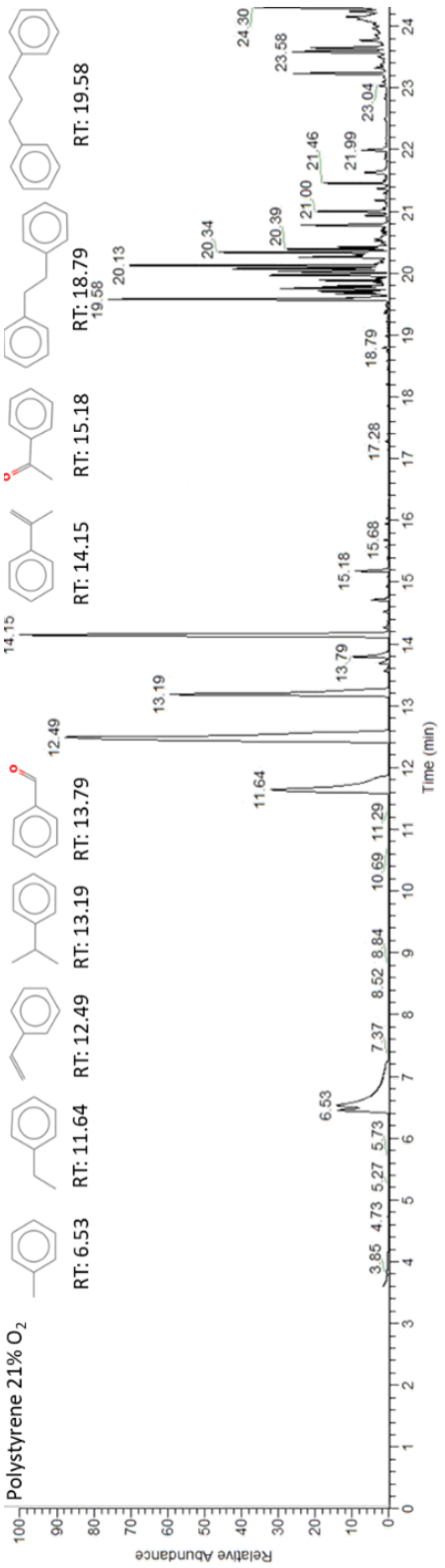

Figure B.3: The total ion chromatogram (TIC) obtained during the pyrolysis of polystyrene under 21 % oxygen. The peaks eluting at 12.49 and 14.15 minutes were identified as the monomer styrene and the pyrolysis product methylstyrene.

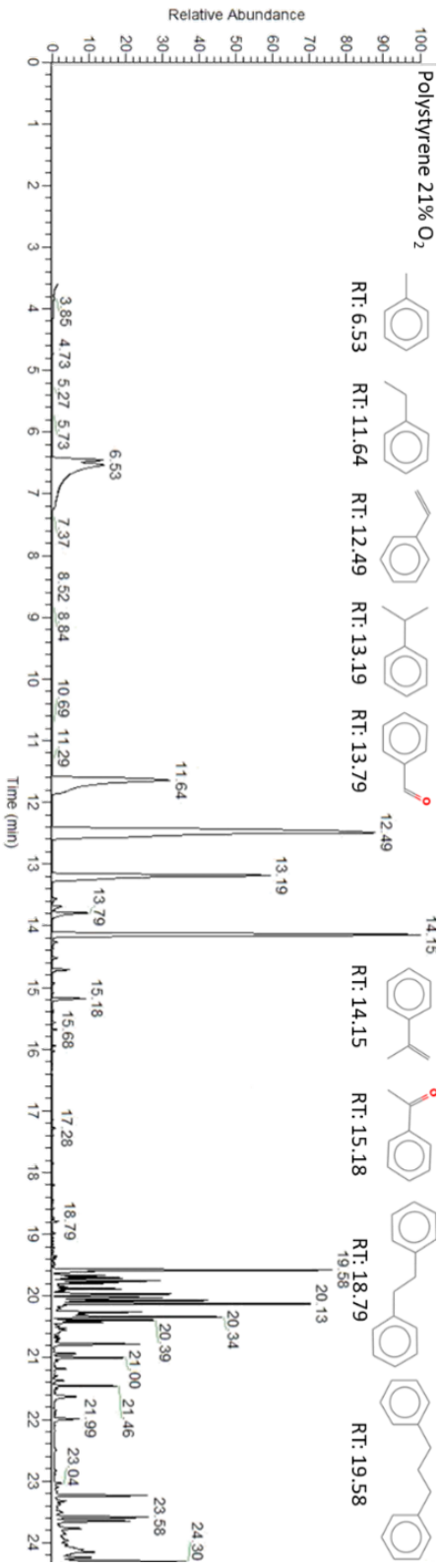

Figure B.4: The total ion chromatogram (TIC) obtained during the pyrolysis of timber (*Picea abies*) under 21 % oxygen. Many of the identified species were aromatic or heteroaromatic with several furans being identified.

Appendix C

Chapter 5: Supplementary Information

"Burn the midnight oil at both ends."

– Courteeners
Hanging Off Your Cloud (More. Again. Forever., 2020)

This page has been intentionally left blank.

C.1 Appendix C

This appendix details the additional information relevant to the content discussed in Chapter 5.

Table C.1: The recorded average heat fluxes and subsequent calculated heat release from char oxidation for PIR and phenolic foam collected under three differing ventilation conditions during the final 100 seconds of each experiment.

Material	**Oxygen Environment / %**	**Average Supplied Heat Flux (500 – 600 s) / kW m^{-2}**	**Heat Release from Char Oxidation / W**
PIR	0	49.9	0
	10	46.0	24.7
	20.9	37.9	76.5
Phenolic Foam	0	56.5	0
	10	35.3	136.0
	20.9	25.4	198.9

Table C.2: The recorded average heat fluxes and subsequent calculated heat release from char oxidation for PIR and phenolic foam collected under three differing ventilation conditions during the final 100 seconds of each experiment. The heat release from char oxidation uses the average supplied heat flux at 0 % oxygen as its baseline, resulting in some minor contributions being noted under inert atmospheres.

Material	**Oxygen Environment / %**	**Supplied Heat Flux (500 – 600 s) / kW m^{-2}**	**Heat Release from Char Oxidation / W**
PIR	0	49.3	3.53
		49.2	4.42
		51.1	0.00
	10	45.3	29.2
		44.6	33.9
		48.1	11.1
	20.9	39.2	68.1
		40.0	62.8
		34.5	98.6
Phenolic Foam	0	54.2	14.9
		57.3	0.00
		58.1	0.00
	10	33.9	145.1
		37.5	121.6
		34.5	141.2
	20.9	21.8	222.3
		28.3	180.5
		26.2	194.0

Appendix D

Chapter 6: Supplementary Information

"Turbulence is constant."

– Maxïmo Park
Doppelgänger Eyes (Stream of Life, 2024)

This page has been intentionally left blank.

D.1 Appendix D

This appendix details the additional information relevant to the content discussed in Chapter 6.

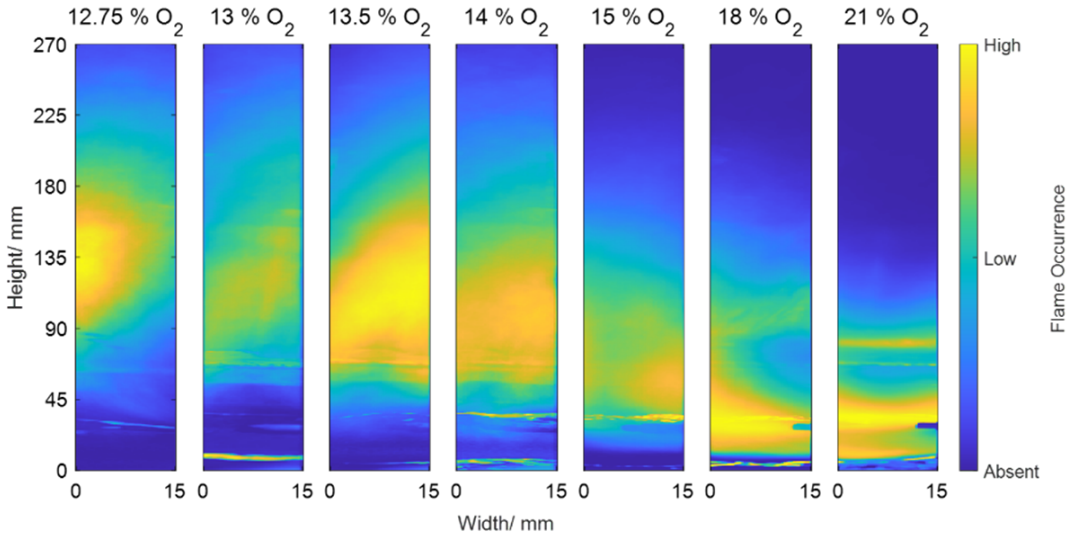

Figure D.1: The average flame occurrence obtained during the steady state combustion of PMMA under a range of oxidative conditions. Yellow areas indicate high flame occurrence, while blue regions denote the absence of a flame.

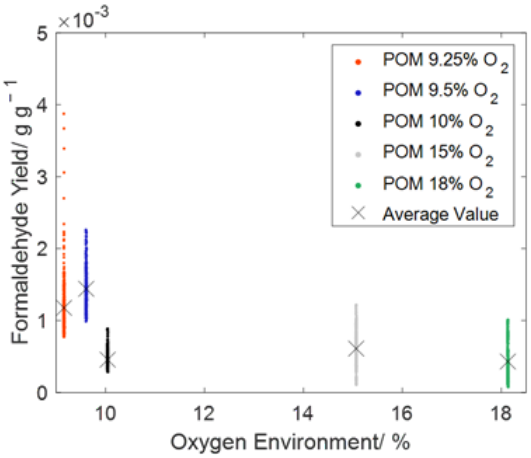

Figure D.2: The Formaldehyde yields obtained during the combustion of POM under a fixed MLR across a range of oxidative environments.

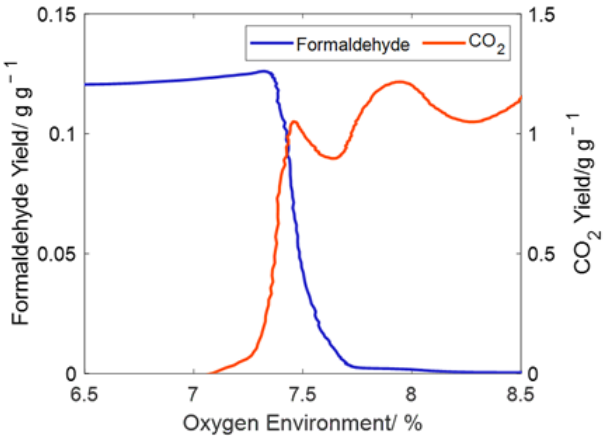

Figure D.3: The yields of formaldehyde and CO_2 obtained during the combustion of POM when sweeping the oxidative conditions between 6.5 % and 8.5 % oxygen. Note that the flame was sustained at lower oxygen percentages than the original series of experiments.